การสังเคราะห์ควอนตัมดอตแคดเมียมซีลีไนด์/ซิงก์ซัลไฟด์ชนิดประจุบวกและการประยุกต์ในการตรวจวัดดีเอ็นเอ

นางสาวจมรพรรณ ยังเจริญยืนยง

วิทยานิพนธ์นี้เป็นส่วนหนึ่งของการศึกษาตามหลักสูตรปริญญาวิทยาศาสตรมหาบัณฑิต
สาขาวิชาเคมี ภาควิชาเคมี
คณะวิทยาศาสตร์ จุฬาลงกรณ์มหาวิทยาลัย
ปีการศึกษา 2560

SYNTHESIS OF CATIONIC CdSe/ZnS QUANTUM DOTS AND APPLICATIONS IN DNA DETECTION

Miss Jamornpan Yangcharoenyuenyong

A Thesis Submitted in Partial Fulfillment of the Requirements
for the Degree of Master of Science Program in Chemistry
Department of Chemistry
Faculty of Science
Chulalongkorn University
Academic Year 2017

Thesis Title	SYNTHESIS OF CATIONIC CdSe/ZnS QUANTUM DOTS AND APPLICATIONS IN DNA DETECTION
By	Miss Jamornpan Yangcharoenyuenyong
Field of Study	Chemistry
Thesis Advisor	Numpon Insin, Ph.D.
Thesis Co-Advisor	Professor Tirayut Vilaivan

Accepted by the Faculty of Science, Chulalongkorn University in Partial Fulfillment of the Requirements for the Master's Degree

.....Dean of the Faculty of Science

(Professor Polkit Sangvanich, Ph.D.)

THESIS COMMITTEE

.....Chairman

(Associate Professor Vudhichai Parasuk, Ph.D.)

.....Thesis Advisor

(Numpon Insin, Ph.D.)

.....Thesis Co-Advisor

(Professor Tirayut Vilaivan)

.....Examiner

(Assistant ProfessorBoosayarat Tomapatanaget, Ph.D.)

.....External Examiner

(Assistant Professor Amara Apilux, Ph.D.)

จมรพรรณ ยังเจริญยืนยง : การสังเคราะห์ควอนตัมดอตแคดเมียมซีลีไนด์/ซิงก์ซัลไฟด์ชนิดประจุบวกและการประยุกต์ในการตรวจวัดดีเอ็นเอ (SYNTHESIS OF CATIONIC CdSe/ZnS QUANTUM DOTS AND APPLICATIONS IN DNA DETECTION) อ.ที่ปรึกษาวิทยานิพนธ์หลัก: อ. ดร.นำพล อินสิน, อ.ที่ปรึกษาวิทยานิพนธ์ร่วม: ศ. ดร.ธีรยุทธ วีไลวัลย์, 86 หน้า.

ในปัจจุบัน อนุภาคนาโนของสารกึ่งตัวนำหรือควอนตัมดอตกำลังเป็นที่สนใจในการนำมาประยุกต์ใช้ทางด้านการตรวจวัดชีวภาพเชิงแสง เนื่องด้วยประสิทธิภาพการเปล่งแสงที่มีความเสถียร โดยชนิดของควอนตัมดอตที่ได้รับความนิยมอย่างกว้างขวางคือควอนตัมดอตชนิดแคดเมียมซีลีไนด์/ซิงก์ซัลไฟด์ หนึ่งในการตรวจวัดที่นำควอนตัมดอตมาประยุกต์ใช้คือการตรวจวัดดีเอ็นเอ โดยอาศัยการเกิดอันตรกิริยาระหว่างประจุลบจากหมู่ฟอสเฟตของดีเอ็นเอกับประจุบวกบนพื้นผิวควอนตัมดอต แต่ด้วยขั้นตอนกระบวนการสังเคราะห์ควอนตัมดอตชนิดแคดเมียมซีลีไนด์/ซิงก์ซัลไฟด์ที่เสถียร ทำให้ได้ควอนตัมดอตชนิดแคดเมียมซีลีไนด์/ซิงก์ซัลไฟด์ที่มีพื้นผิวไม่ชอบน้ำ ดังนั้นในงานวิจัยนี้ จึงทำการเคลือบผิวของควอนตัมดอตชนิดแคดเมียมซีลีไนด์/ซิงก์ซัลไฟด์ให้สามารถกระจายตัวในน้ำได้และมีประจุบวกโดยการสร้างไมเซลล์กับพอลิเมอร์ชนิดพอลิเอทิลีนอิมมีน แต่เนื่องจากพอลิเอทิลีนอิมมีนมีความชอบน้ำสูง เพื่อให้สามารถสร้างไมเซลล์กับผิวควอนตัมดอตได้ ดังนั้นจึงได้ทำการเพิ่มความไม่ชอบน้ำด้วยการดัดแปรหมู่ฟังก์ชั่นเอมีนของพอลิเอทิลีนอิมมีนบางส่วนให้เป็นเอไมด์โดยใช้กรดออกทาโนอิกผ่านกระบวนการเข้าคู่กันโดยใช้ EDC/NHS coupling ในงานวิจัยได้ทำการยืนยันโครงสร้างของพอลิเอทิลีนอิมมีนที่ผ่านการดัดแปรหมู่ฟังก์ชันบางส่วนด้วยเทคนิคอินฟราเรด โปรตอนและคาร์บอนนิวเคลียร์แมกเนติกเรโซแนนซ์และแมสสเปกโตรเมทรี จากผลการพิสูจน์ทราบโครงสร้างสารของควอนตัมดอตชนิดแคดเมียมซีลีไนด์/ซิงก์ซัลไฟด์พบว่าอนุภาคมีเส้นผ่าศูนย์กลางประมาณ 4.60 ±0.53 นาโนเมตรและมีลักษณะเป็นทรงกลม นอกจากนี้จากผลของเครื่องเอกซ์เรย์ดิฟแฟรกชันยังแสดงให้เห็นว่า ควอนตัมดอตที่สังเคราะห์มีทั้งแคดเมียมซีลีไนด์และซิงก์ซัลไฟด์ ในการพิสูจน์ทราบโครงสร้างสารของควอนตัมดอตที่ถูกเคลือบผิวให้มีประจุบวกได้ใช้เทคนิคอัลตราไวโอเลตและวิสิเบิลสเปกโทรสโคปี เทคนิคฟลูออเรสเซนต์สเปกโตรสโคปี เทคนิควัดการกระเพื่อมของความเข้มแสงและเทคนิคกล้องจุลทรรศน์อิเล็กตรอนแบบส่องผ่านในการยืนยัน โดยได้ทำการปรับเปลี่ยนอัตราส่วนระหว่างพอลิเอทิลีนอิมมีนที่ผ่านการดัดแปรและควอนตัมดอต จากผลการวัดขนาดและประจุบนพื้นผิวของควอนตัมดอตที่ผ่านการเคลือบพบว่าควอนตัมดอตที่ผ่านการเคลือบผิวมีขนาดอยู่ในช่วง 250-400 นาโนเมตร และมีประจุพื้นผิวระหว่าง +36 ถึง +40 มิลลิโวลต์ โดยยิ่งอัตราส่วนมากขนาดและประจุยิ่งมีค่าเพิ่มขึ้นตามไปด้วย นอกจากนี้ ยังได้ทำการตรวจวัดสมบัติเชิงแสงของควอนตัมดอตที่ผ่านการเคลือบผิวกับควอนตัมดอตเดิม จากผลการทดลองพบว่าควอนตัมดอตที่ผ่านการเคลือบผิวยังคงสมบัติเชิงแสงไว้ และสามารถเก็บไว้ได้นานถึง 30 วัน ในอัตราส่วนของพอลิเมอร์ต่อควอนตัมดอตที่ดีที่สุดคือ 60 ต่อ 1 โดยโมล และจากผลของกล้องจุลทรรศน์แบบส่องผ่านพบว่าขนาดที่เพิ่มขึ้นมาจากในแต่ละไมเซลล์ประกอบด้วยควอนตัมดอตหลายอนุภาค นอกจากนี้ยังได้ทำการศึกษาการเกิดอันตรกิริยาระหว่างควอนตัมดอตที่ผ่านการเคลือบผิวกับดีเอ็นเอ และดีเอ็นเอที่ถูกตรึงกับเพปไทด์นิวคลิอิกแอซิดหรือพีเอ็นเอ จากผลการตรวจวัดพบว่าควอนตัมดอตสามารถเกิดอันตรกิริยากับดีเอ็นเอได้ ซึ่งสามารถนำไปเป็นประโยชน์ในการศึกษาด้านชีวภาพต่อไปได้

ภาควิชา เคมี ลายมือชื่อนิสิต .....

สาขาวิชา เคมี ลายมือชื่อ อ.ที่ปรึกษาหลัก .....

ปีการศึกษา 2560 ลายมือชื่อ อ.ที่ปรึกษาร่วม .....

5771929823 : MAJOR CHEMISTRY
KEYWORDS: QUANTUM DOTS, SEMICONDUCTOR NANOPARTICLES, MICELLE FORMATION, CATIONIC QUANTUM DOTS, POLY(ETHYLENE)IMINE, DNA DETECTION

JAMORNPAN YANGCHAROENYUENYONG: SYNTHESIS OF CATIONIC CdSe/ZnS QUANTUM DOTS AND APPLICATIONS IN DNA DETECTION. ADVISOR: NUMPON INSIN, Ph.D., CO-ADVISOR: PROF. TIRAYUT VILAIVAN, D.Phil., 86 pp.

Semiconductor nanoparticles or quantum dots (QDs), especially CdSe/ZnS QDs, are of great interest in bioapplications due to their unique size-dependent optical properties and photo-stability. One of the plausible applications of QDs is DNA detection using QDs as a novel fluorescence tool for sensing of DNA using the electrostatic interaction between negative charge of DNA and positive charge on QDs surface. In this work, CdSe/ZnS QDs were synthesized using a hot-solution decomposition process resulting in hydrophobic CdSe/ZnS QDs. To obtain water-soluble and cationic QDs, the surface of QDs were modified with poly(ethylene)imine (PEI) via micelle formation. Because of hydrophilicity of PEI and hydrophobicity of QDs surface, for the formation of micellar structures, PEI was partially acylated with octanoic acid through EDC/NHS-coupling process to increase the hydrophobicity. The the structure of octanoic acid-modified PEI (Oct-PEI) were studied using infrared spectroscopy, ^{1}H and ^{13}C NMR, and mass spectrometry. TEM results showed that diameter of the synthesized CdSe/ZnS QDs are 4.60 ±0.53 nm and are in spherical shapes. Moreover, XRD results also showed that the synthesized QDs contained both of CdSe and ZnS. To characterized the cationic QDs (Oct-PEI/QDs), the UV-Visible spectroscopy, fluorescent spectroscopy, dynamic light scattering analysis and TEM were used. The size and zeta-potentials of the QDs showed that, the sizes and charges of Oct-PEI/QDs were in the range of 250-400 nm and +36 to +40 mV, respectively. The ratio between of Oct-PEI and QDs was varied and it was found that the higher ratio of QDs and Oct-PEI, the larger size and the higher magnitudes of positive charge. The optical properties of cationic QDs was measured and compared with the original QDs. The absorption and emission results showed that the Oct-PEI/QDs still maintained the properties as the original QDs, and the fluorescent signal lasted for 30 days in samples prepared using the Oct-PEI/QDs ratio of 60:1 by mol. TEM results revealed that the increase in sizes of the particles were likely due to micelles contained several individual particles. Moreover, it was found that the Oct-PEI/QDs interacted with DNA and DNA matched peptide nucleic acid (PNA) for investigating the sensing properties. The results showed that the Oct-PEI/QDs can interact with DNA and become potentially useful for biological studies.

Department:	Chemistry	Student's Signature	.....
Field of Study:	Chemistry	Advisor's Signature	.....
Academic Year:	2017	Co-Advisor's Signature	.....

ACKNOWLEDGEMENTS

Firstly, I would like to appreciate Dr. Numpon Insin who is my thesis advisor, gave me valuable assistance not only for the achievement in my thesis successfully completion but also in daily life. Moreover, I appreciate Professor Dr. Tirayut Vilaivan, who is my thesis co-advisor, who also guided me the solution to solve many obstructions in this work.

For valuable comment and advices, I would to thank my thesis committee, Associate Professor Dr. Vudhichai Parasuk, Assistant professor Dr. Boosayarat Tomapatanaget and Dr. Amara Apilux. This research would have not been completed without all of their kindness.

In addition, I would special thanks to all of members of Materials Chemistry and Catalyst Research Unit and Organic Synthesis Research Unit who are always helpful. Particularly, Padtaraporn Chanhom, Wishulada Injumpa, Chalathan Saengruengrit, Kamonlatth Rodponthukwaji, Chayan Charoenpakdee and Nuttapon Jirakittiwut who are my seniors that gave me very useful advises. Moreover, the supporters are also Kullatida Ratchadapiban, Nattakarn Phromsiri, Natthaya Thepphanao, Chonnavee Maneepunti, Apichat Klayanon and Chutima Tangku. They are very important for me and have a lot of contribution in my thesis.

Other special group is my family who gave me everything for my life and be my encouragement for working on this research especially Mr. Choomphol Yangcharoenyeunyong, I hope you can see my successful from the sky.

Finally, this work was partly funded by the Grant for International Research Integration: Chula Research Scholar, Ratchadaphiseksomphot Endowment Fund, CU Graduate School Thesis Grant and Center of Excellence on Petrochemical and Materials Technology, additionally, I would like to thank Department of Chemistry, Faculty of Science, and Chulalongkorn University for laboratory facilities and instruments.

CONTENTS

Page

THAI ABSTRACT iv

ENGLISH ABSTRACT v

ACKNOWLEDGEMENTS vi

CONTENTS vii

LIST OF FIGURES xi

LIST OF TABLES xix

LIST OF SCHEMES xx

LIST OF ABBREVIATIONS xxi

CHAPTER I INTRODUCTION 1

1.1 Statement of the problem 1

1.2 Objectives of this thesis 2

1.3 Scope of this thesis 2

1.4 The benefits of this thesis 3

CHAPTER II THEORIES AND LITERATURE REVIEWS 4

2.1 Nanomaterials 4

2.1.1 Metallic nanoparticles 5

2.1.1.1 Gold nanoparticles (AuNPs) 5

2.1.1.2 Silver nanoparticles (AgNPs) 6

2.1.1.3 Copper nanoparticles (CuNPs) 6

2.1.2 Magnetic nanoparticles (FeNPs) 7

2.1.3 Carbon nanoparticles (CNPs) 8

2.1.4 Semiconductor nanoparticles 9

Page

2.1.4.1 Semiconductor nanocrystal Quantum Dots (QDs) 9
2.1.4.2 Quantum dots (QDs) synthesis techniques 15
2.1.4.2.1 Top-Down Synthesis Processes 15
2.1.4.2.2 Bottom-Up Approach 15
2.1.4.2.2.1 Wet-Chemical Methods 15
1) Sol-gel Process 16
2) Micro-emulsion Process 16
3) Hot-Solution Decomposition Process 16
4) Other synthesis processes 17
2.1.4.2.2.2 Vapor-Phase Methods 17
2.2 Surface modification of QDs 19
2.2.1 Ligand exchange 19
2.2.2 Micelle formation 21
2.3 Poly(ethylene) imine (PEI) 24
CHAPTER III EXPERIMENTS 28
3.1 Instruments 28
3.2 Chemicals 29
3.3 Synthesis of CdSe/ZnS core/shell QDs 30
3.3.1 Synthesis of CdSe core 31
3.3.1.1 Preparation of TOPSe solution 31
3.3.1.2 Preparation of CdSe-precursor mixture 31
3.3.1.3 Synthesis of CdSe-core 31
3.3.2 ZnS-shell coating 31

Page

3.3.2.1 Preparation of CdSe cores 31
3.3.2.2 Preparation of TOPS solution 31
3.3.2.3 ZnS-shell coating 32
3.3.3 Characterization of CdSe/ZnS core/shell QDs 32
3.3.3.1 Ultraviolet-Visible spectroscopy (UV-Vis spectroscopy) 32
3.3.3.2 Fluorescence spectroscopy 32
3.3.3.3 Transmission Electron Microscopy (TEM) 33
3.3.3.4 X-ray Diffractometer (XRD) 33
3.3.3.5 Scanning Electron Microscopy coupled with Energy Dispersive X-ray Spectroscopy (SEM-EDX) 33
3.4 Cationic surface modification of CdSe/ZnS core/shell QDs 33
3.4.1 Partial acylation of PEI by octanoic acid 34
3.4.1.1 Characterization of partially acylated PEI (Oct-PEI) 35
3.4.1.1.1 Fourier Transform Infrared Spectroscopy (FTIR spectroscopy) 35
3.4.1.1.2 Proton and Carbon Nuclear Magnetic Resonance Spectrometry (^{1}H and ^{13}C NMR) 35
3.4.1.1.3 Solubility test 35
3.4.2 Micelle formation between the surface of QDs and Oct-PEI (Oct-PEI/QDs) 35
3.4.2.1 Variation of weight by weight ratio between QDs and Oct-PEI 35
3.4.2.2 Variation of molar ratio between QDs and Oct-PEI 36
3.4.2.3 Characterization of the coated QDs (Oct-PEI/QDs) 36
3.4.2.3.1 Ultraviolet-Visible spectroscopy (UV-Vis spectroscopy) .. 36

Page

3.4.2.3.2 Fluorescence spectroscopy 36
3.4.2.3.3 Dynamic Light Scattering analyzer (DLS) 36
3.4.2.3.4 Transmission Electron Microscopy (TEM) 36
3.4.2.4 Photostability test 37
3.4.2.5 Cytotoxicity test 37
3.5 Application of cationic Oct-PEI/QDs in DNA detection 38
3.5.1 DNA detection onto glass slide 38
3.5.2 DNA detection in solution 39
3.5.2.1 DNA mixed with the cationic Oct-PEI/QDs 39
3.5.2.2 PNA-DNA mixed with the cationic Oct-PEI/QDs 39
CHAPTER IV RESULTS AND DISCUSSIONS 40
4.1 Characterization of the synthesized CdSe/ZnS QDs 40
4.2 Characterization of the partially acylated poly(ethylene)imine (Oct-PEI) 46
4.3 Characterization of the cationic QDs (Oct-PEI/QDs) 50
4.4 Fluorescent response of the cationic QDs in presence of DNA 62
CHAPTER V CONCLUSION 68
REFERENCES 70
Appendix A 76
Appendix B 80
Appendix C 83
VITA 86

LIST OF FIGURES

Figure 2.1 Examples of nanomaterials in different morphologies [2]. 4

Figure 2.2 Color of the AuNP solution with different concentration of kanamycin [5]. 5

Figure 2.3 TEM images of different synthesis method of AgNPs which A) milky mushroom extraction and B) culture supernatant of bacteria [7]. 6

Figure 2.4 TEM image of synthesized copper nanoparticles [9]. 7

Figure 2.5 TEM images of SPIONPs encapsulated with chitosan nanoparticles in scale bar of a) 100 nm, b) 50 nm and c) 20 nm [11]. 7

Figure 2.6 Confocal fluorescence images of HeLa cells which the emissions were recorded in different ranges: A) 420-510 nm, B) 490-560 nm, C) 540-590 nm, and D) 590-750 nm [14]. 8

Figure 2.7 The band gap diagram of a conductor, semiconductor and an insulator [15]. 9

Figure 2.8 Fluorescence images of E. coli having been mixed with QDs/L-cysteine obtained by changing visible (A,C) and UV light (B,D) [17]. 10

Figure 2.9 Solid lines: PL spectra of crude solutions of CdSe, CdTe, and InAs nanocrystals measured at different stages of particle growth. Points: PL quantum efficiency vs position of the PL maximum of size-selected fractions isolated from each crude solution [18]. 11

Figure 2.10 Colloidal suspensions of CdSe QDs [19]. 11

Figure 2.11 Fluorescence of the CdSe/TOPO (dotted line) and CdSe/ZnS (solid line) nanocrystals normalized by their absorption at the excitation wavelength of 470 nm [21]. 12

Figure 2.12 TEM image of CdSe/ZnS nanocrystals [21]. 12

Figure 2.13 Schematic diagram of the synthesis of CdSe/ZnS QDs process [22]. 13

Figure 2.14 Absorption spectra demonstrating the photocatalytic degradation of methyl orange by CdSe (a) and CdSe/ZnS core/shell QDs (b) [22]. 13

Figure 2.15 TEM images of the CdSe QDs a), and CdSe/ZnS core-shell QDs with different shell thickness b), c) and d) [23]. 14

Figure 2.16 Fluorescence spectra of the CdSe/ZnS core-shell QDs (C0, C1, C2, C3) under the excitation of 532 nm in which 0, 1, 2 and 3 referred to the thickness of shell layer [23]. 14

Figure 2.17 Typical room temperature band edge luminescence and absorption spectra for 3.5 nm diameter CdSe crystallites [30]. 18

Figure 2.18 Absorption and emission spectra of TOPO-capped CdSe nanocrystals at room-temperature before (solid lines) and after (dashed lines) surface exchange with allylamine. The inset shows normalized PL spectra [31]. 18

Figure 2.19 Schematic of some of the applicable CdSe quantum dot structures [32]. 20

Figure 2.20 Temporal evolution of the absorption spectra of MUA-coated CdSe nanocrystals in water under the photooxidation conditions. The time progression follows the photooxidation of the nanocrystals from the start of the experiment to the precipitation of nanocrystals [33]. 21

Figure 2.21 Polymer coating of the Nanocrystals [34]. 22

Figure 2.22 TEM images of polymer-coated with four different types of core nanomaterials [34]. 22

Figure 2.23 a) Emission of polymer water solubilized CdSe/ZnS NCs following the addition of dye over time. The emission from the aqueous dye/polymer complex alone is shown in black. b) Schematic of the coupled NP/dye system. c) Absorption spectra of the bare NP, the NP/dye couple, and the dye alone [35]. 23

Figure 2.24 Fluorescence images of HeLa cells transfected by a) PEI-10K at different ratio with DNA, b) PEI-25K at different ratio with DNA and c) copolymer at different ratio with DNA [36]. 24

Figure 2.25 TEM images of PEI-coated onto silica nanoparticles [38]. 25

Figure 2.26 Size distribution of PEI-derivatised QDs in water, measured by light back-scattering. Squares: 800 D PEI, triangles: 25 kD PEI [39]..... 26

Figure 2.27 (A) Schematic representations of the preparing route for PEI/QD nanoparticles; TEM images of QDs (B), PEI/QDs (C), and PEI/QD/miRNA (D) nanoparticles. (E, F, and G) DLS data corresponding to (B, C, and D), respectively [40]. 27

Figure 3.1 Structures of MTT and colored formazan product [44]. 37

Figure 3.2 Reaction scheme for the attachment of aminated DNA to aldehyde-modified glass [45]. 39

Figure 4.1 The synthesized CdSe/ZnS core/shell QDs with difference sizes in hexane under a UV lamp. 40

Figure 4.2 Absorption spectra of the synthesized CdSe core (black line), and CdSe/ZnS core/shell (red line) QDs at room temperature. 42

Figure 4.3 Emission spectra of the synthesized CdSe core (black line), and CdSe/ZnS core/shell (red line) QDs at room temperature with the excitation wavelength 350 nm and applied voltage 700 PMT. 42

Figure 4.4 The bar chart of calculated quantum yield compared between CdSe core and CdSe/ZnS core/shell QDs. 43

Figure 4.5 TEM images of a,c) CdSe core and b,d) CdSe/ZnS core/shell QDs with magnitude of 120 kX. 44

Figure 4.6 XRD pattern of (blue line) CdSe core QDs, (green line) CdSe/ZnS core/shell QDs, (red line) JCPDS no. 19-0191 Cadmium Selenide pattern, and (black line) JCPDS no. 05-0566 Sphalerite Zinc Sulfide pattern. Star (*) refer to the presence of ZnS in CdSe/ZnS QDs..... 45

Figure 4.7 Schematic of EDC/NHS coupling between octanoic acid and PEI. 47

Figure 4.8 IR spectra of Oct-PEI in differentiated percentage of acylation; 20% (red line), 30% (purple line), and 40% (light blue line)..... 47

Figure 4.9 IR spectra of PEI (purple line), octanoic acid (red line), and Oct-PEI (brown line)..... 47

Figure 4.10 ^{1}H NMR spectra of PEI (blue line), octanoic acid (green line), and Oct-PEI (red line)..... 48

Figure 4.11 ^{13}C NMR spectra of PEI (blue line), octanoic acid (green line), and Oct-PEI (red line)..... 49

Figure 4.12. Images of QDs coated with Oct-PEI. a) in $CHCl_3$, b) after evaporated, c) and d) in DI water before and after centrifuge, respectively. The weight ratio between Oct-PEI and QDs is 4:1. 51

Figure 4.13 Images of QDs coated with Oct-PEI dissolved in DI water with the weight ratio between Oct-PEI and QDs were a) 5:1, b) 6:1, c) 7:1, d) 8:1, e) and f) 9:1 which before and after centrifugation. 52

Figure 4.14 Emission spectra of fluorescence titration started with the synthesized CdSe/ZnS core/shell QDs (black line), after adding 10 µL (red line), 50 µL (blue line), 100 µL (green line), 500 µL (pink line), 1 mL (olive-green line), 2 mL (navy-blue line), 3 mL (magenta line), and 4 mL (light-red line) of polymer solution in the ratio of Oct-PEI:QDs was 1:1 by weight or 100:1 by mole. The excitation wavelength was 350 nm with 700 PMT applied voltage. 53

Figure 4.15 Emission spectra of Oct-PEI:QDs with the molar ratio of 100:1 when dispersed in $CHCl_3$ (red line) and DI water (green line). The excitation wavelength was 350 nm with 700 PMT applied voltage..... 53

Figure 4.16 Fluorescence spectrum of the coated QDs dispersed in DI water in the molar ratio between Oct-PEI and QDs of 90:1 using excitation wavelength at 350 nm with 700 PMT applied voltage. 54

Figure 4.17 Emission spectra of the coated QDs dispersed in DI water in the molar ratio between Oct-PEI and QDs of 90:1 when left at room temperature for 1 day

(black line), 7 days (red line), and 15 days (blue line). The excitation wavelength was 350 nm with 700 PMT applied voltage. 55

Figure 4.18 Emission spectra of the coated QDs in different molar ratio between Oct-PEI:QDs of 60:1 (black line), 70:1 (red line), 80:1 (blue line), and 90:1 (green line). The excitation wavelength was 350 nm with 600 PMT applied voltage. 56

Figure 4.19 Emission spectra of the coated QDs in different molar ratio between Oct-PEI:QDs of 60:1 (black line), 70:1 (red line), 80:1 (blue line), and 90:1 (green line). The excitation wavelength was 350 nm with 600 PMT applied voltage. 56

Figure 4.20 Emission spectra of the coated QDs in molar ratio between Oct-PEI and QDs of 60:1 after 1 day (black line), 7 days (red line), 15 days (blue line), and 30 days (pink line). The excitation wavelength was 350 nm with 600 PMT applied voltage. 57

Figure 4.21 Emission spectra of the coated QDs in molar ratio between Oct-PEI and QDs of 70:1 after 1 day (black line), 7 days (red line), 15 days (blue line), and 30 days (pink line). The excitation wavelength was 350 nm with 700 PMT applied voltage. 57

Figure 4.22 Emission spectra of the coated QDs in molar ratio between Oct-PEI and QDs of 80:1 after 1 day (black line), 7 days (red line), 15 days (blue line), and 30 days (pink line). The excitation wavelength was 350 nm with 600 PMT applied voltage. 58

Figure 4.23 TEM images of the coated QDs with different magnification a) 20 kX and b) 40 kX. 60

Figure 4.24 MTT assays of the coated QDs against to L929 cells with the incubation time of 24 hours. 61

Figure 4.25 Images of 140 μM, 40 μL of the cationic QDs reacted with TET DNA (top row, column 1, 3, 5) and Kanamycin DNA (bottom row, column 1, 3, 5) compared with DNA alone (column 2, 4, and 6) under a) normal light, b) and c) UV light in different concentrations which are 1000 nM (column 1,2), 500 nM

(column 3,4), and 250 nM (column 5,6). The green dots onto left sides of glass slide b) were SYBR gold DNA stains with TET (top) and Kanamycin (bottom). 62

Figure 4.26 Absorption spectra of DNA-glass slide (red line) compared with reference glass slide (black line). The absorption was measured in the range of 200-600 nm. 63

Figure 4.27 The mixture between 10 μM of the dG10 strand and 70 μM of the cationic QDs (left) compared with the cationic QDs (right) in phosphate buffer pH7.0 under a) UV lamp and b) normal light; the camera setting was f=8.0, speed shutter=2, ISO 100. 64

Figure 4.28 Images of (P) Nile Red-PNA, (D) T9 DNA complimented with the PNA, (P+D) NR-PNA in combination with DNA and pure the cationic QDs (QDs) at a) before adding QDs into P, D, and P+D, b) suddenly after adding QDs to P, D and P+D, and c) after 1 min of QD addition. The concentration of DNA was 10 μM, PNA and the cationic QDs were 14 μM in 20 μL of phosphate buffer pH 7.0. The camera setting was f=8.0, speed shutter=2, and ISO 100. 65

Figure 4.29 Fluorescent spectra of 0.1 μM the cationic QDs before interacted with 1 μM of NR-PNA and DNA (dark yellow line), after interacted for 0 minute (pink line), 1 minute (dark cyan line), 3 minutes (blue line), 5 minutes (red line), 10 minutes (black line), and the solution of DNA matched NR-PNA before adding QDs (navy line). The excitation wavelength was 350 nm with 700 PMT applied voltage. .. 66

Figure 4.30 Fluorescent spectra of 0.1 μM of the cationic QDs before interacted with 1 μM of DNA (green line), after interacted for 0 minute (black line), 1 minute (dark grey line), 3 minutes (grey line), 5 minutes (lighter grey line), and 10 minutes (the lightest grey line). The excitation wavelength was 350 nm with 700 PMT applied voltage. 67

Figure A1 Graph between peak area of fluorescence VS absorbance at wavelength 480 nm of Rhodamine 6G in 5 different concentrations. 77

Figure A2 Graph between area peak of fluorescence VS absorbance at wavelength 480 nm of CdSe core QDs in 5 different concentrations. 78

Figure A3 Graph between area peak of fluorescence VS absorbance at wavelength 480 nm of CdSe/ZnS core/shell QDs in 4 different concentrations..... 79

Figure B1 Emission spectra of the coated green QDs in molar ratio between Oct-PEI and QDs of 60:1 after 1 day (black line), 7 days (red line), 15 days (blue line), and 30 days (pink line). The excitation wavelength was 350 nm with 700 PMT applied voltage. 81

Figure B2 Emission spectra of the coated green QDs in molar ratio between Oct-PEI and QDs of 70:1 after 1 day (black line), 7 days (red line), 15 days (blue line), and 30 days (pink line). The excitation wavelength was 350 nm with 700 PMT applied voltage. 81

Figure B3 Emission spectra of the coated green QDs in molar ratio between Oct-PEI and QDs of 80:1 after 1 day (black line), 7 days (red line), 15 days (blue line), and 30 days (pink line). The excitation wavelength was 350 nm with 700 PMT applied voltage.

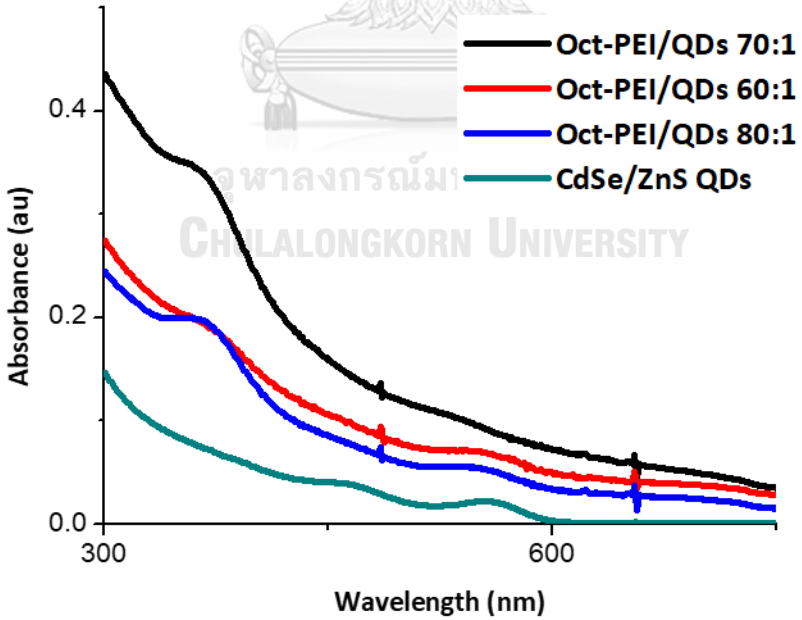

..... 82

Figure B4 Absorption spectra of CdSe/ZnS core/shell QDs (green line) compared with the Oct-PEI/QDs in different molar ratio of 60:1 (red line), 70:1 (black line), and 80:1 (blue line). 82

Figure C1 Fluorescent spectra of 0.1 μM of the cationic QDs before interacted with 1 μM of DNA and NR-PNA (dark yellow line), after interacted for 0 minute (pink line), 1 minute (green line), 3 minutes (blue line), 5 minutes (red line), and 10 minutes (black line). The excitation wavelength was 350 nm with 700 PMT applied voltage. 84

Figure C2 Fluorescent spectra of 0.1 μM of the cationic QDs before interacted with 1 μM of NR-PNA (dark yellow line), after interacted for 0 minute (pink line), 1 minute (green line), 3 minutes (blue line), 5 minutes (red line), and 10 minutes (black line). The excitation wavelength was 350 nm with 700 PMT applied voltage. 85

LIST OF TABLES

Table 3.1 List of instrument 28

Table 3.2 List of chemical 29

Table 4.1 Elemental analysis of CdSe core QDs and CdSe/ZnS core/shell QDs. 46

Table 4.2 Physical properties and dissolved solvents in each percentage of acylation. 50

Table 4.3 Results from Zetasizer of QDs in different ratio of Oct-PEI/QDs 59

Table A4 Parameters of the linear regression of Rhodamine 6G emission 77

Table A5 Parameters of the linear regression of CdSe core QDs emission 78

Table A6 Parameters of the linear regression of CdSe/ZnS core/shell QDs emission 79

LIST OF SCHEMES

Scheme 1 Schematic diagram of synthesis of CdSe/ZnS core/shell QDs [30]..... 30

Scheme 2 Schematic diagram of QDs surface modification via micelle formation..... 34

LIST OF ABBREVIATIONS

HDA	=	hexadecylamine
HDDO	=	hexadecane diol
NPs	=	nanoparticles
Oct-PEI	=	partial acylated poly(ethylene)imine
Oct-PEI/QDs	=	quantum dots coated surface by Oct-PEI
PEI	=	poly(ethylene)imine
QDs	=	quantum dots
TOP	=	trioctylphosphine
TOPO	=	trioctylphosphine oxide
TOPS	=	trioctylphosphine sulfide
TOPSe	=	trioctylphosphine selenide
cm	=	centimeter
g	=	gram
h	=	hour
mL	=	milliliter
min	=	minute
μM	=	micromolar
nm	=	nanometer

CHAPTER I
INTRODUCTION

1.1 Statement of the problem

Colloidal semiconductor nanoparticles or quantum dots (QDs) are inorganic nanoparticles with the sizes of about 2-10 nm. They are widely used as sensors due to their unique optical properties such as broad excitation wavelength and photostable. Besides, their size and band gap are inversely related, resulting in the tunability of their emissions. To apply the QDs in bio-applications, the water-soluble and biocompatible QDs are required.

In a typical synthesis method, the surface of QDs are organic molecules such as Tri-octylphosphine (TOP), Tri-octylphosphine oxide (TOPO), Hexadecylamine (HDA) and Hexadecane diol (HDDO), which exhibited hydrophobic properties. For using the synthesized QDs in bio-applications, their surfaces are needed to be modified to become hydrophilic by coating with hydrophilic molecules or polymers. Ligand exchange and micelle formation are the two common surface modification processes. In this research, the micelle formation is used for the modification process because it can maintain the optical properties of the original QDs comparing to the modified QDs obtained from ligand exchange. The hydrophilic molecules or polymers that are mostly used are neutral or anionic types because there are more stable and less cytotoxic when compared with cationic type. However, in some specific bio-application such as DNA detection, the cationic surface nanoparticles might be helpful. The cationic polymer that becomes of our interest is poly(ethylene)imine (PEI) because of its proton sponge effect. However, there are still some limitation in using PEI since high molecular weight PEI exhibits high cytotoxicity. Therefore, in this research, low molecular weight PEI is used and long-chain amine is partially modified onto the PEI by EDC/NHS coupling for increasing the hydrophobicity and forming the micelle onto the surface of QDs.

To demonstrate the applications of the cationic QDs in biological systems, DNA detection has been studied. The DNA detection is the technique that can be used for

diagnosing genetic diseases and can be very useful in biological studies. Due to their specific base pair interactions, which are Adenine (A), Thymine (T), Cytosine (C) and Guanine (G), in the DNA sequence make the detection becomes effective. There are many researches that have reported the combination of the DNA detection and optical QDs. In this research, the anionic phosphate in DNA sequence is proposed to interact with the cationic surface of QDs via ionic interaction. Moreover, the specificity of the detection is proposed to be from Peptide-nucleic acid (PNA) that can be matched only with the targeted DNA.

1.2 Objectives of this thesis

1.2.1 To synthesize water-dispersible cationic CdSe/ZnS core/shell quantum dots using surface modification with acylated-poly(ethylene) imine (Oct-PEI) via micelle formation.

1.2.2 To investigate the optical properties and cytotoxicity of the cationic QDs.

1.2.3 To apply the synthesized cationic QDs in combination of peptide nucleic acid (PNA) in DNA detection.

1.3 Scope of this thesis

First of all, we synthesize of core/shell quantum dots of CdSe/ZnS via hot injection method and characterize by UV-visible absorption, fluorescence emission spectroscopy and transmission electron microscopy. Then, the surface of the synthesized QDs are coated with partially acylated PEI via micelle formation to produce the cationic QDs, and the zeta-potentials are measured using zeta-sizer analysis. The cationic QDs in combination with PNA are applied in the DNA detection and are investigated by fluorescence spectroscopy. Moreover, the optical properties and stability of the cationic QDs prepared via micelle formation are compared with the cationic QDs prepared via ligand exchange.

1.4 The benefits of this thesis

The expected benefits from this research are that the cationic QDs prepared via micelle formation can be dispersed in aqueous solution and also maintain the optical properties of the original QDs. The resulted QDs are useful tools in the development of fluorescent sensors in various biological studies.

CHAPTER II

THEORIES AND LITERATURE REVIEWS

2.1 Nanomaterials

Nanomaterials are wide classes of materials that have at least one dimension falling less than 100 nm. They can be classified into different classes based on their properties, shapes or sizes. Based on the shape, nanomaterials can be zero dimension (0D), one dimension (1D), two dimension (2D) or even three dimension (3D) [1]. The zero-dimensional (0D) nanomaterials have all the dimensions of not larger than 100 nm e.g. nanoparticles. The one-dimensional (1D) nanomaterials have one dimension outside the nanoscale e.g. nanotubes, nanorods, and nanowires. The two-dimensional (2D) nanomaterials have two dimensions outside the nanoscale e.g. graphene, nanofilms, and nanolayers. The three-dimensional (3D) nanomaterials are the ones without any dimension confined in the nanoscale e.g. dispersions of nanoparticles, bundles of nanowires, and nanotubes as well as multi-nanolayers. Images of examples of nanomaterials were shown in Figure 2.1 [2].

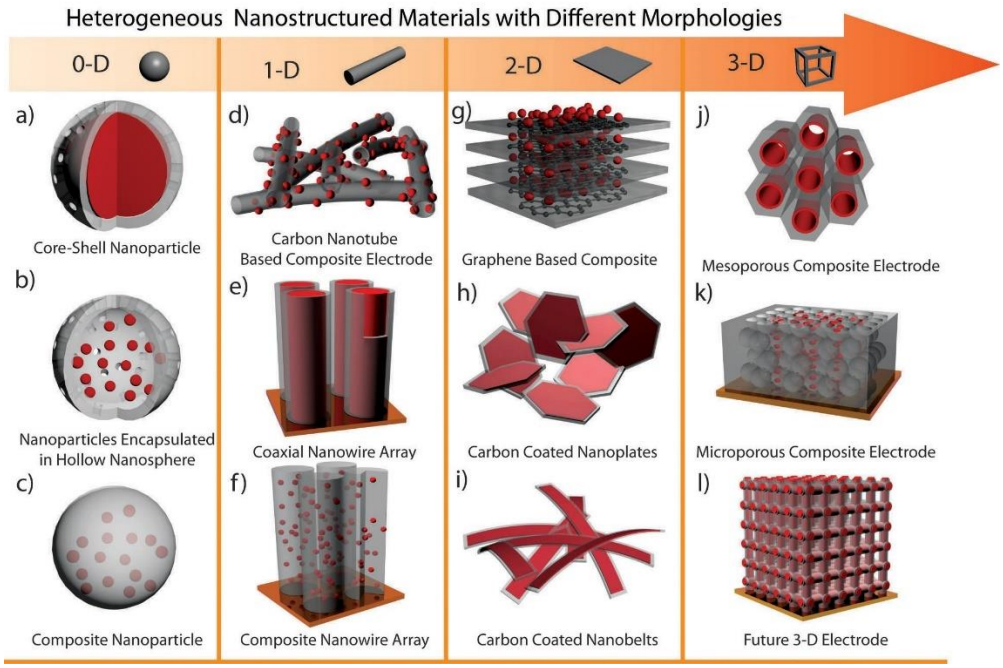

Figure 2.1 Examples of nanomaterials in different morphologies [2].

The nanomaterials are of great scientific interest as they are effectively a bridge between bulk materials and atomic or molecular structures. Due to their small sizes, greater surface area per weight than larger particles make electrons movement confined leading unique properties, which are different from bulk materials that have constant physical properties [3]. Their unique properties such as electrical, magnetic and optical properties show a wide variety potential applications in biomedical, optical, electronic fields, etc. Examples of nanomaterials that are widely used in applications include metallic nanoparticles, magnetic nanoparticles, carbon nanoparticles, and semiconductor nanoparticles.

2.1.1 Metallic nanoparticles

Metallic nanoparticles are nanosized metals with dimensions (length, width or thickness) within the size range of 1-100 nm. They have various properties such as plasmon excitation, quantum confinement, and large surface energies [4]. The metallic nanoparticles, especially gold (Au), silver (Ag), and copper (Cu), have been applied in many fields due to their colloidal stability and less cytotoxicity.

2.1.1.1 Gold nanoparticles (AuNPs)

Gold nanoparticles (AuNPs) are colloidal suspension of nanoparticles of gold. The colloid is usually either an intense red colour or blue/purple colour depending on their sizes. They are the subject of abundant research due to their optical and electronic properties with many potential applications including diagnostic and biomedical applications. For example, Kyung-Mi Song, *et al*. (2011) used AuNPs-based colorimetric method to confirm the binding affinity and interacting region of the ssDNA aptamer for kanamycin as shown in Figure 2.2 [5].

Figure 2.2 Color of the AuNP solution with different concentration of kanamycin [5].

2.1.1.2 Silver nanoparticles (AgNPs)

Silver nanoparticles (AgNPs) are colloidal suspension of nanoparticles of silver. They have been used for a long time and have been registered as a biocidal material in the United States since 1954 as called “colloidal silver”. They are often combined with other substances to develop combined functionalities for using in many fields [6]. Recent years, Sangiliyandi Gurunathan, *et al*. (2015) applied AgNPs in apoptotic potential for targeting MDA-MB-23I human breast cancer cells. Size and surface morphology of the AgNPs were as shown in Figure 2.3 [7].

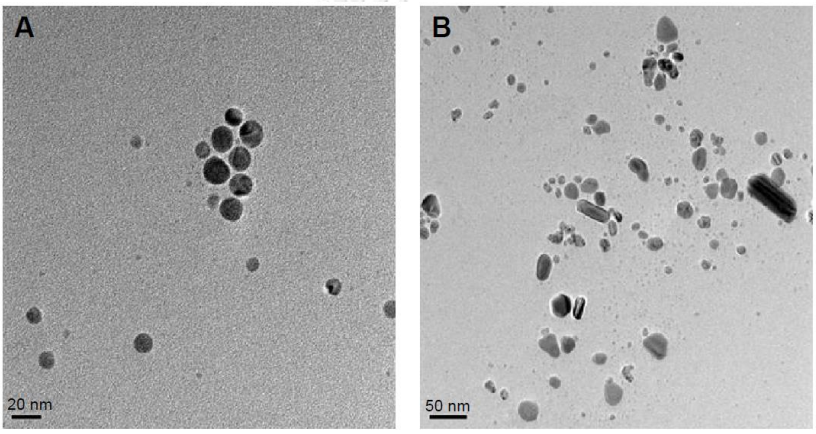

Figure 2.3 TEM images of different synthesis method of AgNPs which A) milky mushroom extraction and B) culture supernatant of bacteria [7].

2.1.1.3 Copper nanoparticles (CuNPs)

Copper nanoparticles (CuNPs) are normally 1 to 100 nm in size. They can be formed by natural processes or through chemical synthesis. They have been attractive due to their novel electronic, mechanical properties, catalytic, and biological applications [8, 9]. For example, Kondaiah Seku, *et al*. (2018) synthesized CuNPs by hydrothermal processes which were spherical in shape as shown in Figure 2.4 [9]. These synthesized CuNPs were also exhibited good antibacterial and antifungal activity against pathogenic strains.

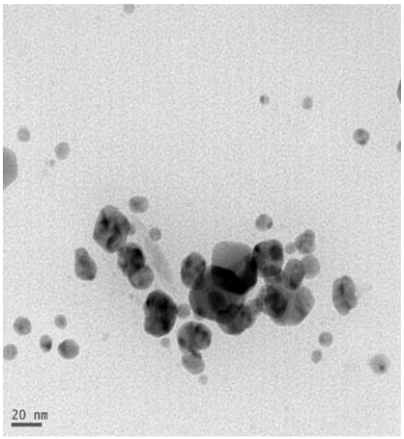

Figure 2.4 TEM image of synthesized copper nanoparticles [9].

2.1.2 Magnetic nanoparticles (FeNPs)

Magnetic nanoparticles (FeNPs) are a class of nanoparticles that can be operated using magnetic fields. They commonly consist of two components, which are a magnetic material such as iron, and a chemical functionalized. The Fe-based NPs, especially iron oxide particles such as magnetite (Fe_3O_4) are of interest in biomedical applications due to their biocompatibility and superparamagnetic behavior that do not retain any magnetism after removal of the magnetic field [10]. For example, Chutimon Sanjai, *et al.* (2014) encapsulated super-paramagnetic iron oxide nanoparticles (SPIONPs) with chitosan-triphosphate nanoparticles for using in MRI technique as an MRI contrast agent [11]. Images of the synthesized SPIONPs are as shown in Figure 2.5.

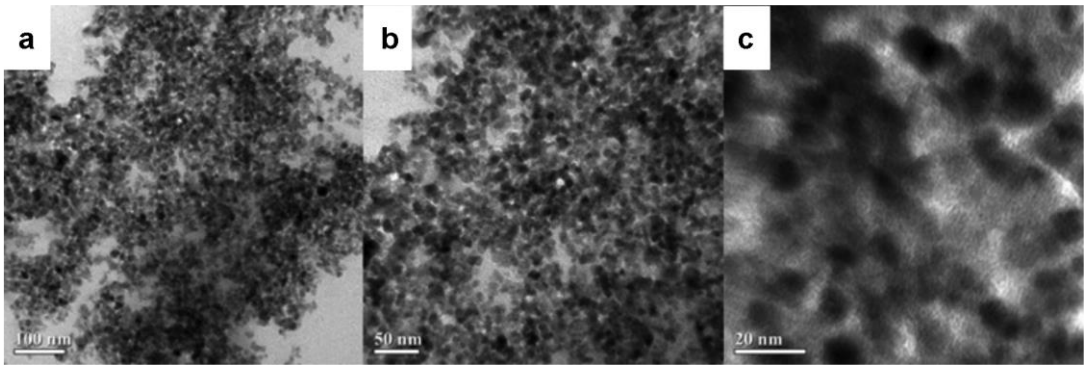

Figure 2.5 TEM images of SPIONPs encapsulated with chitosan nanoparticles in scale bar of a) 100 nm, b) 50 nm and c) 20 nm [11].

2.1.3 Carbon nanoparticles (CNPs)

Carbon nanoparticles are nanosized carbon elements of which at least one dimension is less than 100 nm. They can be created by various method such as carbonization, heating and activation [12]. From their small sizes and low cytotoxicity along with fluorescence make them become of a great interest in delivering medicine and cellular imaging [13]. For example, Hui Ding, *et al.* (2016), synthesized carbon dots (CDs) using one-pot synthesis to obtain full-color light-emitting CDs and applied the synthesized CDs in cellular imaging as shown in Figure 2.6 [14].

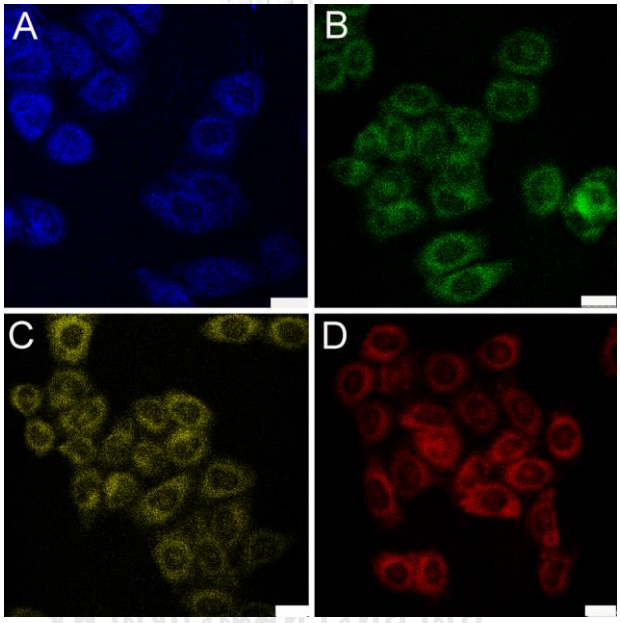

Figure 2.6 Confocal fluorescence images of HeLa cells which the emissions were recorded in different ranges: A) 420-510 nm, B) 490-560 nm, C) 540-590 nm, and D) 590-750 nm [14].

The use of nanoparticles in fluorescence-based sensing has received much attention due to many benefits such as excellent sensitivity, short response time, and low cost. However, for the previously described nanomaterials, there are still some limitation about luminescent life-time and narrow excitation wavelength. In the next topic, we discuss about another type of nanoparticles which could resolve the limitation in fluorescent imaging.

2.1.4 Semiconductor nanoparticles

Materials are classified into three types by their electrical conductivity; conductors, semiconductors, and insulators. As shown in Figure 2.7 [15], in a conductor, conduction band and valence band are overlapped, or the valence band is not filled. For an insulator, band gap between the conduction band and the valence band is large, so the electron from the valence band cannot be excited by thermal energy to the conduction band resulting in no conductivity. For semiconductors, the band gaps are smaller than insulators, and at room temperature, there is enough thermal energy accessible to displace a few electrons from the valence band into the conduction band. As temperature increases, the conductivity of a semiconductor material increases.

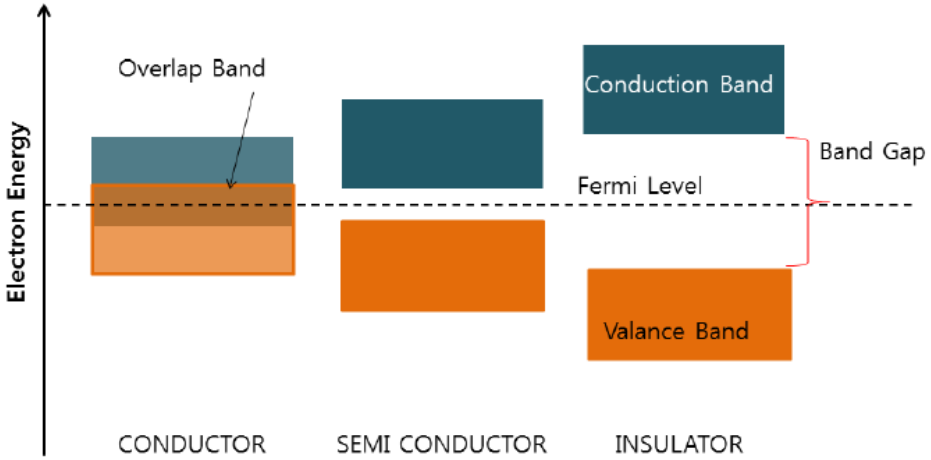

Figure 2.7 The band gap diagram of a conductor, semiconductor and an insulator [15].

In bulk materials, electronic properties semiconductors follow the band structure, when reducing the size into nanoscale, their electronic structures differ from bulk materials, and also show strong luminescence properties [16]. The semiconductor nanoparticles conventionally called quantum dots (QDs)

2.1.4.1 Semiconductor nanocrystal Quantum Dots (QDs)

Quantum Dots (QDs) are semiconductor nanoparticles in sizes of about 2-10 nm consisting of only a few to some hundred atoms which are often

referred to as clusters. Their specific properties are sizes and band gaps energy which inversely related resulting in a tunability of emission. Moreover, with their unique optical properties such as broad excitation and narrow emission spectrum, colloidal and photo-stability make them potentially useful for applications in biological imaging, labeling and sensors. For example, Peng Liu, *et al*. (2009), synthesized CdSe QDs in aqueous medium with L-cysteine as a capping agent for labeling the Escherchia coli (*E. coli*) cells as shown in Figure 2.8 [17]. From the results, the synthesized QDs can be used to label the *E.coli* cells and become useful for biological studies.

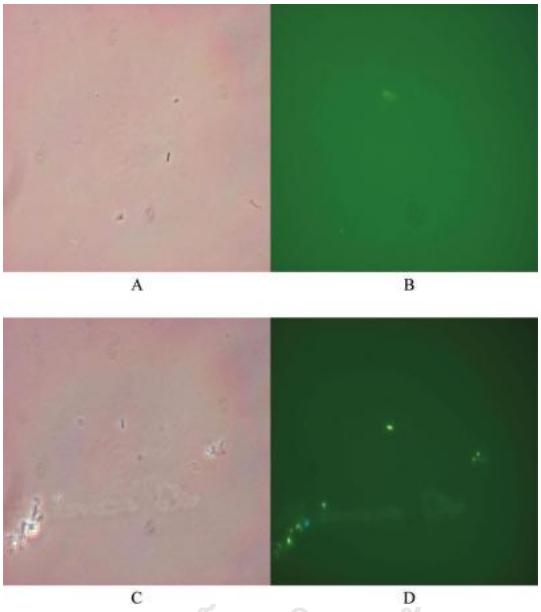

Figure 2.8 Fluorescence images of *E. coli* having been mixed with QDs/L-cysteine obtained by changing visible (A,C) and UV light (B,D) [17].

One type of QDs that become widely used is CdSe QDs due to their colloidal and photo-stability. From the research of Dmitri V. Talapin, *et al*. (2002), it was observed that the photoluminescence efficiencies between both organometallically prepared CdSe and InAs colloids and CdTe nanocrystals synthesized in aqueous medium exhibited the efficiencies relating to size-selected fractions of particle growth [18]. Only organometallically prepared CdSe colloids have the most perfect surface and show the highest efficiency in photoluminescence. The result in Figure 2.9 was also confirmed the photo-stability and narrow size distribution of CdSe.

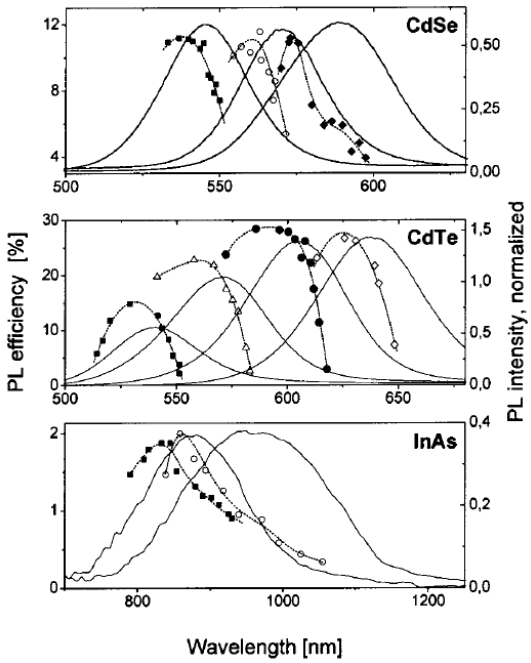

Figure 2.9 Solid lines: PL spectra of crude solutions of CdSe, CdTe, and InAs nanocrystals measured at different stages of particle growth. Points: PL quantum efficiency vs position of the PL maximum of size-selected fractions isolated from each crude solution [18].

Another research about CdSe QDs is reported by Petero Kwizera, *et al*. (2012), that synthesized CdSe QDs by modified the technique of kinetic synthesis which is a safer and simpler method [19]. The result in Figure 2.10 shows the green-yellow to red color of CdSe QDs that are attributed to the increasing size of the QDs indicating the wide range of emission of this QD type.

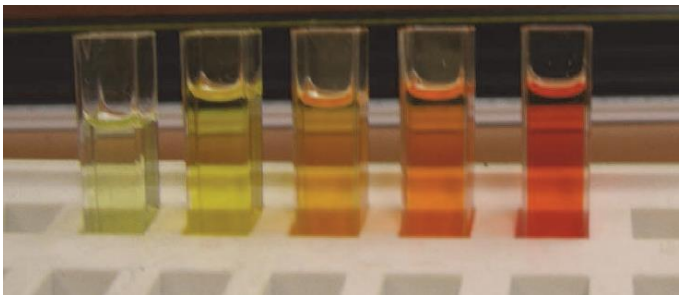

Figure 2.10 Colloidal suspensions of CdSe QDs [19].

In previous research [18], CdSe QDs exhibited a broad band emission related to the surface defects. These surface defects can be reduced by other semiconductor materials such as ZnS, forming core-shell structures [20]. For example, Margaret A. Hines, *et al*. (1996) capped CdSe QDs with ZnS by a two-step single-flask method for enhancing the luminescence properties [21]. From fluorescence result as shown in Figure 2.11 and TEM image as shown in Figure 2.12, the CdSe capped with ZnS could enhance the luminescence properties while the core size remained constant.

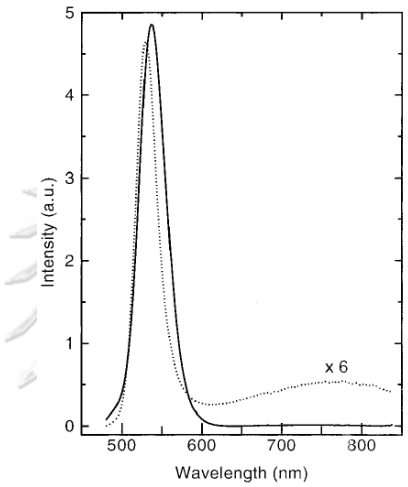

Figure 2.11 Fluorescence of the CdSe/TOPO (dotted line) and CdSe/ZnS (solid line) nanocrystals normalized by their absorption at the excitation wavelength of 470 nm [21].

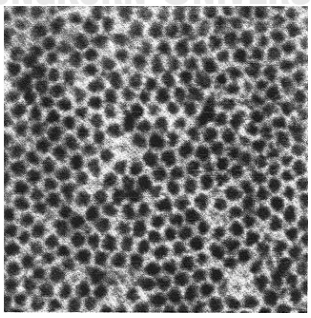

Figure 2.12 TEM image of CdSe/ZnS nanocrystals [21].

For example of using ZnS capped CdSe in core-shell structure, M. Mehrjoo, *et al*. (2017), synthesized CdSe/ZnS core-shell QDs by using a combination of microwave

and photochemical approaches [22]. The schematic diagram of synthesis is as shown in Figure 2.13. The synthesized CdSe/ZnS QDs showed the strong photocatalytic activity to the photo-degradation of methyl orange. The photocatalytic activity of the synthesized QDs were also stronger than CdSe QDs as shown in Figure 2.14.

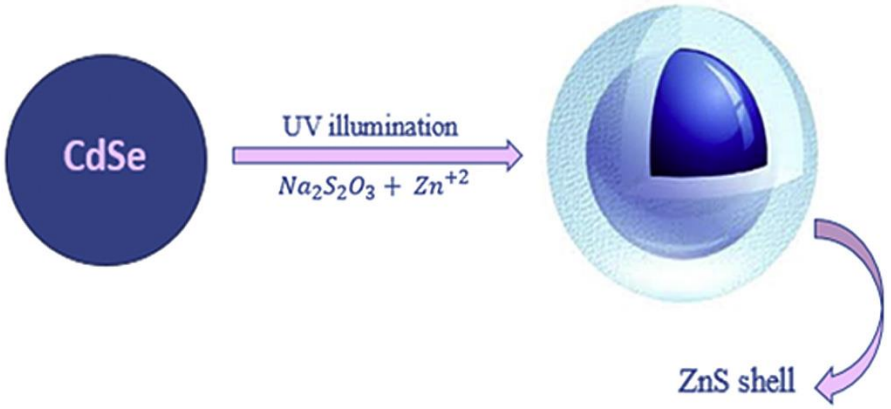

Figure 2.13 Schematic diagram of the synthesis of CdSe/ZnS QDs process [22].

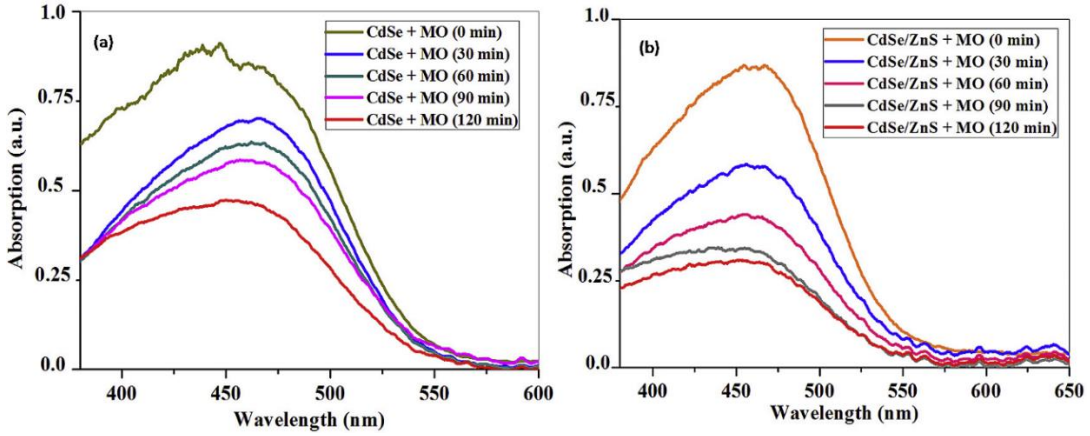

Figure 2.14 Absorption spectra demonstrating the photocatalytic degradation of methyl orange by CdSe (a) and CdSe/ZnS core/shell QDs (b) [22].

Another example research about using CdSe/ZnS was reported by S. Mathew, *et al*. (2015). CdSe/ZnS core-shell QDs were synthesized via micro-emulsion technique and the thickness of ZnS-shell were varied [23]. From TEM images in Figure 2.15 comparing between CdSe core QDs (C0), and CdSe/ZnS QDs (C1, C2 and C3), it was shown that the thicker of ZnS shell, the bigger of particles sizes. Moreover,

fluorescence spectra in Figure 2.16 showed that the thickest of ZnS shell provided the highest fluorescence intensity.

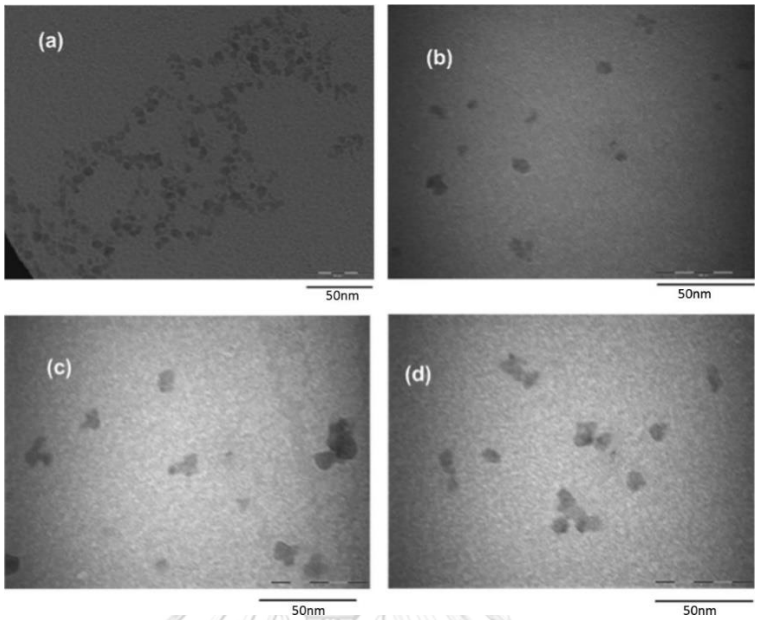

Figure 2.15 TEM images of the CdSe QDs a), and CdSe/ZnS core-shell QDs with different shell thickness b), c) and d) [23].

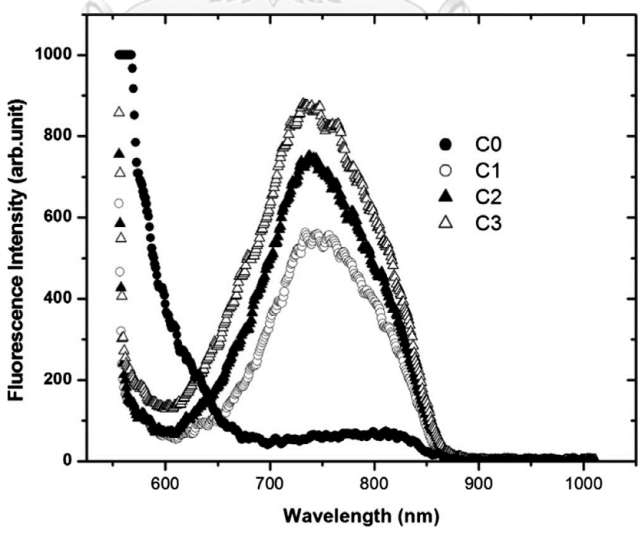

Figure 2.16 Fluorescence spectra of the CdSe/ZnS core-shell QDs (C0, C1, C2, C3) under the excitation of 532 nm in which 0, 1, 2 and 3 referred to the thickness of shell layer [23].

From literature reviews comparing CdSe core QDs and CdSe/ZnS core-shell QDs, in this research we are interested in using CdSe/ZnS core-shell QDs due to their unique optical properties i.e. wide range of excitation wavelength and tunability of emission, photo-stability, and colloidal stability.

2.1.4.2 Quantum dots (QDs) synthesis techniques

There are several routes that have been used to synthesize QDs. All routes were generally aiming at controlling the sizes and shapes, homogeneity of the sizes, and surface coating of the QDs. The processes are classified into a top-down and bottom-up approach [24].

2.1.4.2.1 Top-Down Synthesis Processes

In this process, a bulk semiconductor is thinned to form the QDs. The diameter of the QDs resulting from electron beam lithography, reactive-ion etching and/or wet chemical etching is about 30 nm. The main disadvantages of these processes are the impurities of the resulted QDs and structural imperfections. Therefore, another process, bottom-up approach, become widely used instead of the top-down process.

2.1.4.2.2 Bottom-Up Approach

This approach can be divided into two methods which are wet-chemical methods including sol-gel, micro-emulsion, competitive reaction chemistry, hot-solution decomposition, and electrochemistry, and vapor-phase methods including molecular beam epitaxy (MBE), sputtering, liquid metal ion sources, and aggregation of gaseous monomers.

2.1.4.2.2.1 Wet-Chemical Methods

The main concept of this method is to follow the conventional precipitation methods with careful control of parameters for a single or mixture solutions. The precipitation process compromises both nucleation, which can be homogeneous, heterogeneous or secondary nucleation, and control of the growth of nanoparticles [25]. The homogeneous nucleation occurs when dissolved atoms or

molecules combine and reached a critical size without the assistance of a pre-existing solid interface. The focus-sized QDs can be synthesized by varying factors; i.e., temperature, electrostatic double layer thickness, stabilizers or micelle formation, concentrations of precursors, ratios of anionic to cationic species and solvent.

1) Sol-gel Process

Typically, the main steps in this process are hydrolysis and condensation of metal precursor in acidic or basic medium resulting in sol formation, and followed with polymerization to form a network resulting in gel. This method is occasionally used due to a broad size distribution and a high concentration of defects [26].

2) Micro-emulsion Process

The process includes normal micro-emulsions and reverse micro-emulsions which are oil-in-water and water-in-oil, respectively. The reverse micelle process occurs when two immiscible liquids (polar water and nonpolar alkanes) are mixed and stirred to form the emulsion. In some cases, the polar solvents such as alcohol, may be used instead of water, but there are some disadvantages, which are low yield, and impurities and defects of resulted QDs.

3) Hot-Solution Decomposition Process

This process is a well-known process for the synthesis of QDs by the pyrolysis of organometallic compound at high temperature (~300 °C). A standard procedure involves first degassing and drying of a coordinating solvent which is organometallic compound under vacuum. A mixture of Cd-precursor and selenium precursors, such as tri-*n*-octyl-phosphine (TOP) selenide, is prepared and injected with vigorous stirring into a flask at high temperature. The simultaneous injection of precursors into the flask along with coordinating solvent induces the formation of QDs in homogeneous nucleation. The size of resulted QDs is controlled by the reaction time and temperature. This process has been vastly used in the syntheses of II-VI, IV-VI and III-V QDs. Process parameters and precursors, solvents and coordinating agents, and the purity of the coordinating solvent are the factors that control the size, shape

and overall reaction. An advantage of this synthesis method is the sufficient thermal energy could anneal the defects, resulting in monodispersed QDs. Due to the particles growth rate is relatively slow and the temperature can be modulated, a series of QDs sizes can be prepared from the same precursor bath.

4) Other synthesis processes

Sonic waves or microwaves have been used for synthesis of tiny-sized QDs (1-5 nm) [27]. These waves provide energy to dissociate the precursor and water molecules, resulting in the growth of QDs. Another method that has been used to synthesize QDs is hydrothermal synthesis or similar synthesis process that crystallized inorganic salts from aqueous solution. Crystals from this method can be controlled by pressure and temperature [28].

2.1.4.2.2.2 Vapor-Phase Methods

In this method, QDs occur on a substrate without any patterning due to their self-assembly leading to a growth in an atom-by-atom process [29]. Although, self-assembling of QDs using this method is effective in synthesis of QDs arrays without template, but vacillation in size of QDs often results in inhomogeneous optoelectronic properties.

From the advantages and disadvantages in each synthesis methods; however, the suitable method for synthesis of CdSe/ZnS core-shell QDs is still be the hot-solution decomposition process due to the ability of obtaining a series of QDs sizes preparation and monodispersed QDs. For example, C. B. Murray, *et al*. (1993) synthesized Cd-based QDs, including CdSe, CdS and CdTe, through a hot-solution decomposition process by using tri-*n*-octylphosphine (TOP) and tri-*n*-octylphosphine oxide (TOPO) as organometallic reagents [30]. From their research, it was found that the average size and the size distribution of crystallites in a sample depended on the growth temperature while using TOP/TOPO as solvent coordinating the surface of the crystallites permitted slow steady growth at temperature above 280°C. Figure 2.17 showed the sharp absorption and narrow emission spectrum that indicated the highly

monodisperse and growth of crystallites with few electronic defect sites of the synthesized CdSe.

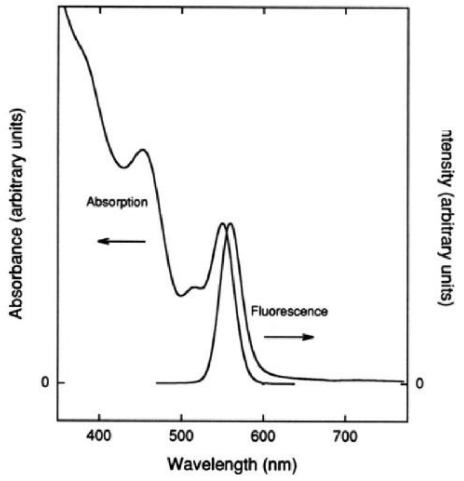

Figure 2.17 Typical room temperature band edge luminescence and absorption spectra for 3.5 nm diameter CdSe crystallites [30].

Another research about synthesis of CdSe/ZnS QDs via a hot-solution decomposition process is reported by Dmitri V. Talapin, *et al*. (2001) of the syntheses of CdSe nanocrystals in a hexadecylamine (HDA), TOPO and TOP mixture [31]. From the result in Figure 2.18, the synthesized CdSe nanocrystals in the system of TOPO-TOP as stabilizing shell cooperated with alkylamine exhibited a high reaction yields and PL quantum efficiency of 50-60%.

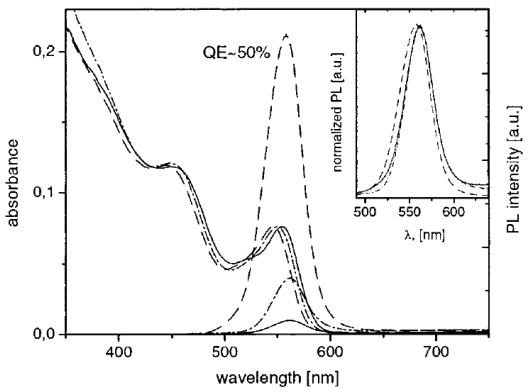

Figure 2.18 Absorption and emission spectra of TOPO-capped CdSe nanocrystals at room-temperature before (solid lines) and after (dashed lines) surface exchange with allylamine. The inset shows normalized PL spectra [31].

According to reviews about the synthesis of efficient QDs via a hot-solution decomposition process and using TOPO, TOP and alkylamine as stabilizing ligands, in this research, we synthesized CdSe/ZnS QDs through a hot-solution decomposition process and use the ligands as described above.

2.2 Surface modification of QDs

Based on the hot-injection synthesis process, the synthesized QDs are hydrophobic. For the use in bio-applications e.g. biosensors, the hydrophilic QDs are required. Therefore, the surface of QDs need to modify to become hydrophilic. Normally, there are 2 routes for the surface modification, which are ligand exchange and micelle formation.

2.2.1 Ligand exchange

Ligand exchange is the process that the desired molecule substitutes the original surface molecules to provide the required properties. The most common substituent is mercapto- or thiol groups. For example, Jeremiah A. Kloepfer, *et al*. (2005) exchanged the TOPO surface ligand with mercaptoacetic acid (MAA) to generate the water-soluble CdSe QDs as shown in Figure 2.19 and exchanged with dihydrolipoic acid (DHLA) for CdSe/ZnS QDs [32]. The CdSe-MAA QDs could be dissolved in H_2O and the CdSe/ZnS-DHLA could be dissolved in PBS buffer with a minimal quenching.

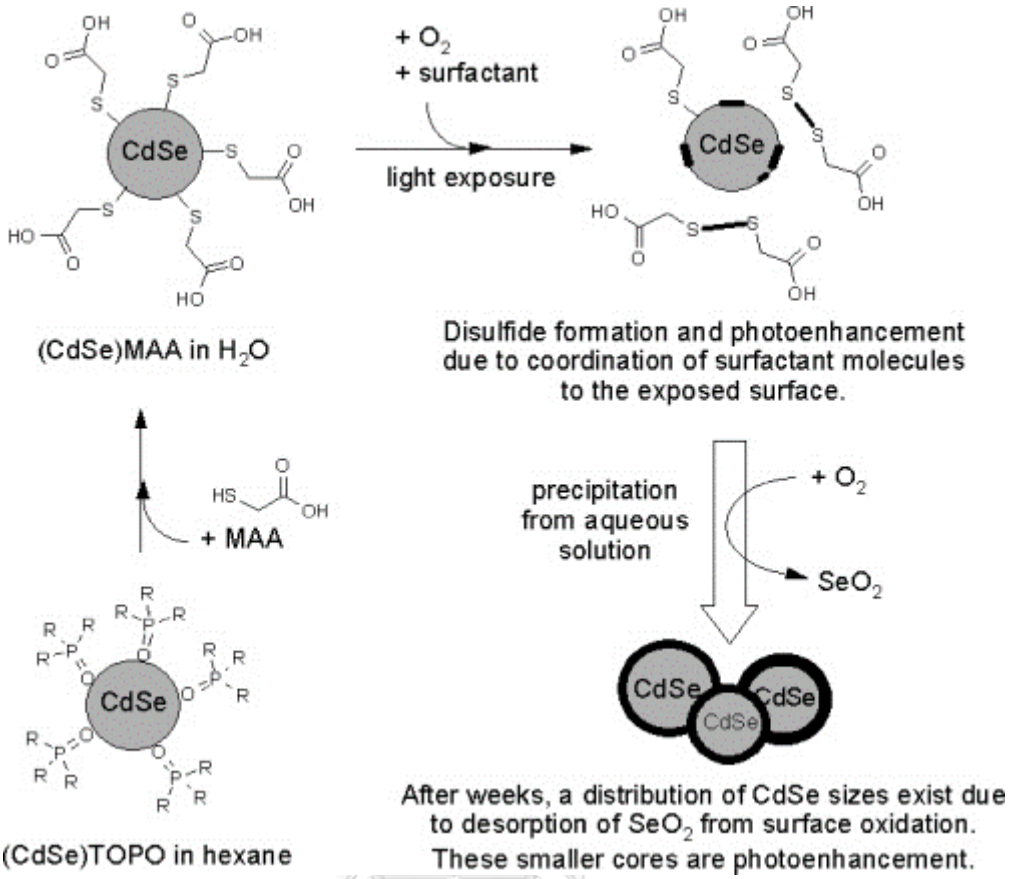

Figure 2.19 Schematic of some of the applicable CdSe quantum dot structures [32].

Another research about ligand exchange process is by Jose Aldana, *et al*. (2001). They studied about the instability of CdSe nanoparticles coated with hydrophilic thiols via ligand exchange [33]. The result showed that the coated 11-mercaptoundecanoic acid (MUA) induced the photooxidation occurring onto the QDs surface that effected the size of nanocrystals and induced a decrease of absorption peak as shown in Figure 2.20.

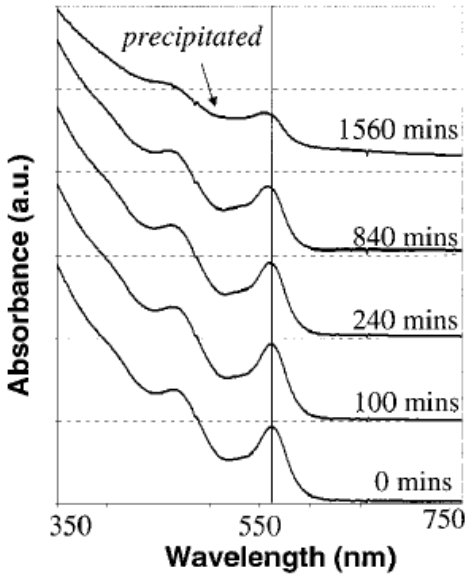

Figure 2.20 Temporal evolution of the absorption spectra of MUA-coated CdSe nanocrystals in water under the photooxidation conditions. The time progression follows the photooxidation of the nanocrystals from the start of the experiment to the precipitation of nanocrystals [33].

There are some researches that reported about the instability of nanocrystals coated surface by ligand exchange process [33]. Therefore, the surface modification via micelle formation process has been of our interest.

2.2.2 Micelle formation

Micelle formation is the process that the amphiphilic molecule forms micellar structures onto the hydrophobic nanoparticles without replacing the original surfactants to produce the hydrophilic nanoparticles. For example, Teresa Pellegrino, *et al*. (2004) coated hydrophobic CdSe/ZnS nanocrystals and other nanoparticles (i.e. $CoPt_3$, Au and Fe_2O_3) with poly(maleic anhydride alt-1-tetradecene).cross-linked bis(6-aminohexyl)amine as shown in Figure 2.21 [34]. The coated nanocrystals become water-soluble and their major physical properties were still remained in the water such as the fluorescence of CdSe/ZnS. Moreover, from TEM images in Figure 2.22 showed no large aggregates of particles, other than the formation of a monolayer.

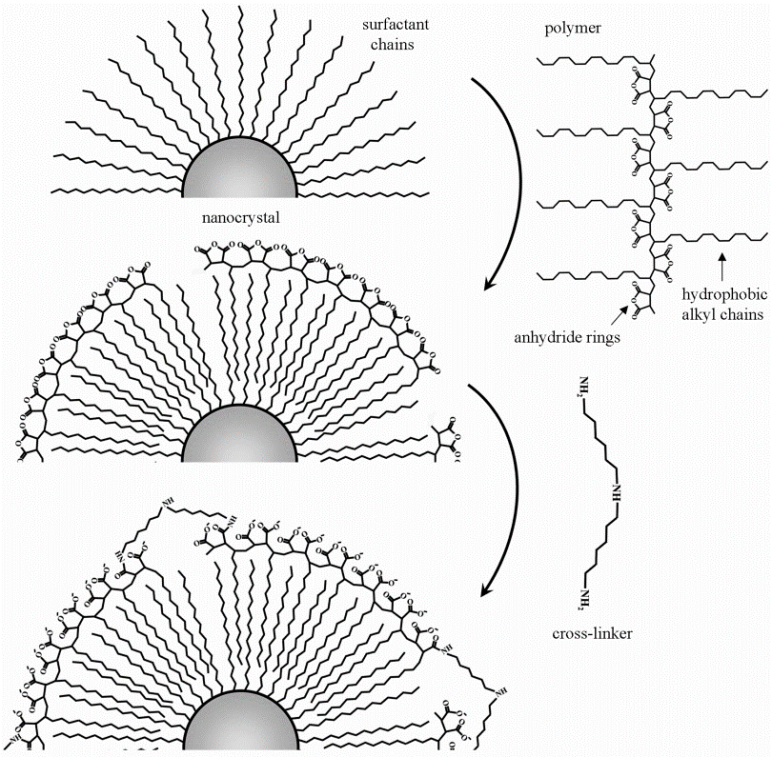

Figure 2.21 Polymer coating of the Nanocrystals [34].

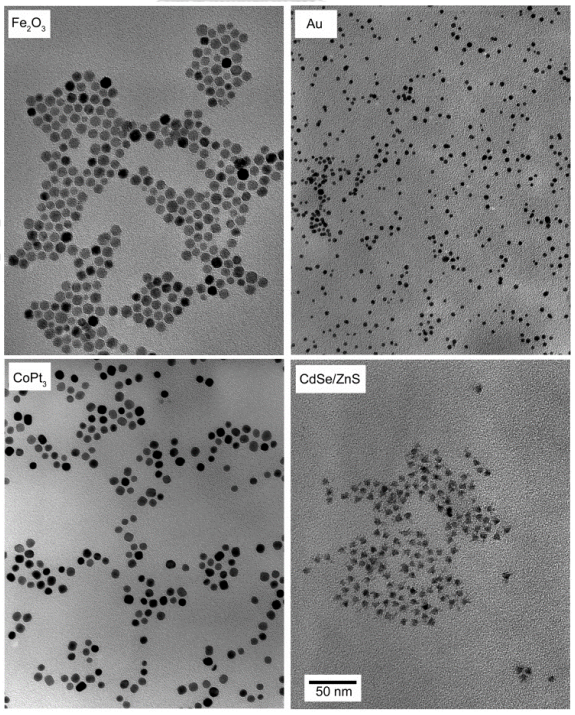

Figure 2.22 TEM images of polymer-coated with four different types of core nanomaterials [34].

Another research that modified the surface of QDs via micelle formation is reported by Yingchuan Chen, *et al*. (2008). The surface of CdSe/ZnS NPs were coated with polyacrylic acid 40% modified with octylamine for conjugating the QDs with dye [35]. From the results as shown in Figure 2.23, the water-soluble CdSe/ZnS emitted at 580 nm and successfully conjugated with dye (BODIPY).

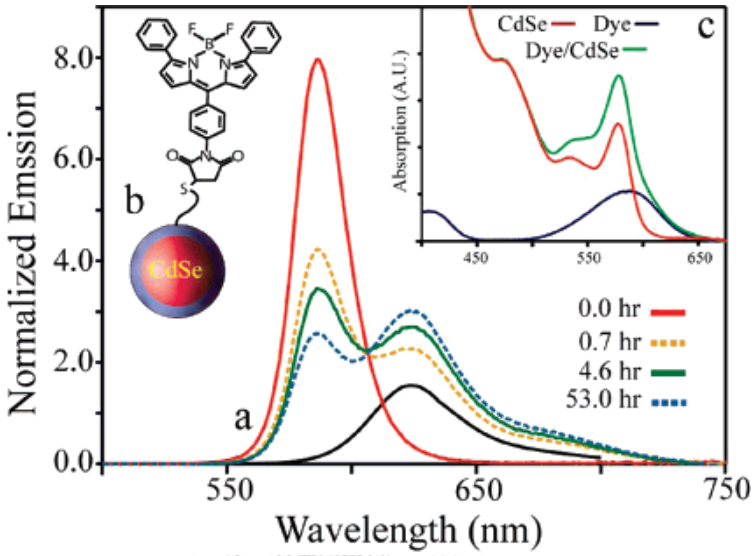

Figure 2.23 a) Emission of polymer water solubilized CdSe/ZnS NCs following the addition of dye over time. The emission from the aqueous dye/polymer complex alone is shown in black. b) Schematic of the coupled NP/dye system. c) Absorption spectra of the bare NP, the NP/dye couple, and the dye alone [35].

According to many reviews, the surface modification via micelle formation process could maintain the optical properties of QDs better than ligand exchange process. The common amphiphilic molecules that were used for coating the nanoparticles are anionic polymers, while their cross-linking properties could stabilize the micellar structure of the particles. In bio-applications, not only anionic surface QDs that were required but in some specific bio-applications such as DNA detection, the cationic surface QDs are also preferred. Thus, in this work we modify the surface of QDs with the cationic polymer via micelle formation process to produce the cationic water-soluble QDs.

2.3 Poly(ethylene) imine (PEI)

Poly(ethylene) imine or PEI is a cationic polymer that has been of interest in bio-applications such as DNA complexation and gene delivery, due to their sponge effect and cationic water-solubility. For example, Huayu Tian, *et al*. (2007) synthesized polyethylenimine-poly(γ-benzyl L-glutamate) copolymer (PEI-PBLG) and investigated its properties in biological studies [36]. From the results in Figure 2.24, the copolymer could be conjugated with DNA and also imaged the HeLa cells.

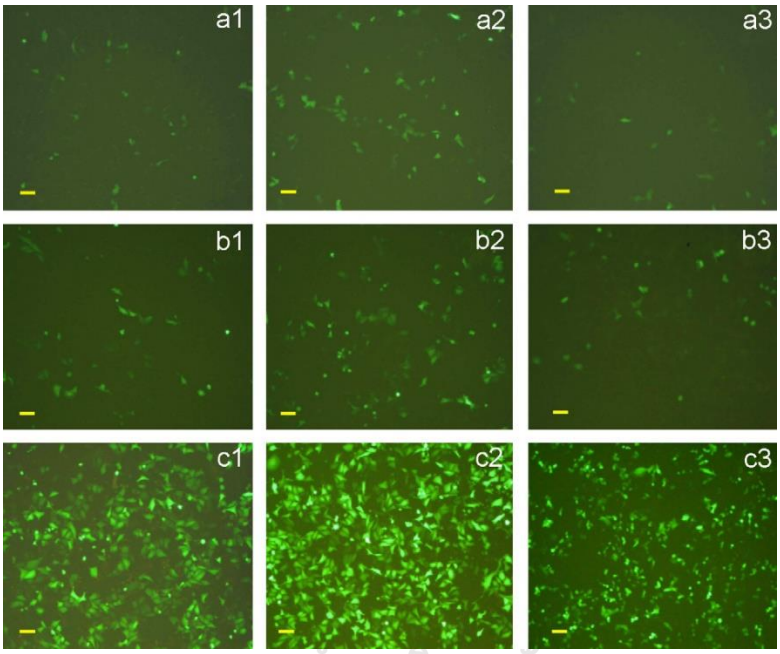

Figure 2.24 Fluorescence images of HeLa cells transfected by a) PEI-10K at different ratio with DNA, b) PEI-25K at different ratio with DNA and c) copolymer at different ratio with DNA [36].

Moreover, there are many researches studied about PEI onto nanoparticles surface. For example, Sethu Kalidhasan, *et al*. (2017) capped copper nanoparticles (CuNPs) with branched-PEI for depositing onto montmorillonite (MK10) and quartz sand, and studied the degradation of atrazine [37]. The PEI capped CuNPs are stable with no significant amount of copper leaching was found.

Another research that studied about PEI and NPs is Hayrettin Tumturk, *et al*. (2016). The branched-PEI was grafted onto the surfaces of silica nanoparticles aiming at obtaining the cationic silica nanoparticles [38]. These cationic nanoparticles were used to study the enzyme immobilization using the electrostatic interaction between positively charged surfaces of nanoparticles and negatively charged enzyme. TEM image in Figure 2.25 showed that PEI-coated silica nanoparticles have a clear spherical shape and core-shell structure, indicating that silica nanoparticles were wrapped in the PEI molecule.

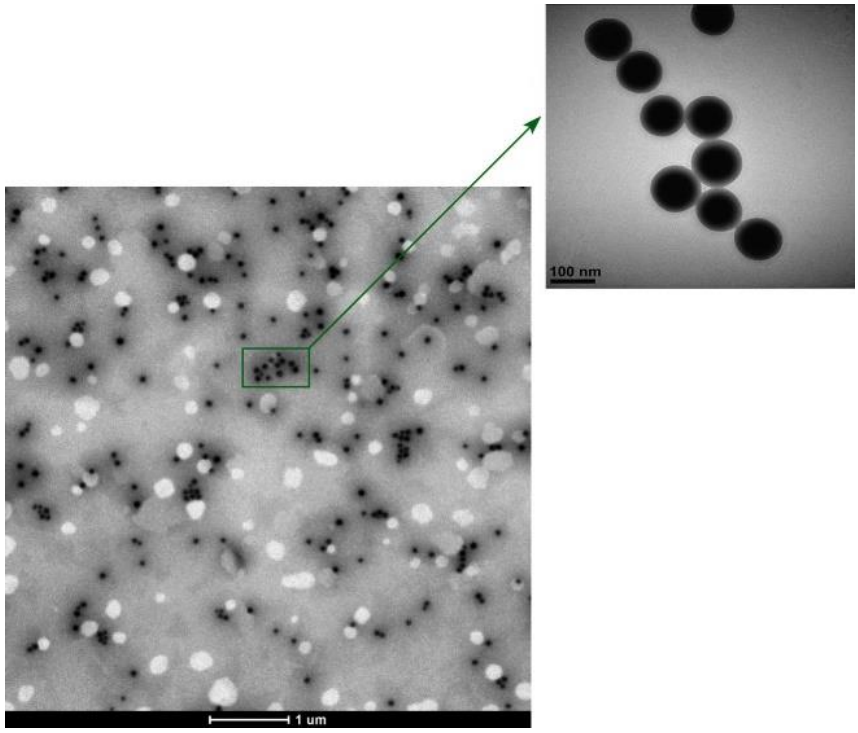

Figure 2.25 TEM images of PEI-coated onto silica nanoparticles [38].

QDs also have been reported to be cooperated with PEI. For example, Thomas Nann, *et al.* (2005) presented the new phase-transfer method of CdSe/ZnS QDs using hyperbranched PEI via ligand exchange [39]. The result in Figure 2.26 showed that the coated QDs with low molecular weight PEI (800 D) resulted in a smaller hydrodynamic diameter than the QDs using the high molecular weight PEI (25 kD). Moreover, more than 99% of the QDs were found within two peaks, indicating a very good electrostatic stabilization in water.

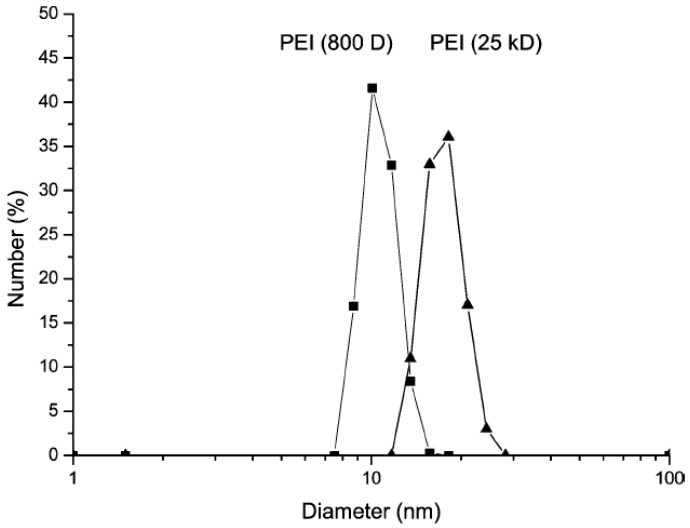

Figure 2.26 Size distribution of PEI-derivatised QDs in water, measured by light back-scattering. Squares: 800 D PEI, triangles: 25 kD PEI [39].

Another research that combined PEI and QDs is reported by Gaofeng Liang, *et al*. (2016). The surface of CdSe/ZnS QDs were capped with PEI for delivering RNA (miR-26a plasmid) into HepG2 cells and bio-imaging purposes [40]. The cationic PEI were capped onto anionic QDs via electrostatic interaction. From the results, the miR-26a-loaded QD nanocomplexes can reach the target cells, which is beneficial in biomedical applications. The schematic representations and characterizations of the nanocomplexes were shown in Figure 2.27.

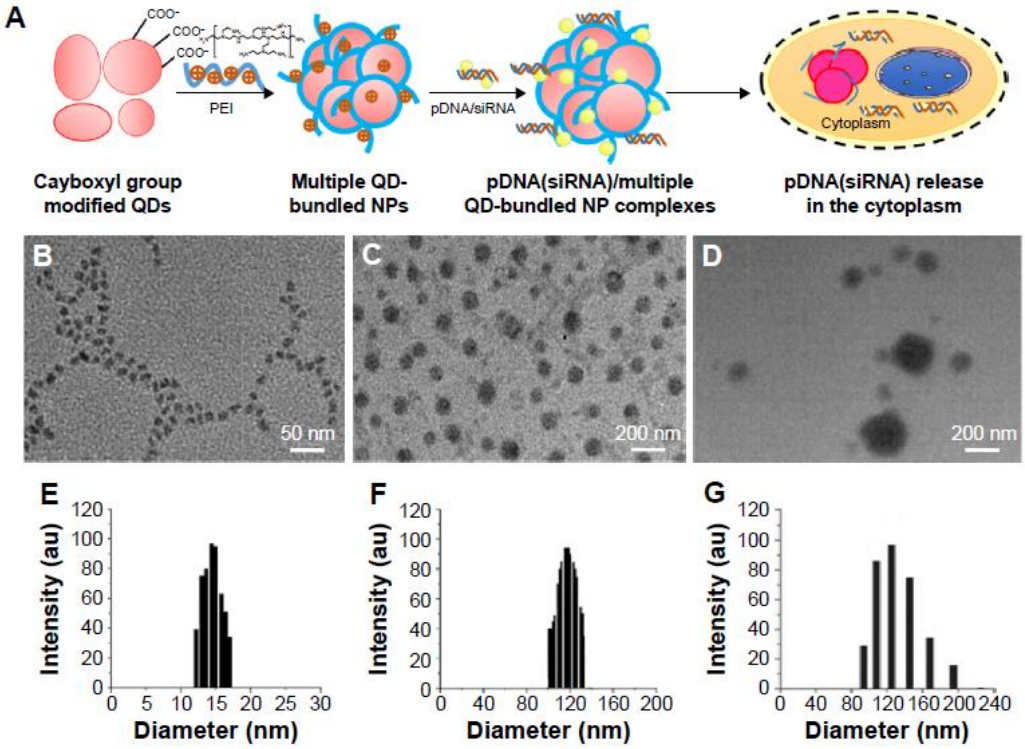

Figure 2.27 (A) Schematic representations of the preparing route for PEI/QD nanoparticles; TEM images of QDs (B), PEI/QDs (C), and PEI/QD/miRNA (D) nanoparticles. (E, F, and G) DLS data corresponding to (B, C, and D), respectively [40].

From literature reviews about coating CdSe/ZnS QDs with PEI, there are not any researches reporting the PEI coated the surface of QDs via direct micelle formation. Therefore, in this work, we are interested in coating the surface of CdSe/ZnS QDs with octanoic acid-modified branched-PEI (800 D) and applying these cationic QDs in DNA detection.

CHAPTER III

EXPERIMENTS

The experimental section is divided into three parts. First part is the synthesis of CdSe/ZnS core/shell QDs, the second part is the cationic surface modification, and the last part is the application of QDs in DNA detection.

3.1 Instruments

Table 3.1 List of instrument

Characterization techniques	Models
UV-Visible spectrophotometry	HP8453 (Agilent)
UV-Visible spectrophotometry	UV-2550 (Shimadzu)
Fluorescence spectrofluorometry	Cary Eclipse (Agilent)
X-ray diffractometry	D/MAX 2200 (Rigaku)
Transmission Electron Microscopy	Model TECNAI 20 (Philips)
Dynamic light scattering	Zetasizer Nano ZS (Malvern)
Fourier Transform Infrared Spectroscopy	Nicolet™ 6700 (Thermo Fisher Scientific)
^{1}H, ^{13}C NMR spectrometry	Bruker 400 MHz (Bruker)
Scanning Electron Microscopy	JSM-IT100 (JEOL)
Rotary evaporator	R-114 (BUCHI)
Freeze dryer	Shell Freeze System (LABCONCO)
Centrifuge	Rotofix 32A, Mikro 200/200R (Hettich)
Balance	AB204-S (Mettler Toledo)
Temperature Controller	PCD-33A (SCM premier)

Magnetic Stirrer	Hei-Tec (Heidolph), WH220-HT (Wiggens)

3.2 Chemicals

Table 3.2 List of chemical

Chemicals	**Supplier**
Ammonia solution 25%, NH_3	Merck
Cadmium acetylacetonate, $Cd(C_2H_7O_2)_2$	Sigma-Aldrich
Chloroform, $CHCl_3$	RCI Labscan
EDAC hydrochloride, $C_8H_{18}ClN_3$	Chem-Impex
Ethanol, C_2H_5OH	Merck
Glacial Acetic acid, CH_3COOH	Merck
1,2-Hexadecanediol, $CH_3(CH_2)_{13}CHOHCH_2OH$	Sigma-Aldrich
Hexadecylamine, $CH_3(CH_2)_{15}NH_2$	Sigma-Aldrich
Hexane, $CH_3(CH_2)_4CH_3$	Merck
N-hydroxysuccinimide, $C_4H_5NO_3$	Chem-Impex
2-(*N*-morpholino)ethanesulfonic acid, $C_6H_{13}NO_4S$	Sigma-Aldrich
Nitric acid 65%, HNO_3	Merck
Octanoic acid, $CH_3(CH_2)_6COOH$	Sigma-Aldrich
Polyethylenimine branched, $H(NHCH_2CH_2)_nNH_2$ (MW800)	Sigma-Aldrich
Selenium Powder, Se	Riedel-de Haen

Sodiumborohydride, $NaBH_4$	Sigma-Aldrich
Sodium dodecyl sulfate, $CH_3(CH_2)_{11}OSO_3Na$	Sigma-Aldrich
Sulfur Powder, S	Sigma-Aldrich
Trioctylamine, $(CH_3(CH_2)_7)_3N$	Sigma-Aldrich
Tri-octylphosphine, $(CH_3(CH_2)_7)_3P$	Sigma-Aldrich
Tri-octylphosphine oxide, $(CH_3(CH_2)_7)_3PO$	Sigma-Aldrich
Zinc acetate dihydrate, $Zn(CH_3COO)_2{\cdot}2H_2O$	Sigma-Aldrich

3.3 Synthesis of CdSe/ZnS core/shell QDs

CdSe/ZnS core/shell QDs were synthesized by a hot-solution decomposition process as shown in Scheme 1 using TOP as coordinating solvent, TOPO and alkylamine as stabilizing ligands for avoiding an aggregation of nanoparticles [41]. The synthesis were divided into two parts; synthesis of CdSe core and ZnS-shell coating.

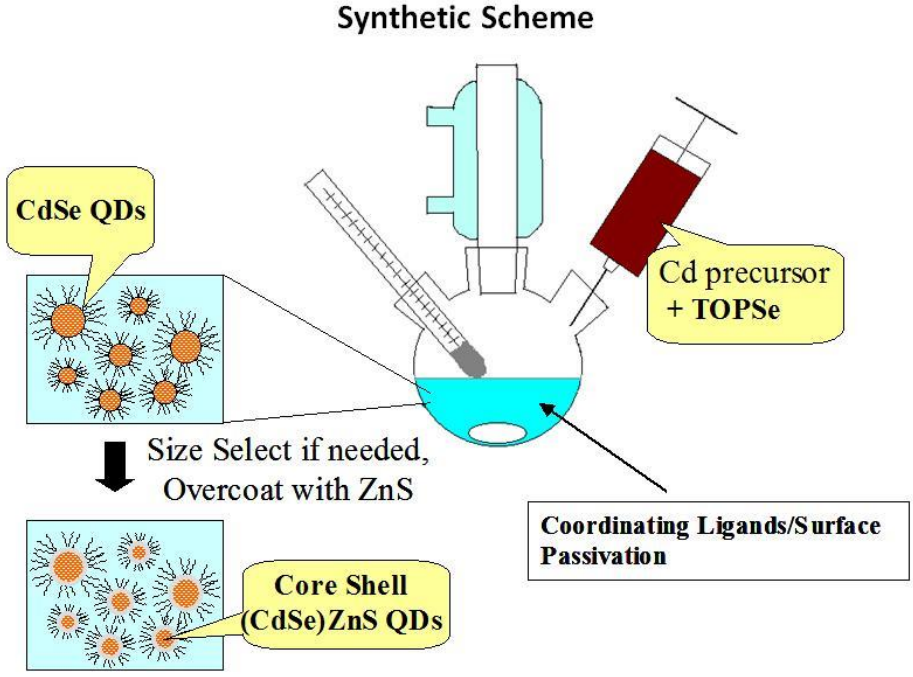

Scheme 1 Schematic diagram of synthesis of CdSe/ZnS core/shell QDs [30].

3.3.1 Synthesis of CdSe core

3.3.1.1 Preparation of TOPSe solution

Selenium powder (5.92 g) was added into a 125 mL-erlenmeyer flask capped with a septum and pumped under vacuum for 30 minutes. After that 50 mL of TOP was added into the flask under nitrogen atmosphere. The mixture was stirred for 24 h to become clear solution.

3.3.1.2 Preparation of CdSe-precursor mixture

Cadmium-2,4-pentanedionate (0.076 g) and HDDO (1.7 g) were added into a 20 mL-vial with a septum and pumped under vacuum for 30 minutes. After that 4 mL of TOP was added under nitrogen atmosphere and stirred under vacuum for 1 hour at 100°C. Then the solution was cooled down to room temperature and the previously prepared 6 mL of TOPSe solution was injected to produce CdSe precursor mixture.

3.3.1.3 Synthesis of CdSe-core

HDA (5.75 g) and TOPO (6.25 g) were added into a 100 mL three-necked bottle and pumped under vacuum for 30 minutes. Then 3.4 mL of TOP was added under nitrogen atmosphere and heated to 140°C under vacuum for 2 hours to remove the moisture. After that the CdSe-precursor mixture was injected into the solution that heated to 360°C and stabilized at 160°C for 30 minutes to produce the CdSe-core QDs.

3.3.2 ZnS-shell coating

3.3.2.1 Preparation of CdSe cores

10 mL of CdSe cores that were dissolved in hexane was precipitated with EtOH by centrifuge. The precipitate was re-dissolved with hexane of minimal volume.

3.3.2.2 Preparation of TOPS solution

Sulfur powder (0.0641 g) was dissolved in 5 mL TOP under nitrogen atmosphere to produce the TOPS solution.

3.3.2.3 ZnS-shell coating

Zinc acetate dihydrate (0.21 g) and HDA (1.636 g) were added into a 100 mL-three-necked-bottle and pumped under vacuum for 30 minutes. Then 5 mL of tri-octylamine was added under nitrogen atmosphere and heated to 120°C under vacuum for 30 minutes to remove the moisture. Next, solution of the prepared CdSe cores was injected into this solution at 60°C under nitrogen atmosphere and left under vacuum at 100°C for 30 minutes to remove hexane. After that the prepared TOPS solution was injected drop by drop into the stirring reaction mixture at 150°C to produce the CdSe/ZnS core/shell QDs.

3.3.3 Characterization of CdSe/ZnS core/shell QDs

3.3.3.1 Ultraviolet-Visible spectroscopy (UV-Vis spectroscopy)

The absorption spectra of the synthesized CdSe core QDs and CdSe/ZnS core/shell QDs were recorded on HP8453 UV-Vis spectrophotometer (Agilent, USA) from 350 nm to 700 nm at room temperature. The absorbance at 480 nm was used to calculate the quantum yields of the nanoparticles.

3.3.3.2 Fluorescence spectroscopy

The emission spectra of the synthesized CdSe core QDs and CdSe/ZnS core/shell QDs were measured using Cary Eclipse Fluorescence spectrofluorometer (Agilent, CA). The excitation wavelength was at 350 nm for regular measurement and at 480 nm, which provided the maximum quantum yield of the compared rhodamine dye in the calculation of the quantum yields of the nanoparticles.

The quantum yields of CdSe core QDs and CdSe/ZnS QDs were calculated by comparing with Rhodamine 6G as the standard fluorescence dye according to Equation 3.1 [42].

$$Q = Q_R \left(\frac{m}{m_R}\right)\left(\frac{n^2}{n_R^2}\right)$$

Q = Quantum yield

m = Slope of the linear regression between the peak area of fluorescent signal and absorbance at excitation

n = Refractive index of solvent

R = Quantum yield of Rhodamine 6G standard of 0.95 [43]

3.3.3.3 Transmission Electron Microscopy (TEM)

Sizes and morphologies of CdSe core QDs and CdSe/ZnS core/shell QDs were measured using Model TECNAI20 transmission electron microscope (Philips, US) at Burapha University. Samples were prepared by depositing droplet onto carbon film with 300 mesh copper grids.

3.3.3.4 X-ray Diffractometer (XRD)

The crystalline phases of CdSe core QDs and CdSe/ZnS core/shell QDs were characterized by D/MAX 2200 X-ray Diffractometer (Rigaku, Japan) with Cu-K_{α} radiation at an accelerating voltage of 40 kV and an applied current of 30 mA.

3.3.3.5 Scanning Electron Microscopy coupled with Energy Dispersive X-ray Spectroscopy (SEM-EDX)

The compositions of CdSe core QDs and CdSe/ZnS core/shell QDs were confirmed by JSM-IT100 Scanning Electron Microscope (JEOL) equipped with Energy Dispersive X-ray Spectroscop at an accelerating voltage of 20 kV. Samples were prepared by depositing onto carbon tape.

3.4 Cationic surface modification of CdSe/ZnS core/shell QDs

The hydrophobic surface of as-synthesized CdSe/ZnS core/shell QDs required further modification to be applied in applications involving biological systems such as DNA detection. The hydrophilic QDs especially cationic surface should make it compatible with biological system. In this work, the synthesized CdSe/ZnS QDs surface were modified with partially acylated PEI in a micellar form as shown in Scheme 2.

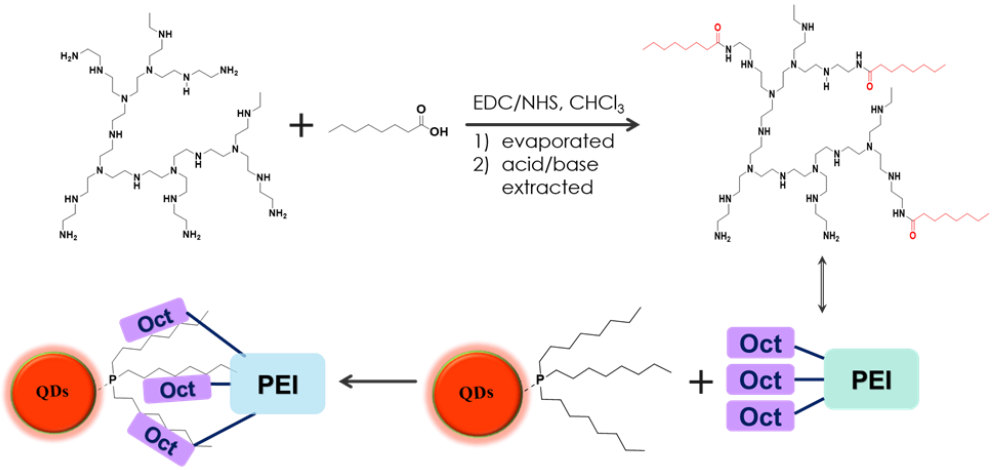

Scheme 2 Schematic diagram of QDs surface modification via micelle formation.

3.4.1 Partial acylation of PEI by octanoic acid

Branched poly(ethylene)imine-ethylene diamine (MW 800) was 20%, 30% and 40% acylated with octanoic acid. First, 1.25 mL of octanoic acid was activated with excess EDC and NHS in 7 mL of chloroform for 3 hours. Next, the activated acid was added drop by drop into the solution of PEI (2 mL of PEI dissolved in 5 mL of chloroform) under nitrogen atmosphere and the coupling was left to proceed for 18 hours. Then, the chloroform in the mixture was evaporated and the remaining mixture was washed twice with DI water to remove the reagents and unreacted PEI. Then, the mixture was re-dissolved in chloroform and adjusted to pH ~4 by adding nitric acid to extract the modified polymer from unreacted acid. After adjusting the pH, the mixture was left for 2 hours, after which become separated into two layers, which are aqueous layer and organic layer. Then, the aqueous layer was adjusted to pH 11 by adding ammonia to completely remove unreacted acid out of the modified polymer. The modified polymer (Oct-PEI) was washed with DI until it was neutral, left dried in a freeze dryer and stored at 4 °C. The optimum acylated percentage was used to modify onto the surface of QDs.

3.4.1.1 Characterization of partially acylated PEI (Oct-PEI)

3.4.1.1.1 Fourier Transform Infrared Spectroscopy (FTIR spectroscopy)

Functional groups of Oct-PEI were characterized using Nicolet™ 6700 Fourier Transform Infrared Spectroscopy (Thermo Fisher Scientific, USA) equipped with a mercury-cadmium telluride (MCT) detector and compared the results with PEI.

3.4.1.1.2 Proton and Carbon Nuclear Magnetic Resonance Spectrometry (^{1}H and ^{13}C NMR)

The functional groups of Oct-PEI and PEI were confirmed by Bruker 400 MHz ^{1}H and ^{13}C NMR spectrometer (Bruker, UK). Samples of about 0.02 g were dissolved in an appropriate deuterated solvent and transferred to NMR tube for measuring the chemical shift of proton and carbon.

3.4.1.1.3 Solubility test

The Oct-PEI (1 mg) with different molar ratios between PEI and octanoic acid were dissolved in ethanol, iso-propanol, DI water and chloroform.

3.4.2 Micelle formation between the surface of QDs and Oct-PEI (Oct-PEI/QDs)

3.4.2.1 Variation of weight by weight ratio between QDs and Oct-PEI

The synthesized CdSe/ZnS core/shell QDs 1 mL were centrifuged by adding solvent mixture of methanol and ethanol (volume ratio 1:1), dried and weighed. The Oct-PEI was added 4-9 folds of the weight of QDs and dissolved in 5 mL of chloroform. The pH of the Oct-PEI solution was adjusted to ~5.5 by adding 10 µL of glacial acetic acid. Then the solution of QDs specify concentration, dissolved in 1 mL of chloroform, was slowly added drop by drop into the solution of Oct-PEI and the reaction mixture was left overnight. Then, the chloroform in the mixture was evaporated and the coated QDs was slowly re-dissolved in DI water. The unbound excess polymer were removed by dialysis and the coated QDs (Oct-PEI/QDs) were stored in the refrigerator.

3.4.2.2 Variation of molar ratio between QDs and Oct-PEI

The synthesized CdSe/ZnS core/shell QDs 1 mL was centrifuged by adding solvent mixture between methanol and ethanol (ratio 1:1), and the mole of QDs were calculated. The Oct-PEI was weighted and added into solution of the dried QDs with the molar ratio of 100, 90, 80, 70, and 60 per 1 mole of QDs, and 5 mL of chloroform was added to disperse the mixture. Then the dispersion of Oct-PEI and QDs was mixed following the step in 3.4.2.1.

3.4.2.3 Characterization of the coated QDs (Oct-PEI/QDs)

3.4.2.3.1 Ultraviolet-Visible spectroscopy (UV-Vis spectroscopy)

The absorption spectra of Oct-PEI/QDs with different ratios of Oct-PEI and QDs were measured using HP8453 UV-Vis spectrophotometer (Agilent, USA) from 350 to 700 nm at room temperature. The Oct-PEI/QDs were dissolved in DI water and the results were compared with the original QDs and PEI/QDs prepared via ligand exchange process without acylation of octanoic acid.

3.4.2.3.2 Fluorescence spectroscopy

The emission spectra of Oct-PEI/QDs were measured using Cary Eclipse Fluorescence spectrofluorometer (Agilent, CA) from 400 nm to 700 nm. The excitation wavelength was 350 nm with the PMT voltage of 700.

3.4.2.3.3 Dynamic Light Scattering analyzer (DLS)

Sizes and zeta-potential of the Oct-PEI/QDs were measured by Zetasizer Nano ZS (Malvern, UK) at 25°C. The Oct-PEI/QDs in 200 µL DI water were diluted in 1 mL of PBS buffer pH 7.0.

3.4.2.3.4 Transmission Electron Microscopy (TEM)

Shapes and structures of the Oct-PEI/QDs were characterized using Model TECNAI20 Transmission Electron Microscope (Philips, US) at Burapha University. Samples were prepared by depositing a QDs droplet onto carbon film with 300 mesh copper grids.

3.4.2.4 Photostability test

The Oct-PEI/QDs in DI water were kept in the refrigerator at 4°C, and the fluorescence intensity was measured after 1 day, 2 days, 3 days, 4 days, 5 days, 6 days, 7 days, 2 weeks, 3 weeks, 4 weeks, and 1 month.

3.4.2.5 Cytotoxicity test

The cytotoxicity of the Oct-PEI/QDs in Oct-PEI:QDs ratio of 60:1, 70:1, and 80:1 was studied by measuring the cell viability using the MTT (3-(4,5-dimethylthiazol-2-yl)-2,5-diphenyltetrazolium bromide) tetrazolium reduction assay as shown in Figure 3.1 [44]. The MTT will enter the cells and pass into the mitochondria where it is reduced from yellow to a dark purple formazan product. Mouse fibroblast L929 cells were used as a cell model. Cells were grown in Dulbecco's Modified Eagles Medium (DMEM, Gibco, US) supplemented with 4 mM of **L**-glutamax, 1% Na-pyruvate, 100 U·mL^{-1} penicillin and 10% fetal bovine serum (FBS) (all from OBCR-laboratories, Thailand), in a humid atmosphere at 37°C. The L929 cells were cultured in 96-well plates (10,000 cells in 200 µL of DMEM per well). After 24 hours of incubation to bring the cells to confluence, the cell culture medium was replaced with fresh culture medium containing materials (Oct-PEI/QDs) at a concentration 10 and 100 µg.mL^{-1}. After 24 hours of incubation with different materials at 37°C, the 20 µL of 5 mg·mL^{-1} MTT assay stock solution in PBS was added to each well and further incubated for 1.5 h at 37 °C. Finally, the medium containing unreacted dye was removed, and 150 µL per well DMSO was added to dissolve the achieved purple formazan crystals resulting from the viable cells. The absorbance was measured in a BioTek Elx80 at a wavelength of 570 nm.

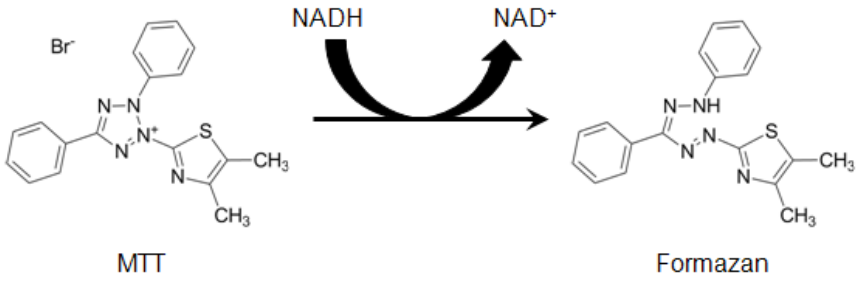

Figure 3.1 Structures of MTT and colored formazan product [44].

3.5 Application of cationic Oct-PEI/QDs in DNA detection

DNA detection of the cationic QDs were investigated into 2 systems; i.e. on glass slide and in solution. All of DNA strands and PNA were from Organic Synthesis Research Unit, Thailand.

3.5.1 DNA detection onto glass slide

Aminated TET DNA (5'-H_2N-CGT ACG GAA TTC GCT AGC CCC CCG GCA GGC CAC GGC TTG GGT TGG TCC CAC-3') and Kanamycin DNA (5'-H_2N-TGG GGG TTG AGG CTA AGC CGA-3') were used for investigating the DNA detection of cationic QDs. The DNAs were attached to the surface of glass slide via a protocol reported by Zammatteo, *et al*. (2000) [45]. The reaction of DNA attachment is shown in Figure 3.2. Firstly, the DNAs were denatured for 10 minutes at 100°C and diluted to 250, 500, and 1000 nM in 0.1 M of 2-(*N*-morpholino) ethanesulfonic acid (MES) pH 6.5 buffer. Then, 50 µL of the DNA solutions were dispended onto SuperAldehyde2 glass slide (Arrayit Corporation, USA) surfaces. Then, the dispended glass slide was incubated for 1 hour at 20°C in a humid chamber and washed with 0.1% of sodium dodecylsulfate (SDS) and milliQ water twice. The washed glass slide was incubated for 5 minutes with freshly prepared sodium borohydride solution (2.5 mg of sodium borohydride dissolved in 750 µL of PBS solution and 250 µL of ethanol). Finally, the glass slide was heated in water at 95 °C for 3 minutes to remove the sodium borohydride. After the attachment of DNA to glass slide surface, 40 µL of the optimum cationic Oct-PEI/QDs were dropped onto the glass slide to react with each DNA in each concentrations. After incubating 30 minutes at room temperature, the glass slide was washed with milliQ water. The results were collected by taking photos under a UV lamp using CANON EOS M camera. The absorption spectra were measured by UV-2550 UV-Visible spectrophotometer (Shimadzu, Japan) from 200 nm to 600 nm at 25°C.

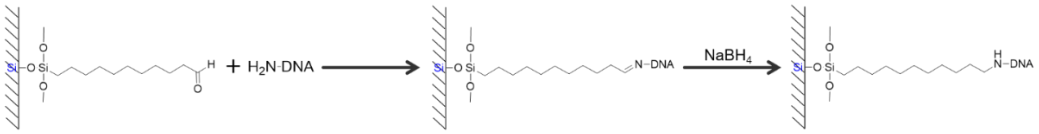

Figure 3.2 Reaction scheme for the attachment of aminated DNA to aldehyde-modified glass [45].

3.5.2 DNA detection in solution

In this system, the DNA detection were separated into 2 parts which were only DNA mixed with cationic Oct-PEI/QDs and PNA-DNA mixed with cationic Oct-PEI/QDs.

3.5.2.1 DNA mixed with the cationic Oct-PEI/QDs

A short sequence DNA such as dG10 DNA (TTTTTTTTTT) was used for studying the action of the cationic Oct-PEI/QDs in DNA detection. The dG10 DNA (TTTTTTTTTT) (166 μM, 10 μL) was mixed with the cationic Oct-PEI/QDs (140 μM, 10 μL) in 10 mM phosphate pH 7 buffer. After that, the result was taken a photo by CANON EOS M camera.

3.5.2.2 PNA-DNA mixed with the cationic Oct-PEI/QDs

For investigating the DNA detection of the cationic QDs employing peptide nucleic acid (or PNA), T9 DNA (TTTTTTTTT) and PNA that conjugated with Nile Red dye (AC-Lys-AAAA(NR)AAAAA-LysNH_2) were used. Four samples were prepared in the phosphate pH 7 buffer with the final volume 20 μL. PNA 1 μL was mixed with 2 μL of the Oct-PEI/QDs, 1 μL of DNA mixed with 2 μL of the Oct-PEI/QDs, 1 μL of PNA mixed with 1 μL of DNA and 2 μL of the Oct-PEI/QDs, and only 2 μL of the Oct-PEI/QDs. All of samples were studied the changes in emission spectra using a fluorescence microscope at the excitation wavelength of 350 nm and 550 nm.

CHAPTER IV

RESULTS AND DISCUSSIONS

In this chapter, we explained and discussed the results from characterization techniques. The results are divided into 4 parts; i.e. characterization of the synthesized CdSe/ZnS core/shell QDs, characterization of the partially acylated poly(ethylene)imine (Oct-PEI), characterization of the cationic QDs (Oct-PEI/QDs), and investigation of the responses of the cationic QDs in DNA detection.

4.1 Characterization of the synthesized CdSe/ZnS QDs

CdSe/ZnS QDs were synthesized via a hot-solution decomposition process using TOPO, TOP, and HDA as stabilizing ligands resulting in different emission colors, including green, yellow and red, as shown in Figure 4.1 [41]. The CdSe core QDs were increased in the photo-stability after coating ZnS shell [21]. Both CdSe core QDs and CdSe/ZnS core/shell QDs exhibited the hydrophobic properties and were dispersed in hexane with stability at room temperature. For comparing the optical properties between CdSe core QDs and CdSe/ZnS core/shell QDs, the absorption and emission spectra of them were measured in the range of 350 nm to 700 nm and absorbance at wavelength 480 nm was used for calculating the quantum yield using rhodamine 6G (Ø = 0.95) as a reference standard.

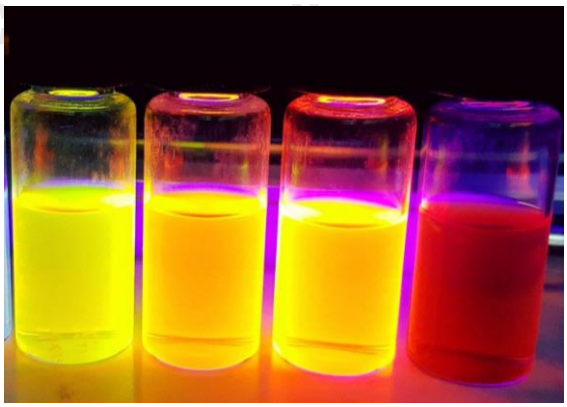

Figure 4.1 The synthesized CdSe/ZnS core/shell QDs with difference sizes in hexane under a UV lamp.

From the absorption spectra measured using a UV-Visible spectroscopy in Figure 4.2, the synthesized QDs showed the broad absorption character and the first absorption peak of both types of QDs were at 534 nm which related to the green luminescence color. Moreover, emission spectra was measured by fluorescence spectroscopy in Figure 4.3. Comparison between CdSe core and CdSe/ZnS core/shell QDs at the excitation wavelength 480 nm showed that the emission spectrum of CdSe/ZnS core/shell QDs was normal distribution and showed higher intensity than the signal of CdSe core QDs with a small blue shift. These results indicated that after CdSe core QDs were coated with ZnS shell, they were still maintained the photo-properties of the core QDs and also increased the colloidal stability of particles [21]. In addition, the as-synthesized CdSe/ZnS core/shell QDs were also increased in the photo-properties of QDs as observed by higher quantum yield. From the bar chart in Figure 4.4, the quantum yields of QDs were calculated from Equation 3.1 [42]. The synthesized CdSe core QDs, CdSe/ZnS core/shell QDs, and rhodamine 6G were prepared at least 3 different concentrations for measuring and plotting the graph to find the slope. The plots between peak area of fluorescence and absorbance of the QDs were shown in **Appendix A**. The result showed that the calculated quantum yield of the as-synthesized CdSe/ZnS core/shell QDs (49%) was higher than the CdSe core QDs (24%). These results indicated that coating ZnS shell can increase the photo-properties and colloidal stability of QDs as have been reported previously [21].

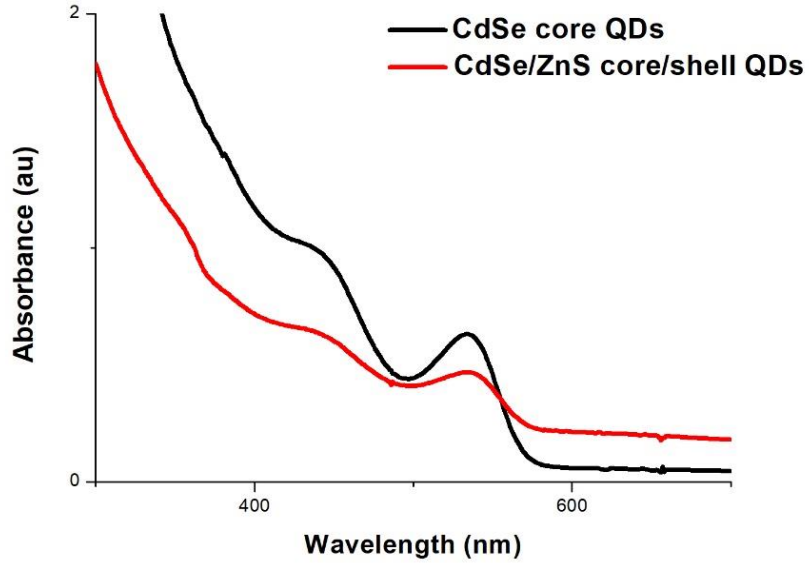

Figure 4.2 Absorption spectra of the synthesized CdSe core (black line), and CdSe/ZnS core/shell (red line) QDs at room temperature.

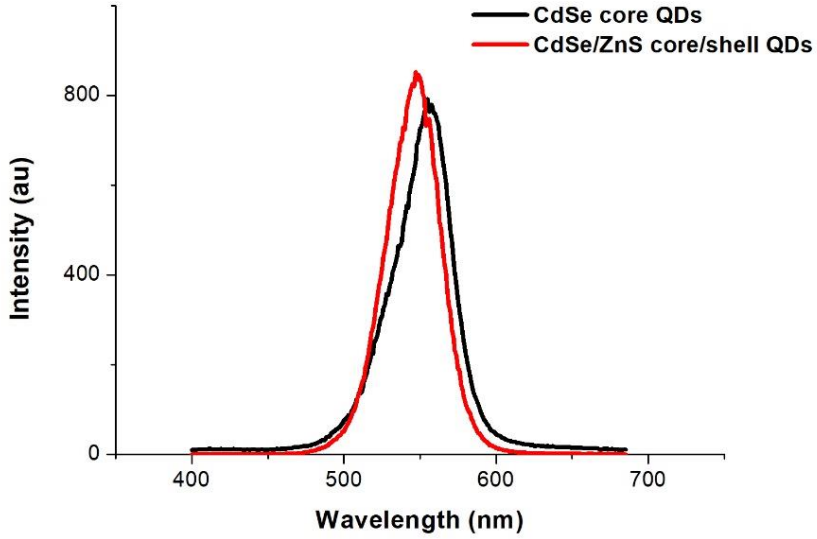

Figure 4.3 Emission spectra of the synthesized CdSe core (black line), and CdSe/ZnS core/shell (red line) QDs at room temperature with the excitation wavelength 350 nm and applied voltage 700 PMT.

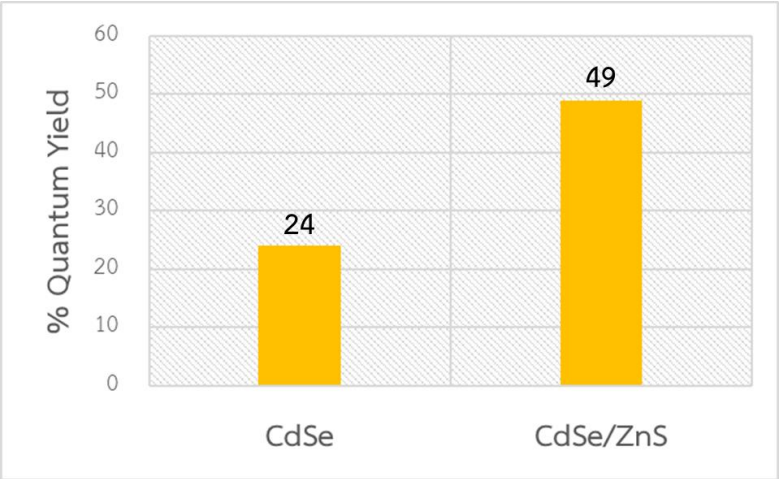

Figure 4.4 The bar chart of calculated quantum yield compared between CdSe core and CdSe/ZnS core/shell QDs.

To measure sizes and investigate the morphologies of QDs, the as-synthesized CdSe core QDs and CdSe/ZnS core/shell QDs were dispersed in hexane, and then deposited onto carbon film with 300 mesh copper grids and characterized by TEM. From TEM images, the average diameter of CdSe/ZnS core/shell QDs particles was 4.59 ±0.53 nm (figure 4.5 b) which not much increased from the CdSe core QDs that was 4.20 ±0.58 nm (figure 4.5 a). The size of QDs was controlled by adjusting the amount of the cadmium precursor, as observed that the smaller size CdSe core (3.35 ±0.43 nm) and CdSe/ZnS core/shell (3.96 ±0.49 nm) QDs (Figure 4.5 c and d) were obtained when reduced the amount of added cadmium. These results showed that the particles of the synthesized QDs are monodispersed and did not induce the aggregation after coating ZnS shell.

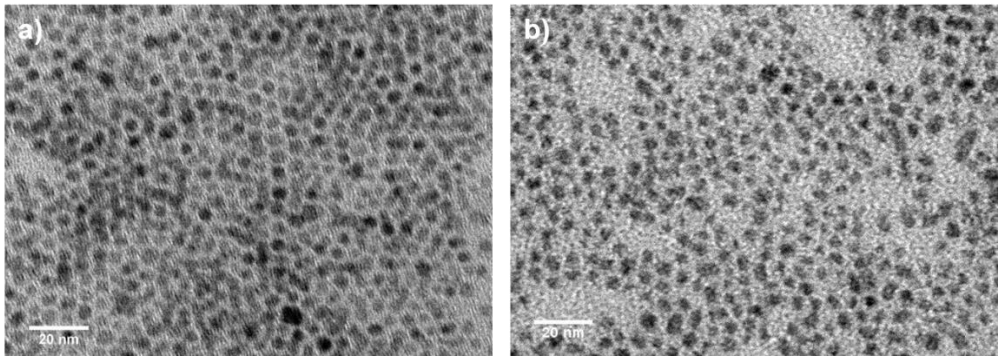

Figure 4.5 TEM images of a,c) CdSe core and b,d) CdSe/ZnS core/shell QDs with magnitude of 120 kX.

To investigate the composition of the as-synthesized QDs, XRD spectra of the synthesized CdSe core and CdSe/ZnS core/shell QDs were compared with the pattern of Cadmium Selenide and Sphalerite Zinc Sulfide as shown in Figure 4.6. The results showed that XRD patterns of both synthesized QDs exhibited the nanocrystals character of a broad XRD signal. In case of the synthesized CdSe core QDs pattern, the strong characteristic peaks in the position of cadmium selenide appeared, and the same pattern also were found in the synthesized CdSe/ZnS core/shell QDs XRD pattern. Moreover, the XRD pattern of the synthesized CdSe/ZnS core/shell QDs also showed some small characteristic peaks of sphalerite zinc sulfide indicating the ZnS shell were obtained.

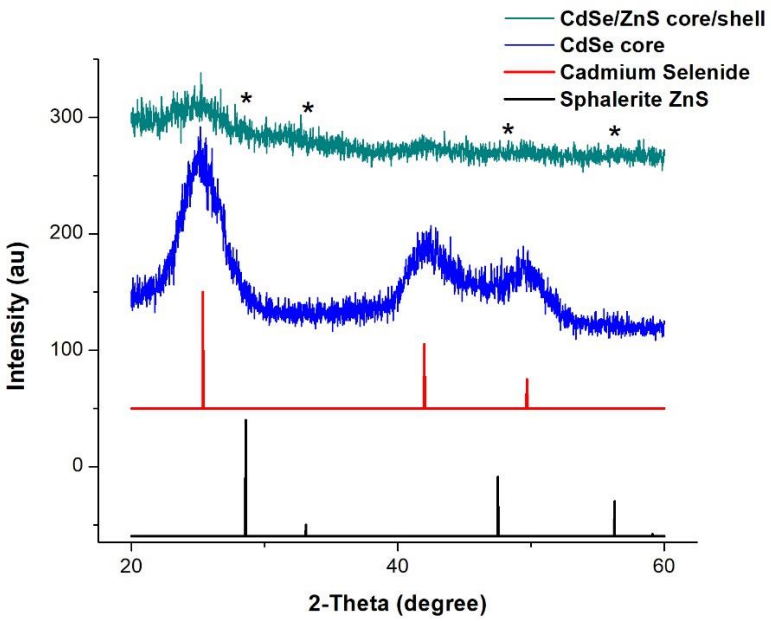

Figure 4.6 XRD pattern of (blue line) CdSe core QDs, (green line) CdSe/ZnS core/shell QDs, (red line) JCPDS no. 19-0191 Cadmium Selenide pattern, and (black line) JCPDS no. 05-0566 Sphalerite Zinc Sulfide pattern. Star (*) refer to the presence of ZnS in CdSe/ZnS QDs.

In order to confirm the composition of the as-synthesized QDs, the elemental composition was analyzed by SEM-EDX technique. From Table 4.1, comparison between the synthesized CdSe/ZnS core/shell QDs and the synthesized CdSe core QDs, the CdSe/ZnS core/shell QDs showed the significant %mass of zinc and sulfur, corresponding to formation of the ZnS shell. Moreover, the proportion between cadmium and selenium in the synthesized CdSe/ZnS core/shell QDs was similar to the synthesized CdSe core QDs.

Table 4.1 Elemental analysis of CdSe core QDs and CdSe/ZnS core/shell QDs.

CdSe (core)		CdSe/ZnS (core/shell)	
Formula	Mass%	Formula	Mass%
Cd	22.61	Cd	7.27
Se	22.16	Se	6.62
Zn	-	Zn	2.40
S	-	S	0.46
P	4.11	P	3.10
O	8.66	O	8.56

From the results of absorption and emission spectra, TEM images, XRD patterns, and SEM-EDX, we could conclude that as-synthesized QDs via a hot-solution decomposition process are nanocrystals of monodispersed and spherical shapes. The synthesized CdSe/ZnS core/shell QDs contained both of CdSe and ZnS and improved in the photo-properties, providing the colloidal stability and photo-stability.

4.2 Characterization of the partially acylated poly(ethylene)imine (Oct-PEI)

Poly(ethylene)imine or PEI was increased in hydrophobicity for forming micellar structure on the surface of QDs by partial acylation with octanoic acid to display the amphiphilic properties. Octanoic acid (CH3(CH2)6COOH) was activated to be used in partial functionalization of the amine groups in PEI to amide group through EDC/NHS coupling as shown in Figure 4.7. In this work, PEI was partially acylated in 20%, 30% (in Figure 4.7), and 40%. From the IR spectra of the partially acylated PEI, which we called Oct-PEI, in Figure 4.8, it can be observed that the peak of carbonyl of amide group (O=C-N) appeared in the spectra of all Oct-PEI with different percentage of acylation (1645 cm^{-1}, for 20% and 30%, and 1642 cm^{-1}, for 40%, respectively) [46]. Moreover, the Oct-PEI spectrum was also compared with PEI and octanoic acid as shown in Figure 4.9. The results confirmed the presence of amide bonds in Oct-PEI because the peak of new carbonyl of amide group was present in neither spectrum of PEI nor spectrum of octanoic acid.

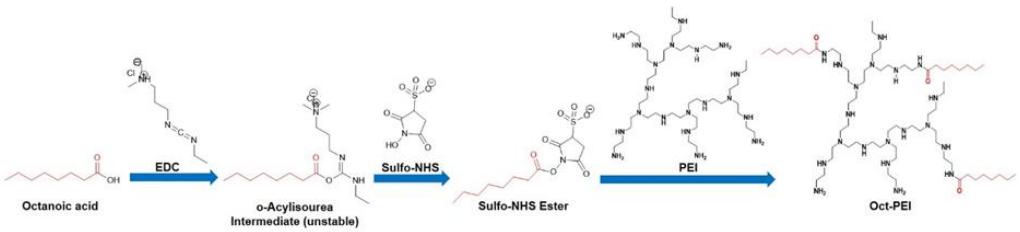

Figure 4.7 Schematic of EDC/NHS coupling between octanoic acid and PEI.

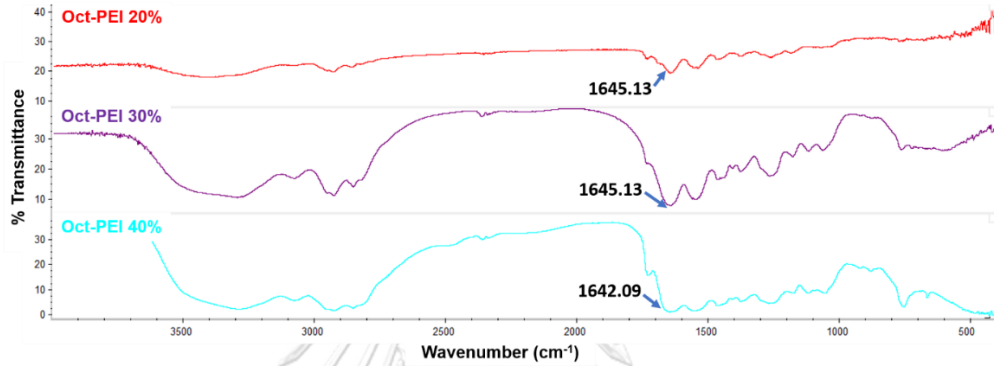

Figure 4.8 IR spectra of Oct-PEI in differentiated percentage of acylation; 20% (red line), 30% (purple line), and 40% (light blue line).

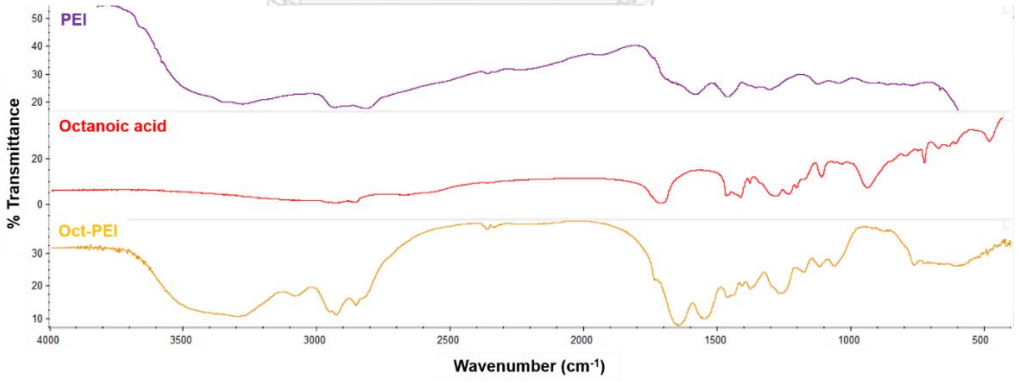

Figure 4.9 IR spectra of PEI (purple line), octanoic acid (red line), and Oct-PEI (brown line).

To confirm the partial acylation of PEI, the proton nuclear magnetic resonance (^{1}H NMR) and the carbon-13 nuclear magnetic resonance (^{13}C NMR) spectroscopy were used. The ^{1}H NMR spectra of Oct-PEI in Figure 4.10 showed that signals of saturated

alkane proton [47] belonging to octyl chain (C8) of octanoate group at 0.910 and 1.293 ppm, which are at the same position as octanoic acid . The signal at 1.609 ppm, which is the same position as in PEI referred to the position of CH_2N protons. For the ^{13}C NMR spectra in Figure 4.11, the spectrum of Oct-PEI was quite similar to octanoic acid, but the carbonyl carbon of amide at the position around 160-185 ppm was not visible. The much reduced intensity of carbonyl carbon peak is well known and distinguish, the signal from noisy background can be difficult [48, 49] From NMR results indicated that the Oct-PEI combined the characteristic signals of both octanoic acid and PEI.

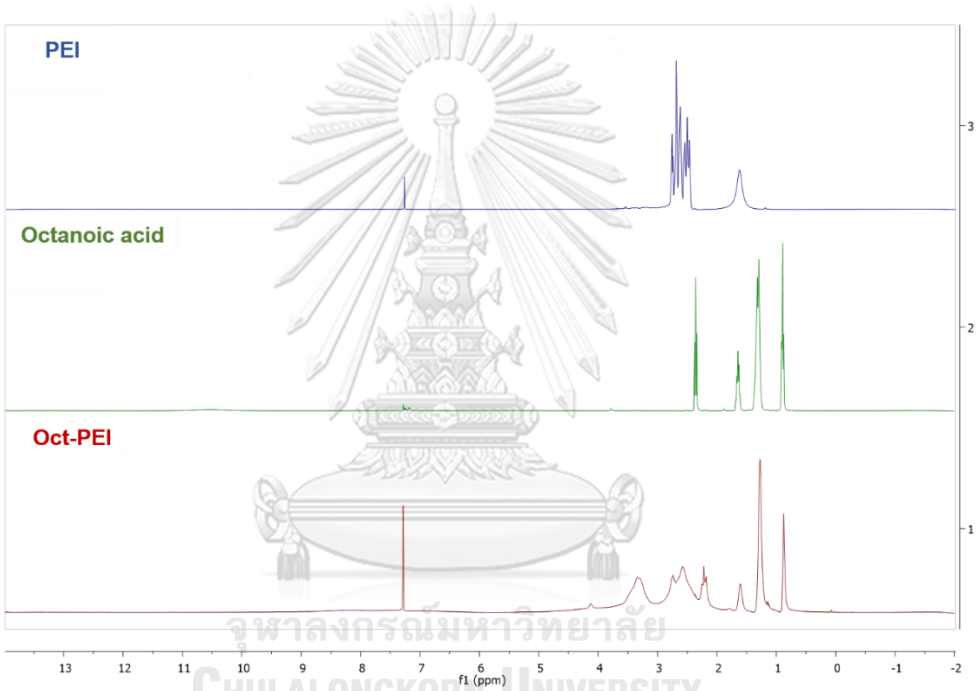

Figure 4.10 ^{1}H NMR spectra of PEI (blue line), octanoic acid (green line), and Oct-PEI (red line).

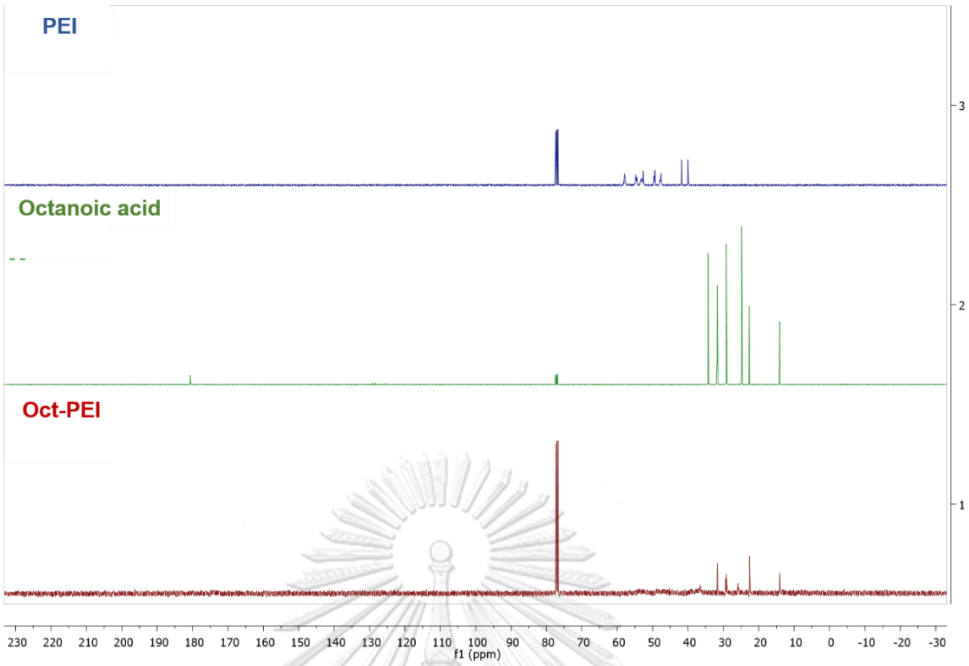

Figure 4.11 ^{13}C NMR spectra of PEI (blue line), octanoic acid (green line), and Oct-PEI (red line).

To confirm the percentage of acylation in PEI, the ^{1}H NMR spectra of Oct-PEI in Figure 4.10 was integrated. The fraction between the integration number of octanoic acid's protons and PEI's proton in Oct-PEI was 3:1, which referred to 30% acylation of PEI by octanoic acid.

Moreover, the physical properties and solubility of Oct-PEI of different percentage of acylation were also observed. Due to our aim of using acylated PEI modified onto the surface of QDs, the amphiphilic polymer is needed to construct the micellar structure on the QDs. From the Table 4.2, only 30% acylated PEI exhibited the amphiphilic properties that it could be dissolved in both of polar solvents such as ethanol, iso-propanol, and DI water, and non-polar solvent such as chloroform. Thus, in this work, the 30% acylated PEI was chosen for continuing our study of coating the Oct-PEI onto the surface of QDs.

Table 4.2 Physical properties and dissolved solvents in each percentage of acylation.

% of Acylation	Physical Properties	Solvents
20	Dark brown color solid	Ethanol and DI
30	Dark yellow color solid	Ethanol, iso-propanol, DI and Chloroform
40	Pale yellow color solid	Chloroform

4.3 Characterization of the cationic QDs (Oct-PEI/QDs)

For coating the 30% partially acylated PEI onto the surface of QDs via micelle formation, the pH of solution and the ratio between polymer and QDs were adjusted to find the optimum proportion leading to cationic QDs with good water solubility and maintain fluorescent properties. The micelle formation method was modified from the previous research [50]. Firstly, the Oct-PEI was weighed (4 folds excess by weight) and added to the dried QDs and the pH was adjusted to induce the amphiphilic forms of polymer. From Figure 4.13, the mixture between QDs and Oct-PEI in chloroform gave a clear solution with orange emission, which was similar to as-synthesized QDs (Figure 4.13 a). After the evaporation (Figure 4.13 b), the orange fluorescence of QDs was still remained. However, after dispersed in DI water and centrifugation (Figure 4.13 c and d), the mixture was slightly turbid and separated into two layers, in which the top layer was the QDs. These results implied that the ratio between Oct-PEI and QDs in 4:1 by weight was not an optimum ratio for forming the micellar structure.

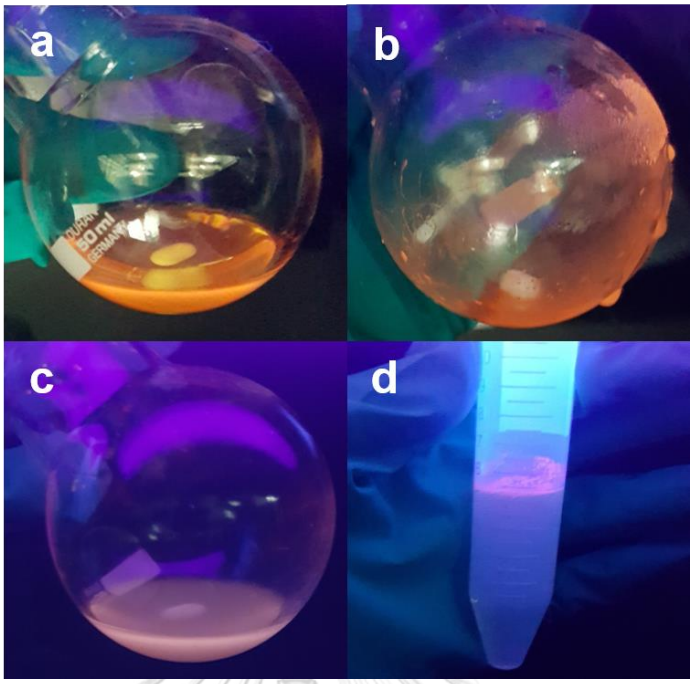

Figure 4.12. Images of QDs coated with Oct-PEI. a) in $CHCl_3$, b) after evaporated, c) and d) in DI water before and after centrifuge, respectively. The weight ratio between Oct-PEI and QDs is 4:1.

Due to the results from the weight ratio between Oct-PEI and QDs of 4:1, we suspected that the amount of polymer might be not enough, so we increased the ratio between Oct-PEI and QDs to 5:1. From the results in Figure 4.14 a), the coated QDs dispersed in DI water also gave a turbid solution. This phenomenon also occurred with other Oct-PEI ratios as shown in Figure 4.14 b, c, d, and e. Moreover, the higher weight ratio of the polymer to QDs, the larger decrease in the fluorescence of QDs was observed. After centrifugation, the layer of QDs moved from top to bottom layer at high ratio (Figure 4.14 f) compared with a low ratio (Figure 4.13 d). These experiments indicated that the weight ratios between Oct-PEI and QDs range of 4:1 to 9:1 were still not the optimum ratio for micelle formation.

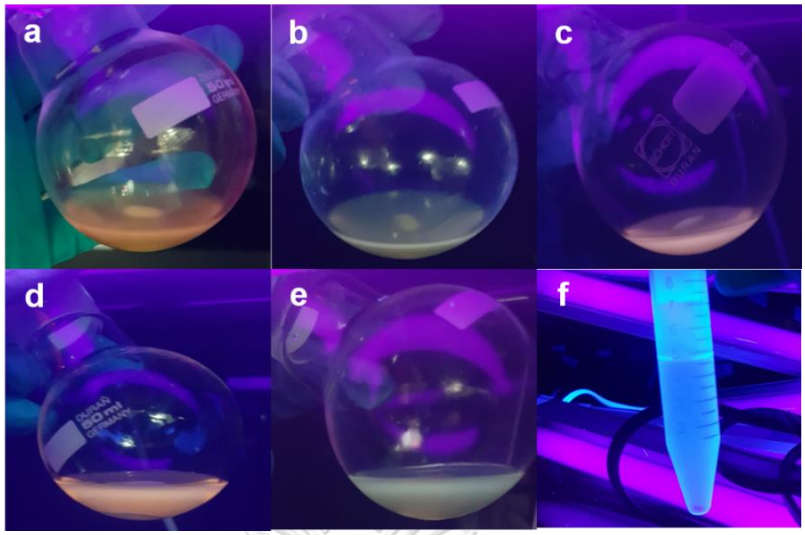

Figure 4.13 Images of QDs coated with Oct-PEI dissolved in DI water with the weight ratio between Oct-PEI and QDs were a) 5:1, b) 6:1, c) 7:1, d) 8:1, e) and f) 9:1 which before and after centrifugation.

From the variation of weight ratio in coating the surface of QDs, was also observed that with too high amount of polymer, a low fluorescent signal of QDs was observed. Therefore, the weight ratio between Oct-PEI and QDs was reduced. The fluorescence titration was investigated by using the weight ratio of 1:1 in chloroform. At this weight ratio, the molar ratio of Oct-PEI per QDs calculated from the fraction between mole of Oct-PEI and mole of QDs was around 100:1. From Figure 4.15, two emission wavelengths were observed around 470 nm and 600 nm, corresponding to Oct-PEI and QDs, respectively. The fluorescence signals of QDs were dramatically decreased when we added a higher volume of Oct-PEI solution. After leaving for 1 day and dispersing in DI water, the fluorescence spectrum of coated QDs in DI water was observed and compared with coated QDs in chloroform as shown in Figure 4.16. From the results, the emission of coated QDs in DI water appeared at the position of QDs at 610 nm, which was slightly shifted from the original QDs and did not obviously appear before 1 day. The delay in exhibiting the fluorescent of QDs Indicated that the micelle formation between Oct-PEI and the surface of QDs occurred slowly and needed time to stabilize the surface. However, the molar ratio of 100:1 (Oct-PEI:QDs) still was not the optimum ratio because the fluorescent intensity of coated QDs was low (10 times

less than the original QDs of the same concentration). Therefore, the molar ratio between Oct-PEI and QDs of less than 100:1 were further investigated.

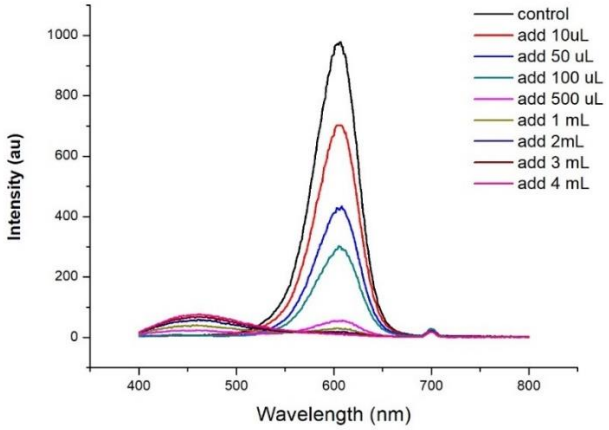

Figure 4.14 Emission spectra of fluorescence titration started with the synthesized CdSe/ZnS core/shell QDs (black line), after adding 10 µL (red line), 50 µL (blue line), 100 µL (green line), 500 µL (pink line), 1 mL (olive-green line), 2 mL (navy-blue line), 3 mL (magenta line), and 4 mL (light-red line) of polymer solution in the ratio of Oct-PEI:QDs was 1:1 by weight or 100:1 by mole. The excitation wavelength was 350 nm with 700 PMT applied voltage.

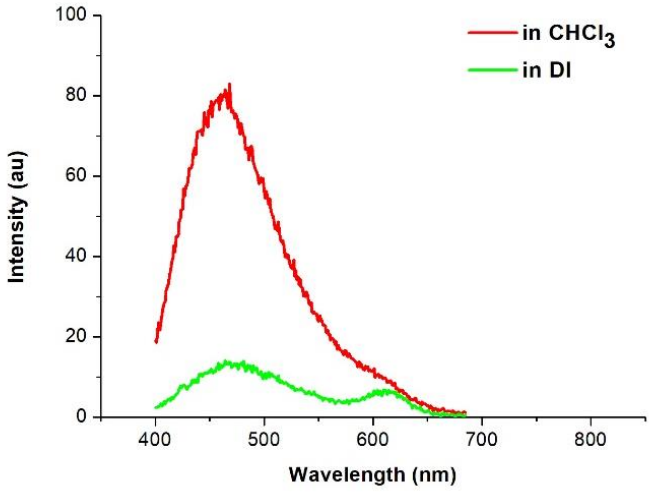

Figure 4.15 Emission spectra of Oct-PEI:QDs with the molar ratio of 100:1 when dispersed in $CHCl_3$ (red line) and DI water (green line). The excitation wavelength was 350 nm with 700 PMT applied voltage.

The molar ratio between Oct-PEI and QDs 90:1 was observed as shown in Figure 4.17. The result showed that at this ratio, the fluorescent intensity of QDs was higher than the one from the ratio 100:1 (Figure 4.16 green line). The result showed that this molar ratio (90:1) was more suitable for coating the surface of QDs than the molar ratio of 100:1. Moreover, Figure 4.18 also showed that the fluorescence signal increased after collecting for 7 days. From these results indicated that the best time for aging the coated particles was 7 days and reducing the molar ratio between Oct-PEI and QDs could increase the fluorescence of QDs. Thus, the possible minimum ratio was investigated.

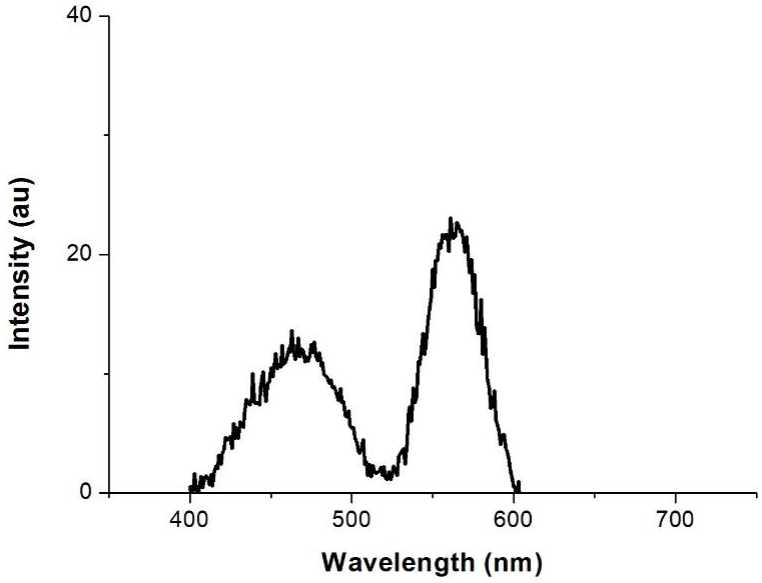

Figure 4.16 Fluorescence spectrum of the coated QDs dispersed in DI water in the molar ratio between Oct-PEI and QDs of 90:1 using excitation wavelength at 350 nm with 700 PMT applied voltage.

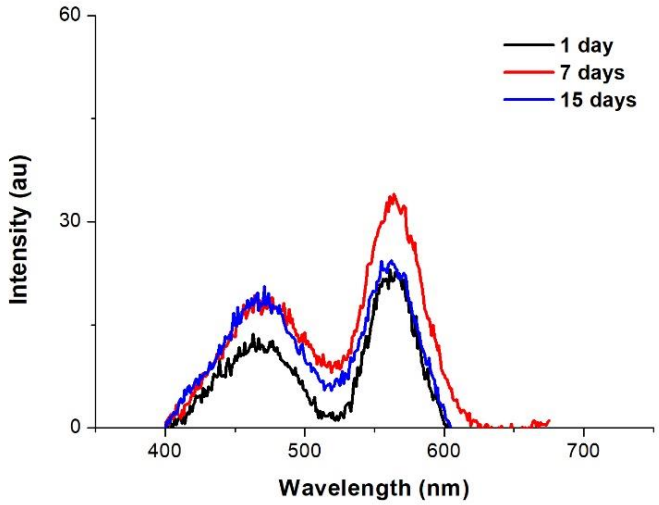

Figure 4.17 Emission spectra of the coated QDs dispersed in DI water in the molar ratio between Oct-PEI and QDs of 90:1 when left at room temperature for 1 day (black line), 7 days (red line), and 15 days (blue line). The excitation wavelength was 350 nm with 700 PMT applied voltage.

To investigate the optimum molar ratio between Oct-PEI and QDs, the coated QDs was observed at different Oct-PEI/QDs molar ratios in range of 50:1 to 90:1. From the result in Figure 4.19 showed that the Oct-PEI/QDs provided the highest intensity at the molar ratio of 80:1 and at the molar ratio of 60:1 provided the higher intensity than 70:1 and 90:1, respectively. These results did not show the expected trend that higher ratio should provide lower intensity of fluorescence. For the coated QDs at the molar ratio of 50:1 in Figure 4.20, did not disperse in buffer and lost the fluorescence properties. This imply that at this low molar ratio, the amount of polymer was too little to maintain the stability of the QDs and caused a severe aggregation of the QDs. Therefore, the optimum molar ratio between Oct-PEI and QDs that could give QDs dispersed in water with good stability and fluorescence was in range of 60:1 to 80:1.

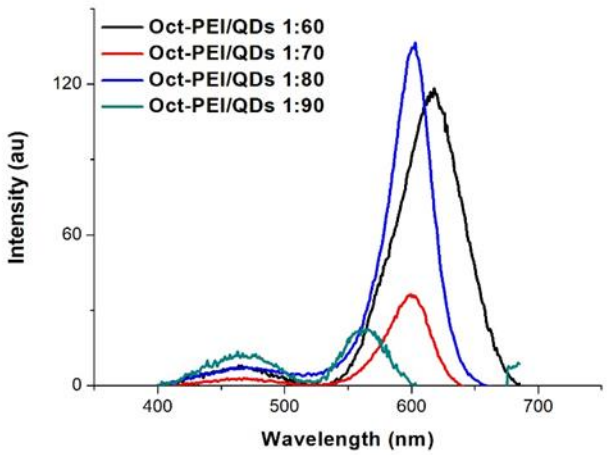

Figure 4.18 Emission spectra of the coated QDs in different molar ratio between Oct-PEI:QDs of 60:1 (black line), 70:1 (red line), 80:1 (blue line), and 90:1 (green line). The excitation wavelength was 350 nm with 600 PMT applied voltage.

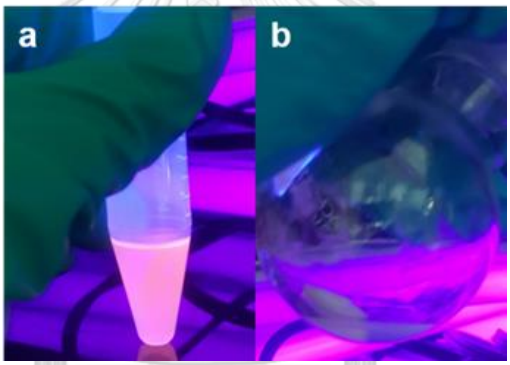

Figure 4.19 Emission spectra of the coated QDs in different molar ratio between Oct-PEI:QDs of 60:1 (black line), 70:1 (red line), 80:1 (blue line), and 90:1 (green line). The excitation wavelength was 350 nm with 600 PMT applied voltage.

To study the stability of each molar ratio between Oct-PEI and QDs in range of 60:1 to 80:1, the emission spectrum of the coated QDs were monitored for 30 days. At the molar ratio between Oct-PEI and QDs of 60:1 as shown in Figure 4.21, the fluorescent intensity of QDs after left for 7 days was dramatically increased from Day 1 and the intensity was roughly the same for the following 30 days.

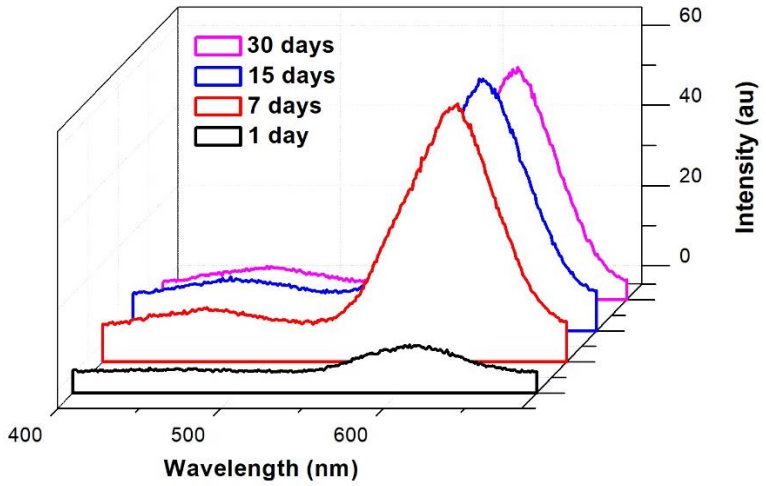

Figure 4.20 Emission spectra of the coated QDs in molar ratio between Oct-PEI and QDs of 60:1 after 1 day (black line), 7 days (red line), 15 days (blue line), and 30 days (pink line). The excitation wavelength was 350 nm with 600 PMT applied voltage.

For the molar ratio between Oct-PEI and QDs of 70:1, the emission spectra were shown in Figure 4.22. The results showed that the fluorescent intensity was dramatically increased after 14 days. Then, the fluorescent intensity was gradually decreased during 30 days which was different from the results of the molar ratio 60:1.

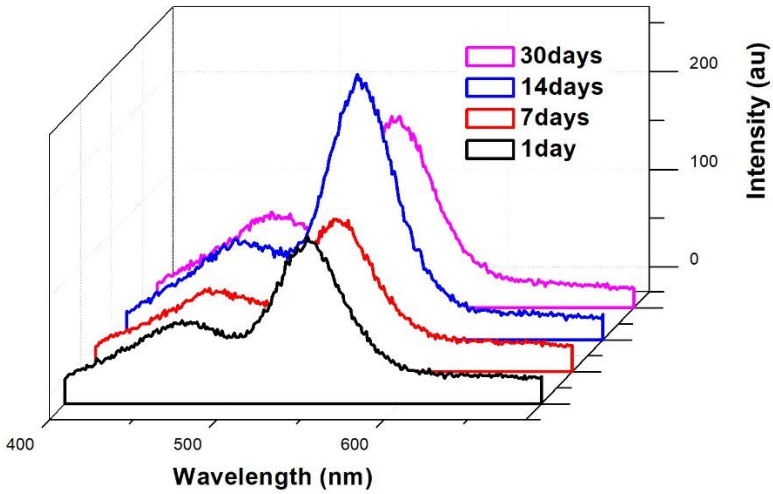

Figure 4.21 Emission spectra of the coated QDs in molar ratio between Oct-PEI and QDs of 70:1 after 1 day (black line), 7 days (red line), 15 days (blue line), and 30 days (pink line). The excitation wavelength was 350 nm with 700 PMT applied voltage.

Another investigated molar ratio between Oct-PEI and QDs was 80:1 that shown in Figure 4.23. The emission spectra showed that the fluorescent intensity stabilized for 15 days and then was decreased on Day 30.

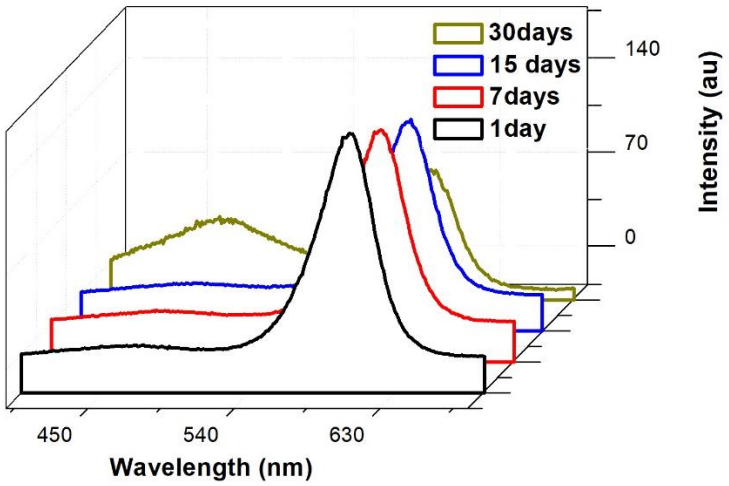

Figure 4.22 Emission spectra of the coated QDs in molar ratio between Oct-PEI and QDs of 80:1 after 1 day (black line), 7 days (red line), 15 days (blue line), and 30 days (pink line). The excitation wavelength was 350 nm with 600 PMT applied voltage.

The emission spectra of the coated QDs in different molar ratio between Oct-PEI and QDs (Figure 4.18, 4.21, 4.22, and 4.23) showed that the coated QDs at the molar ratio of 80:1 was the most stable during the 15 days period test, relating to the highest fluorescent intensity in Figure 4.19. However, a slight decrease in the fluorescence was observed after 30 days. Moreover, due to the large amount of polymer (80 folds of mole of QDs), the fluorescent signal of polymer could interfere the fluorescent signal of QDs of smaller sizes as shown in **Appendix B**.

For the molar ratio between Oct-PEI and QDs of 70:1 and 90:1, their fluorescent signals were not stable due to the instability of fluorescent intensity in 70:1 and the obviously decreased of fluorescent intensity in 90:1. On the other hand, in the molar ratio of 60:1, the fluorescent intensity was drastically increased in the first week after coating and stayed constant for 30 days referred to the aging time of the particles. From the stability results in combination with the result in Figure 4.19, the molar ratio

of 80:1 provided the highest intensity followed by the molar ratio of 60:1, 70:1 and 90:1, respectively.

To confirm the cationic surfaces of the particles, sizes and zeta-potential of the coated QDs were measured using zeta sizer nanoZs instrument. The results in Table 4.2 showed that all coated QDs have a positive charge, and at the molar ratio of 80:1, the resulted QDs exhibited the highest potential (+62.5 mV) and gave the largest diameter (390 nm) when compared to the others. Furthermore, the smallest size and zeta-potential of the QDs at the molar ratio 90:1 indicated that the micelle formation between Oct-PEI and the QDs might not be completed and it could induce the aggregation of particles resulting in the instability of the optical properties.

Table 4.3 Results from Zetasizer of QDs in different ratio of Oct-PEI/QDs.

Materials	Size (d.nm)	Zeta-potential (mV)
Oct-PEI/QDs 60:1	267.2	+36.9
Oct-PEI/QDs 70:1	252.8	+38.1
Oct-PEI/QDs 80:1	390.7	+62.5
Oct-PEI/QDs 90:1	200	+20.5

Due to the large sizes of the coated QDs were measured as in Table 4.3, TEM technique was used to confirm whether the QDs experienced aggregation. The TEM images in Figure 4.24 showed that the sizes of the coated particles become larger than the original synthesized CdSe/ZnS core/shell QDs similar to the results in Table 4.3 confirming the micelle formation between Oct-PEI and QDs occurred in which each particles did not aggregate (Figure 4.24 a). Moreover, in Figure 4.24 b also showed that each micelle included many individual QDs particles caused of the retention of optical properties of QDs in the coated QDs.

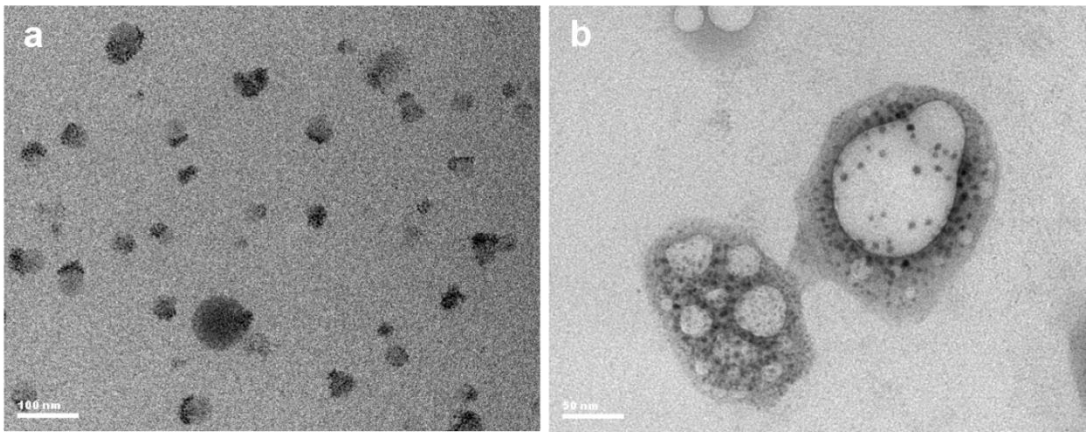

Figure 4.23 TEM images of the coated QDs with different magnification a) 20 kX and b) 40 kX.

Moreover, to investigate whether the prepared QDs are suitable for biological application, the cytotoxicity of the coated QDs in the molar ratio between Oct-PEI and the QDs of 80:1, 70:1, and 60:1 was studied against to Fibroblast L929 cells by MTT assays. From the cytotoxicity result in Figure 4.25, it was found that the QDs with the molar ratio of 60:1 provided the highest percentage of cell viability, while the molar ratio of 70:1 and 80:1 gave the lowest percent. The cytotoxicity of the QDs with high percentage of Oct-PEI might be related to the properties of the original PEI that highly positive charge leading in proton sponge effect caused in death cell [51]. However, the QDs prepared with 70:1 showed a little higher cytotoxicity that the QDs from 80:1 likely because the instability of the QDs with molar ratio 70:1 that could have a higher chance for QD particles release or aggregation. For the as-synthesized QDs, the cytotoxicity could not be tested because they were not hydrophilic enough to apply in the system.

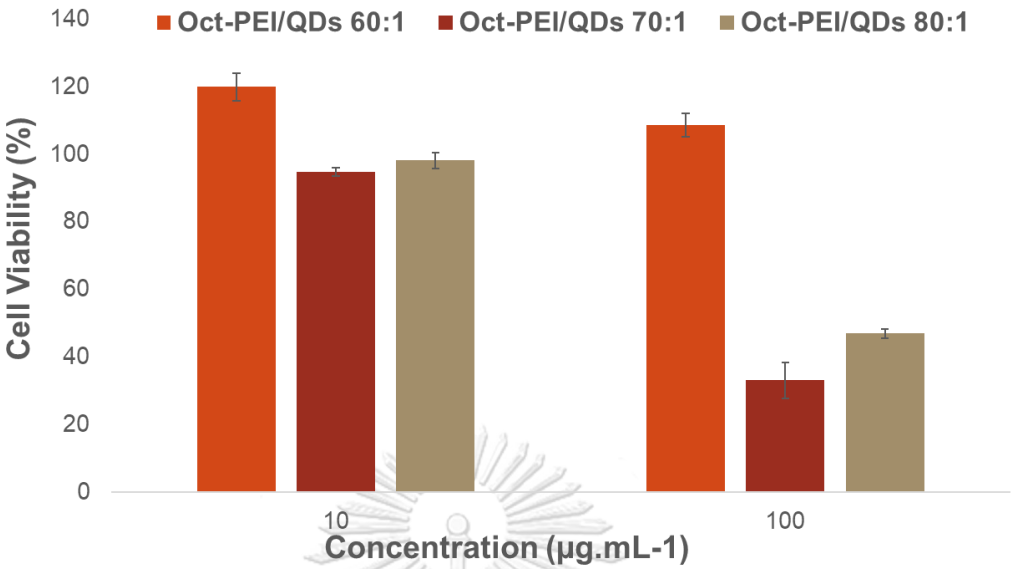

Figure 4.24 MTT assays of the coated QDs against to L929 cells with the incubation time of 24 hours.

Therefore, results from the characterization of the coated QDs including the absorption spectra in **Appendix B** could confirm that the coated QDs provided the cationic surfaces and also maintained the fluorescent properties of the QDs. The optimum molar ratio between Oct-PEI and QDs for providing the highest fluorescent signal was 80:1. In the next section, for applying in DNA detection, the small sizes of QDs which emitted green fluorescence of around 540 nm were preferred for investigating and combining with other optical tools. For studying the changes in the fluorescent signal in response to the presence of DNA, the cationic QDs with the molar ratio between Oct-PEI and QDs of 60:1 was chosen to avoid the interference of the polymer fluorescence signal that will be occurred in the high molar ratio of between Oct-PEI and QDs. Moreover, the stability of the coated green QDs in different molar ratio and effect of the polymer were also shown in **Appendix B**.

4.4 Fluorescent response of the cationic QDs in presence of DNA

The cationic QDs with the molar ratio between Oct-PEI and QDs of 60:1 was applied in the DNA detection. The detection was studied onto the solid support system by using SuperAldehyde2 glass slide. The amine-terminated DNA was fixed onto the glass slide via a standard reductive amination reaction. From Figure 4.26, the cationic QDs were mixed with the different DNA concentrations onto the DNA conjugated glass slide to find the optimum proportion for the electrostatic interaction between positive charges of QDs and negative charges of DNA. After adding the cationic QDs and incubating for 30 minutes, the color and fluorescent of the cationic QDs were evidenced before washing (Figure 4.26 a and b). But after the glass slide was washed with milliQ water (Figure 4.26 c), both of DNA strands (TET and KMY) and the cationic QDs were invisible in the photograph taken under UV light. These results might be interpreted as either the attachment of the DNA strands to the glass slide was not successful, the cationic QDs could not interact with the DNA as proposed, or the signal was too weak to be observed with naked eyes. Therefore, the absorbance of the glass slide was directly measured to gain further insights into the problems.

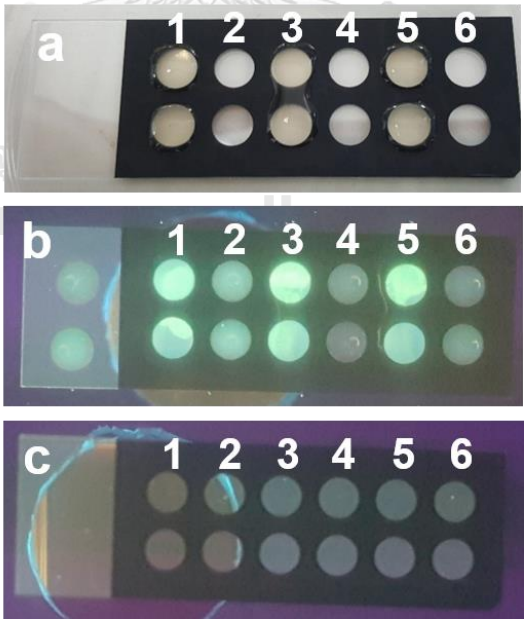

Figure 4.25 Images of 140 μM, 40 μL of the cationic QDs reacted with TET DNA (top row, column 1, 3, 5) and Kanamycin DNA (bottom row, column 1, 3, 5) compared with DNA alone (column 2, 4, and 6) under a) normal light, b) and c) UV light in different

concentrations which are 1000 nM (column 1,2), 500 nM (column 3,4), and 250 nM (column 5,6). The green dots onto left sides of glass slide b) were SYBR gold DNA stains with TET (top) and Kanamycin (bottom).

To measure the absorbance of the DNA-glass slide compared with the reference glass slide, the Diffuse Reflectance UV-visible spectroscopy (DR-UV) was used. From the absorption spectra in Figure 4.27 showed that, the absorbance at 260 nm which belonged to DNA strands could not be identified on both the DNA-immobilize glass slide and the reference glass slide [52]. So we could not confirm whether the DNA strands were successfully attached onto the glass slide.

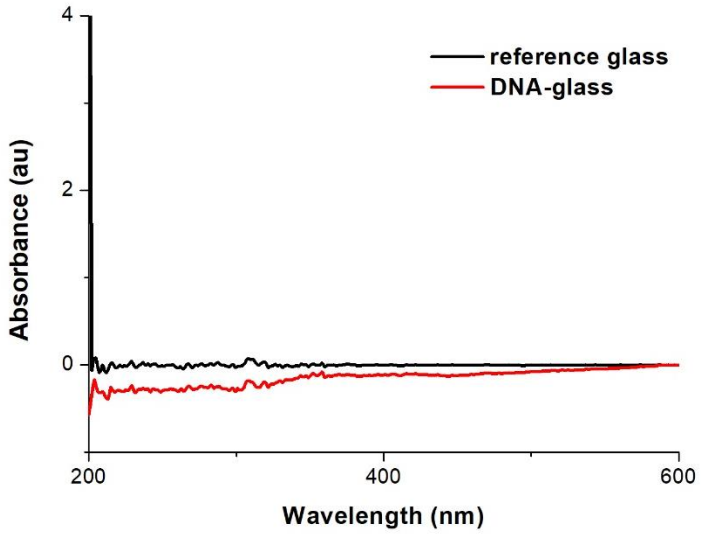

Figure 4.26 Absorption spectra of DNA-glass slide (red line) compared with reference glass slide (black line). The absorption was measured in the range of 200-600 nm.

On the other hand, to confirm the interaction between the cationic QDs and DNA strands, the detection in solution was performed. From Figure 4.28, a model DNA sequence (dGGGGGGGGGG) was mixed with the cationic QDs. The results showed that the fluorescence of the cationic QDs was not quenched after mixing with DNA in Figure 4.28 a) but the mixture become turbid due to the precipitation as shown in Figure 4.28 b). The turbidity of mixture indicated that the electrostatic interaction between the positively charge of the QDs surface and the negatively charge of the DNA strand had

indeed occurred. These results could confirm the occurrence of the electrostatic interaction between the QDs and DNA.

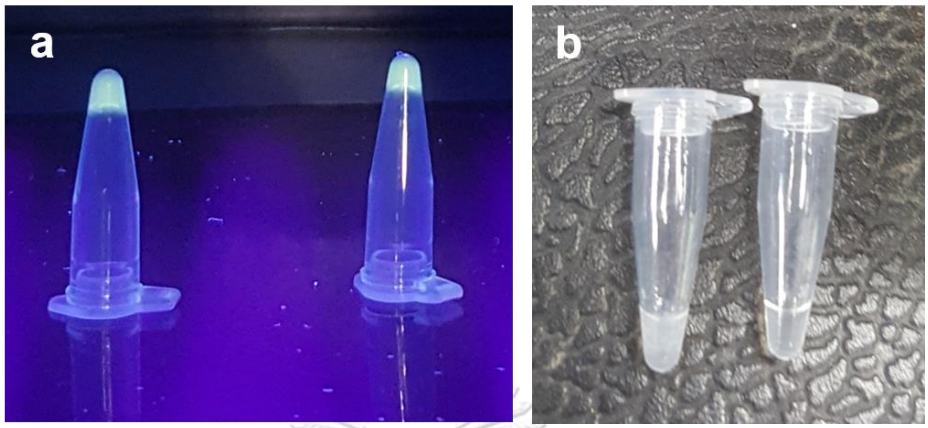

Figure 4.27 The mixture between 10 μM of the dG10 strand and 70 μM of the cationic QDs (left) compared with the cationic QDs (right) in phosphate buffer pH7.0 under a) UV lamp and b) normal light; the camera setting was f=8.0, speed shutter=2, ISO 100.

From these promising results, the cationic QDs were evaluated in combination with peptide nucleic acid (PNA) probe for FRET-based detection of DNA. The PNA sequence was labeled with Nile Red (AC-Lys-AAAA(NR)AAAAA-LysNH2) (NR-PNA) and was used as the acceptor fluorophore to get the energy transfer from the QDs, which should be possible only after the formation of PNA-DNA hybrids. Figure 4.29 showed that after adding the cationic QDs into the DNA solution, the solution become green fluorescence which was brighter than pure QDs as shown in Figure 4.29 b) and gently decreased fluorescence after 1 minute but still brighter than the QDs (Figure 4.29 c). From this result indicated that the interaction between the DNA strand and the cationic QDs might increase the fluorescence of the QDs. Moreover, for the mixture of the cationic QDs that contained NR-PNA (both of P and P+D), their fluorescence colors changed from red to orange after adding the cationic QDs (Figure 4.29 b). However, the color change again after leaving for 1 minute, therefore the color change could not be clearly observed by naked eyes. In order to get a clearer observation, fluorescence spectra were measured at different time interval.

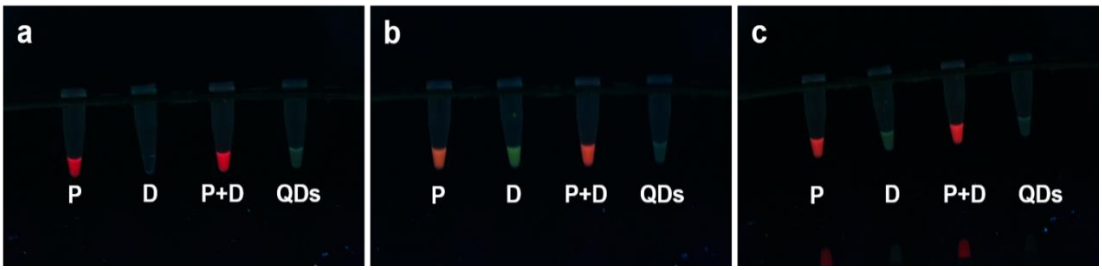

Figure 4.28 Images of (P) Nile Red-PNA, (D) T9 DNA complimented with the PNA, (P+D) NR-PNA in combination with DNA and pure the cationic QDs (QDs) at a) before adding QDs into P, D, and P+D, b) suddenly after adding QDs to P, D and P+D, and c) after 1 min of QD addition. The concentration of DNA was 10 μM, PNA and the cationic QDs were 14 μM in 20 μL of phosphate buffer pH 7.0. The camera setting was f=8.0, speed shutter=2, and ISO 100.

To investigate the interaction between NR-PNA and DNA with the cationic QDs in solution, the fluorescence spectra of mixture were measured every 30 seconds for 10 minutes as described in **Appendix C**. From the results in Figure 4.30 showed that, the fluorescence intensity of the cationic QDs were not decreased while the fluorescence intensity of the NR-PNA were not also increased from the originals which gave the same results as presence of DNA. These results did not follow the FRET principle that the fluorescent intensity of the donor (the cationic QDs) should decrease due to the electrons transferring to acceptor (NR dye in PNA) [53]. Therefore, these results could indicate that, FRET between the cationic QDs and NR-PNA hybridized with DNA was not occurred.

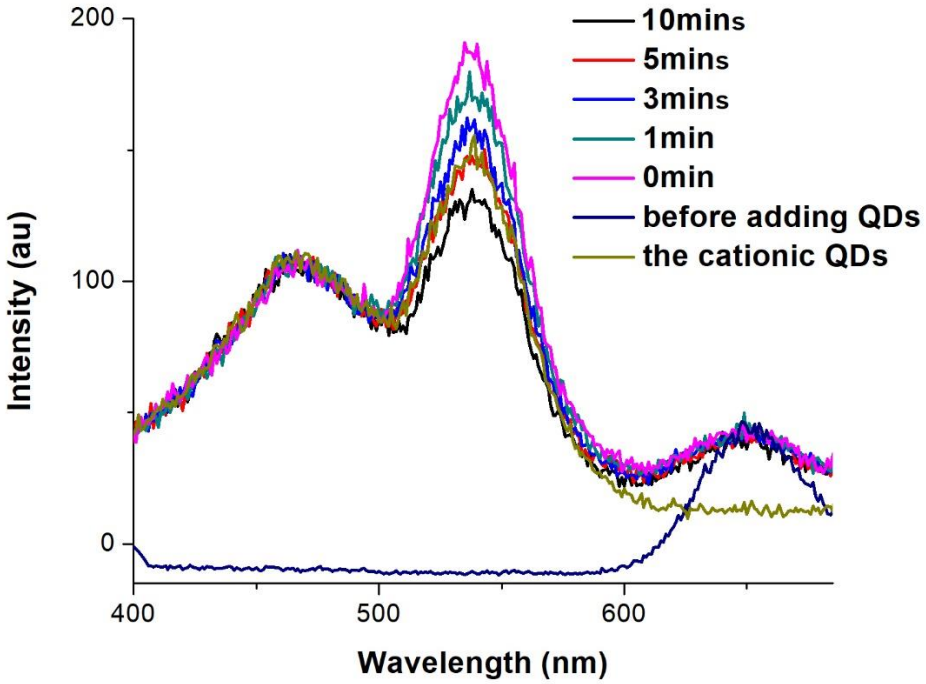

Figure 4.29 Fluorescent spectra of 0.1 μM the cationic QDs before interacted with 1 μM of NR-PNA and DNA (dark yellow line), after interacted for 0 minute (pink line), 1 minute (dark cyan line), 3 minutes (blue line), 5 minutes (red line), 10 minutes (black line), and the solution of DNA matched NR-PNA before adding QDs (navy line). The excitation wavelength was 350 nm with 700 PMT applied voltage.

To study the interaction between the cationic QDs and DNA, the fluorescence spectra at different time interval were monitored as shown in Figure 4.31. The results showed that, the fluorescent intensity of the cationic QDs initially increased rapidly to 32.05% of the original intensity. The signal then started to decrease, and returned to the original signal in around 5 min. At 10 minutes, the fluorescent intensity was slightly lower than the pure cationic QDs. These results indicated that the interaction with DNA could increase the fluorescent intensity of QDs briefly, but the signal gradually quenched to the original level within 5 minutes and was further quenched quenched when left for longer period.

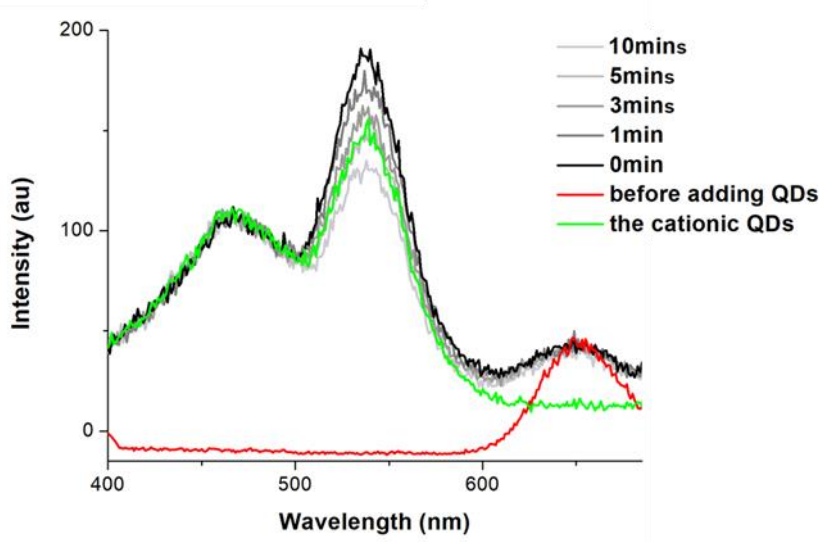

Figure 4.30 Fluorescent spectra of 0.1 μM of the cationic QDs before interacted with 1 μM of DNA (green line), after interacted for 0 minute (black line), 1 minute (dark grey line), 3 minutes (grey line), 5 minutes (lighter grey line), and 10 minutes (the lightest grey line). The excitation wavelength was 350 nm with 700 PMT applied voltage.

The results above suggested that the DNA does interact with the cationic QDs, resulting in a slight fluorescent increase in a time-dependent fashion. The use of QDs in combination with Nile red-labeled acpcPNA probe for the detection of DNA was attempted, but unfortunately could be responded in DNA detection system whether occurrence the PNA with the limitation time of 5 minutes resulting in an increase of emission of the QDs.

CHAPTER V
CONCLUSION

The original hydrophobic CdSe/ZnS core/shell QDs have been successfully synthesized using TOPO, TOP, HDA, and HDDO as surfactant ligands. The CdSe/ZnS core/shell QDs were increased in the efficiency in the fluorescence with the calculated quantum yield of 49%, which was higher than that of the CdSe core QDs (24%). Moreover, as-synthesized CdSe/ZnS core/shell QDs also exhibited the nanocrystal properties as the XRD pattern matched to Cadmium Selenide pattern and Sphalerite-Zinc Sulfide pattern with the diameter size of 4.59 ±0.53 nm measured from TEM.

For applying as-synthesized CdSe/ZnS core/shell QDs in biological applications, the surfaces of the nanoparticles were modified to become hydrophilic in a micellar form with the modified polymer. The modified polymer used in this work was 30% acylated of octanoic acid to poly(ethylene)imine. The results confirmed that poly(ethylene)imine was attained the hydrophobic and hydrophilic parts from the amide functional group at 1645.13 cm^{-1} in Fourier Transform Infrared Spectroscopy (FT-IR), the position of saturated alkane proton at 0.910 and 1.293 ppm, the amine proton at 1.609 ppm, and the ratio of integration of proton from the octanoic acid and PEI in ^{1}H Nuclear Magnetic Resonance (^{1}H-NMR).

Surface of CdSe/ZnS QDs were successfully modified to become positively charge via micelle formation with the 30% acylated poly(ethylene)imine. From the adjustment of the ratio between the polymer and QDs, the optimum ratio for obtaining the cationic QDs with good fluorescence and stability was 60:1 molar ratio of Oct-PEI:QDs. At this ratio, the cationic QDs exhibited the sizes of 267.2 d.nm and the zeta-potential of +36.9 mV. The cationic QDs also provided the water-solubility, fluorescence and colloidal stability for at least 30 days.

For the fluorescent response in the presence of DNA of the cationic CdSe/ZnS QDs, the electrostatic interaction between negatively charged of DNA and positively charged of QDs surface has occurred. The interaction between DNA and QDs can be observed by the turbidity of the mixed solution. Furthermore, in the presence of Peptide Nucleic Acids (PNA) attached with Nile Red, the fluorescence of the cationic QDs were not interfered by the dye on PNA, although the expected FRET could not be observed in the presence of DNA target.

For further investigations, this micellar form cationic CdSe/ZnS core/shell QDs could be involved in bio-applications especially the specific anionic biological species due to their effective positively charged and the colloidal stability for 30 days with high percentage of cell viability. However, the more carefully designed systems have to be created and investigated to be able to use these new cationic QDs.

REFERENCES

[1] Khan, I., Saeed, K., and Khan, I. Nanoparticles: Properties, applications and toxicities. Arabian Journal of Chemistry (2017).

[2] Quora. [Online]. Available from: www.quora.com/What-is-the-difference-between-one-two-three-and-zero-dimensional-nanomaterials [1 June 2018]

[3] Hawk's Perch Technical Writing, L. [Online]. 2016. Available from: www.understandingnano.com/nanoparticles.html [1 June 2018]

[4] Mirela, D. [Online]. 2009. Available from: www.ung.si/~sstanic/teaching/Seminar/2009/20091214_Dragomir_MetNP.pdf [1 June 2018]

[5] Song, K.M., et al. Gold nanoparticle-based colorimetric detection of kanamycin using a DNA aptamer. Anal Biochem 415(2) (2011): 175-81.

[6] Reidy, B., Haase, A., Luch, A., Dawson, K.A., and Lynch, I. Mechanisms of Silver Nanoparticle Release, Transformation and Toxicity: A Critical Review of Current Knowledge and Recommendations for Future Studies and Applications. Materials (Basel) 6(6) (2013): 2295-2350.

[7] Gurunathan, S., Park, J.H., Han, J.W., and Kim, J.H. Comparative assessment of the apoptotic potential of silver nanoparticles synthesized by Bacillus tequilensis and Calocybe indica in MDA-MB-231 human breast cancer cells: targeting p53 for anticancer therapy. Int J Nanomedicine 10 (2015): 4203-22.

[8] Wikipedia. [Online]. Available from: https://en.wikipedia.org/wiki/Copper_nanoparticle [17 May 2018]

[9] Seku, K., Reddy Ganapuram, B., Pejjai, B., Mangatayaru Kotu, G., and Golla, N. Hydrothermal synthesis of Copper nanoparticles, characterization and their biological applications. International Journal of Nano Dimension 9(1) (2018): 7-14.

[10] Ma, Z. and Liu, H. Synthesis and surface modification of magnetic particles for application in biotechnology and biomedicine. China Particuology 5(1-2) (2007): 1-10.

[11] Sanjai, C., Kothan, S., Gonil, P., Saesoo, S., and Sajomsang, W. Chitosan-triphosphate nanoparticles for encapsulation of super-paramagnetic iron oxide as an MRI contrast agent. Carbohydr Polym 104 (2014): 231-7.

[12] AZONANO. [Online]. 2013. Available from: www.azonano.com/article.aspx?ArticleID=4149 [1 June 2018]

[13] Sun, X. and Lei, Y. Fluorescent carbon dots and their sensing applications. TrAC Trends in Analytical Chemistry 89 (2017): 163-180.

[14] Ding, H., Yu, S.B., Wei, J.S., and Xiong, H.M. Full-Color Light-Emitting Carbon Dots with a Surface-State-Controlled Luminescence Mechanism. ACS Nano 10(1) (2016): 484-91.

[15] Mahato, N., Ansari, M.O., and Cho, M.H. Production of Utilizable Energy from Renewable Resources: Mechanism, Machinery and Effect on Environment. Advanced Materials Research 1116 (2015): 1-32.

[16] Bangal, M., et al. Semiconductor Nanoparticles. Hyperfine Interactions 160(1) (2005): 81-94.

[17] Liu, P., Wang, Q., and Li, X. Studies on CdSe/l-cysteine Quantum Dots Synthesized in Aqueous Solution for Biological Labeling. The Journal of Physical Chemistry C 113(18) (2009): 7670-7676.

[18] Talapin, D.V., Rogach, A.L., Shevchenko, E.V., Kornowski, A., Haase, M., and Weller, H. Dynamic Distribution of Growth Rates within the Ensembles of Colloidal II–VI and III–V Semiconductor Nanocrystals as a Factor Governing Their Photoluminescence Efficiency. Journal of the American Chemical Society 124(20) (2002): 5782-5790.

[19] Kwizera, P., Angela, A., Wekesa, M., Uddin, M.J., and Shaikh, M.M. Synthesis and Characterization of CdSe Quantum Dots by UV-Vis Spectroscopy. 2012.

[20] Abbasi, S., Molaei, M., and Karimipour, M. CdSe and CdSe/CdS core-shell QDs: New approach for synthesis, investigating optical properties and application in pollutant degradation. Luminescence 32(7) (2017): 1137-1144.

[21] Hines, M.A. and Guyot-Sionnest, P. Synthesis and Characterization of Strongly Luminescing ZnS-Capped CdSe Nanocrystals. The Journal of Physical Chemistry 100(2) (1996): 468-471.

[22] Mehrjoo, M., Molaei, M., and Karimipour, M. A novel process for synthesis of CdSe/ZnS core-shell QDs and their application for the Methyl orange (MO) degradation. Materials Chemistry and Physics 201 (2017): 165-169.

[23] Mathew, S., et al. Effect of ZnS shell on optical properties of CdSe–ZnS core–shell quantum dots. Optical Materials 39 (2015): 46-51.

[24] Bera, D., Qian, L., Tseng, T.-K., and Holloway, P.H. Quantum Dots and Their Multimodal Applications: A Review. Materials 3(4) (2010): 2260-2345.

[25] Burda, C., Chen, X., Narayanan, R., and El-Sayed, M.A. Chemistry and Properties of Nanocrystals of Different Shapes. Chemical Reviews 105(4) (2005): 1025-1102.

[26] Sashchiuk, A., Lifshitz, E., Reisfeld, R., Saraidarov, T., Zelner, M., and Willenz, A. Optical and Conductivity Properties of PbS Nanocrystals in Amorphous Zirconia Sol-Gel Films. Journal of Sol-Gel Science and Technology 24(1) (2002): 31-38.

[27] Zhu, J., Koltypin, Y., and Gedanken, A. General Sonochemical Method for the Preparation of Nanophasic Selenides: Synthesis of ZnSe Nanoparticles. Chemistry of Materials 12(1) (2000): 73-78.

[28] Xie, Y., Qian, Y., Wang, W., Zhang, S., and Zhang, Y. A Benzene-Thermal Synthetic Route to Nanocrystalline GaN. Science 272(5270) (1996): 1926.

[29] Swihart, M.T. Vapor-phase synthesis of nanoparticles. Current Opinion in Colloid & Interface Science 8(1) (2003): 127-133.

[30] Murray, C.B., Norris, D.J., and Bawendi, M.G. Synthesis and characterization of nearly monodisperse CdE (E = sulfur, selenium, tellurium) semiconductor nanocrystallites. Journal of the American Chemical Society 115(19) (1993): 8706-8715.

[31] Talapin, D.V., Rogach, A.L., Kornowski, A., Haase, M., and Weller, H. Highly Luminescent Monodisperse CdSe and CdSe/ZnS Nanocrystals Synthesized in a Hexadecylamine–Trioctylphosphine Oxide–Trioctylphospine Mixture. Nano Letters 1(4) (2001): 207-211.

[32] Kloepfer, J.A., Bradforth, S.E., and Nadeau, J.L. Photophysical Properties of Biologically Compatible CdSe Quantum Dot Structures. The Journal of Physical Chemistry B 109(20) (2005): 9996-10003.

[33] Aldana, J., Wang, Y.A., and Peng, X. Photochemical Instability of CdSe Nanocrystals Coated by Hydrophilic Thiols. Journal of the American Chemical Society 123(36) (2001): 8844-8850.

[34] Pellegrino, T., et al. Hydrophobic Nanocrystals Coated with an Amphiphilic Polymer Shell: A General Route to Water Soluble Nanocrystals. Nano Letters 4(4) (2004): 703-707.

[35] Chen, Y., Thakar, R., and Snee, P.T. Imparting Nanoparticle Function with Size-Controlled Amphiphilic Polymers. Journal of the American Chemical Society 130(12) (2008): 3744-3745.

[36] Tian, H., et al. Gene transfection of hyperbranched PEI grafted by hydrophobic amino acid segment PBLG. Biomaterials 28(18) (2007): 2899-2907.

[37] Kalidhasan, S., Dror, I., and Berkowitz, B. Atrazine degradation through PEI-copper nanoparticles deposited onto montmorillonite and sand. Sci Rep 7(1) (2017): 1415.

[38] Tumturk, H. and Yuksekdag, H. Acetylcholinesterase immobilized onto PEI-coated silica nanoparticles. Artif Cells Nanomed Biotechnol 44(2) (2016): 443-7.

[39] Nann, T. Phase-transfer of CdSe@ZnS quantum dots using amphiphilic hyperbranched polyethylenimine. Chem Commun (Camb) (13) (2005): 1735-6.

[40] Liang, G., et al. Polyethyleneimine-coated quantum dots for miRNA delivery and its enhanced suppression in HepG2 cells. Int J Nanomedicine 11 (2016): 6079-6088.

[41] Yang, P. and Zhou, G. Phase transfer of hydrophobic QDs for water-soluble and biocompatible nature through silanization. Materials Research Bulletin 46(12) (2011): 2367-2372.

[42] Povrozin, Y. and Terpetschnig, E. Measurement of fluorescence quantum yields on ISS instrumentation using vinci. 2008, ISS Technical Note. 1-8.

[43] Kubin, R.F. and Fletcher, A.N. Fluorescence quantum yields of some rhodamine dyes. Journal of Luminescence 27(4) (1982): 455-462.

[44] Riss, T.L., et al. Cell viability assays. Assay Guidance Manual (2016): 1-31.

[45] Zammatteo, N., et al. Comparison between different strategies of covalent attachment of DNA to glass surfaces to build DNA microarrays. Anal Biochem 280(1) (2000): 143-50.

[46] UCLA. [Online]. 2000. Available from: https://webspectra.chem.ucla.edu/irtable.html [1 Jun 2018]

[47] University, M.C.-M.S. [Online]. Available from: www2.chemistry.msu.edu/faculty/reusch/orgpage/nmr.htm [6 June 2018]

[48] UNM. [Online]. Available from: http://www.unm.edu/~orgchem/304L%20pages/09%2013C%20shift%20chart%20304.pdf [6 June 2018]

[49] Introduction to Carbon NMR [Online]. Available from: http://www2.ups.edu/faculty/hanson/Spectroscopy/NMR/CNMR.htm [5 June 2018]

[50] Ruanmai, S. and Koonsombutkul, K. Surface modification of semiconductor nanoparticles using copolymer for biological and environmental applications. Bachelor, Chemistry Chulalongkorn University, 2555.

[51] Yue, H. and Ma, G. Polymeric micro/nanoparticles: Particle design and potential vaccine delivery applications. Vaccine 33(44) (2015): 5927-5936.

[52] Technology, O.G. [Online]. 2011. Available from: www.ogt.com/resources/literature/483_understanding_and_measuring_variations_in_dna_sample_quality [23 Aug 2011]

[53] Sekar, R.B. and Periasamy, A. Fluorescence resonance energy transfer (FRET) microscopy imaging of live cell protein localizations. The Journal of Cell Biology 160(5) (2003): 629.

APPENDIX

Appendix A

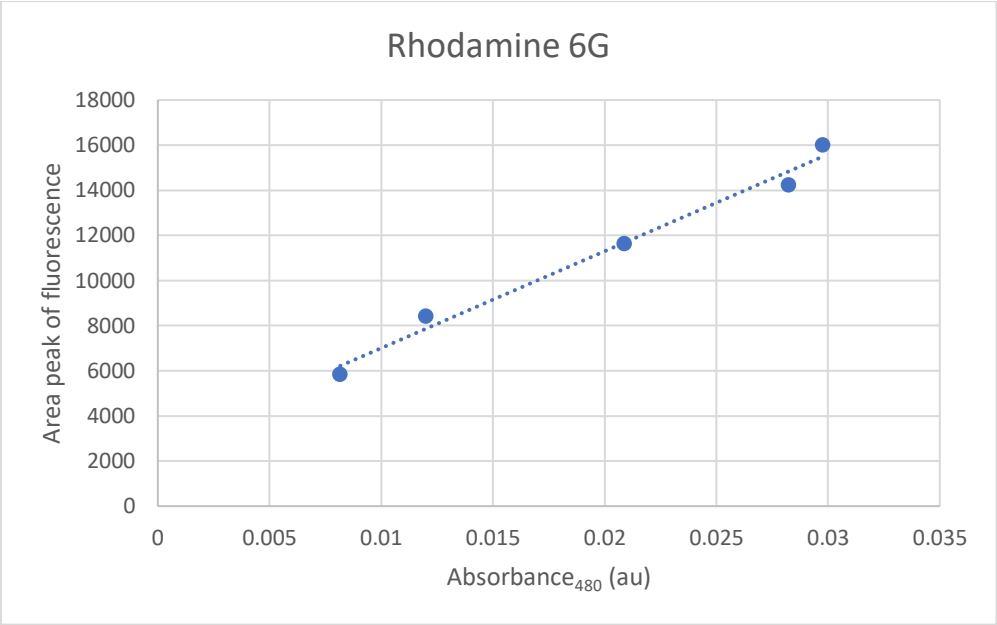

Figure A1 Graph between peak area of fluorescence VS absorbance at wavelength 480 nm of Rhodamine 6G in 5 different concentrations.

Table A4 Parameters of the linear regression of Rhodamine 6G emission

Rhodamine 6G in each concentrations	Abs_{480}	Area peak of fluorescence
R1	0.008164913	5833.941858
R2	0.012015176	8416.71831
R3	0.020902015	11629.32908
R4	0.028240778	14217.43146
R5	0.029772613	16008.74245

Linear equation : $y = 429470x + 2709.5$; $R^2 = 0.9841$

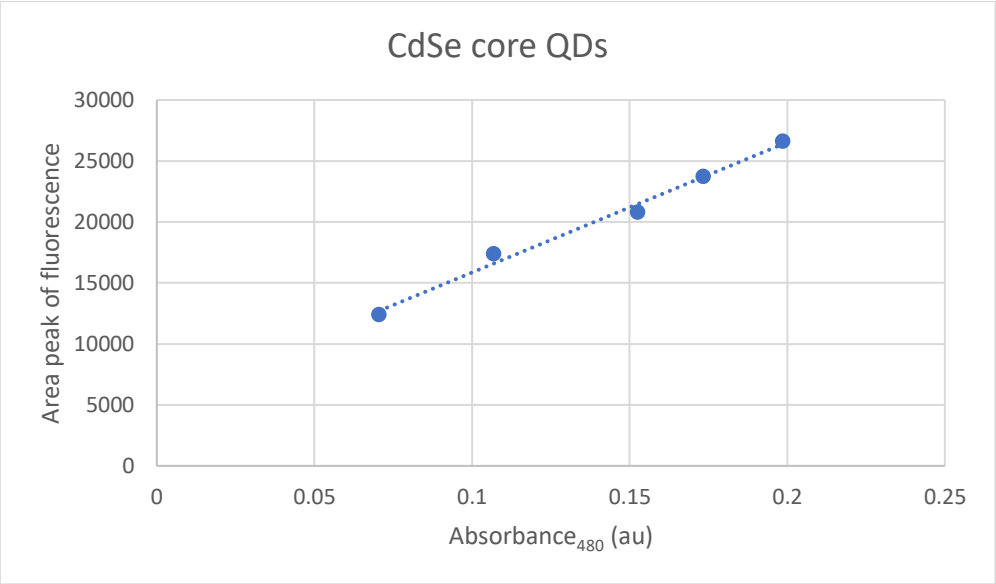

Figure A2 Graph between area peak of fluorescence VS absorbance at wavelength 480 nm of CdSe core QDs in 5 different concentrations.

Table A5 Parameters of the linear regression of CdSe core QDs emission

CdSe core QDs in each concentrations	Abs_{480}	Area peak of fluorescence
C1	0.0705724	12397.16949
C2	0.106948	17398.72591
C3	0.1527311	20779.58628
C4	0.1734927	23700.99734
C5	0.1986822	26623.22064

Linear equation : y = 106772x +5180.1 ; R^2 = 0.9894

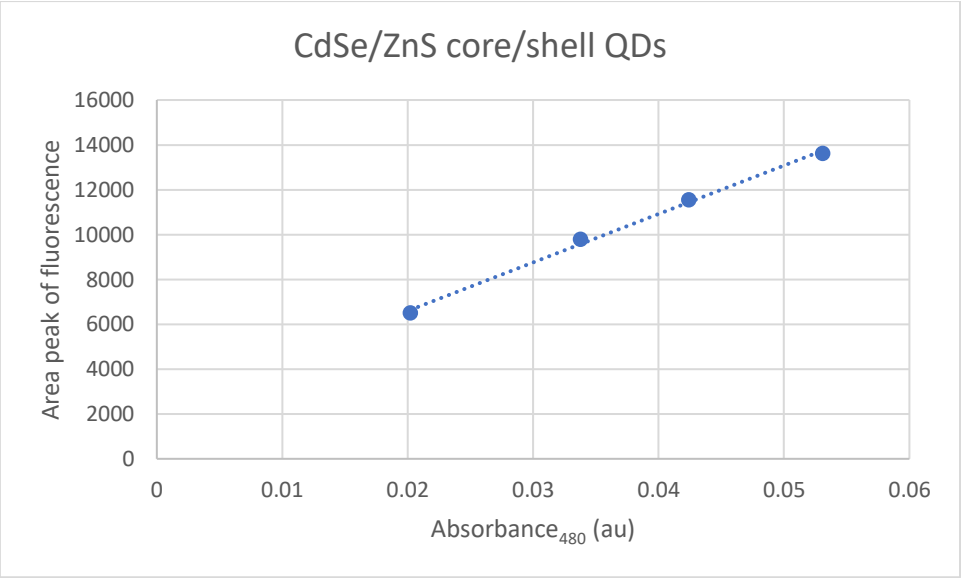

Figure A3 Graph between area peak of fluorescence VS absorbance at wavelength 480 nm of CdSe/ZnS core/shell QDs in 4 different concentrations.

Table A6 Parameters of the linear regression of CdSe/ZnS core/shell QDs emission

CdSe/ZnS core/shell in each concentrations	Abs_{480}	Area peak of fluorescence
S1	0.020205645	6499.748392
S2	0.03380277	9767.100395
S3	0.042424135	11528.78214
S4	0.053078759	13606.08589

Linear equation : $y = 216119x + 2272.4$; $R^2 = 0.997$

Appendix B

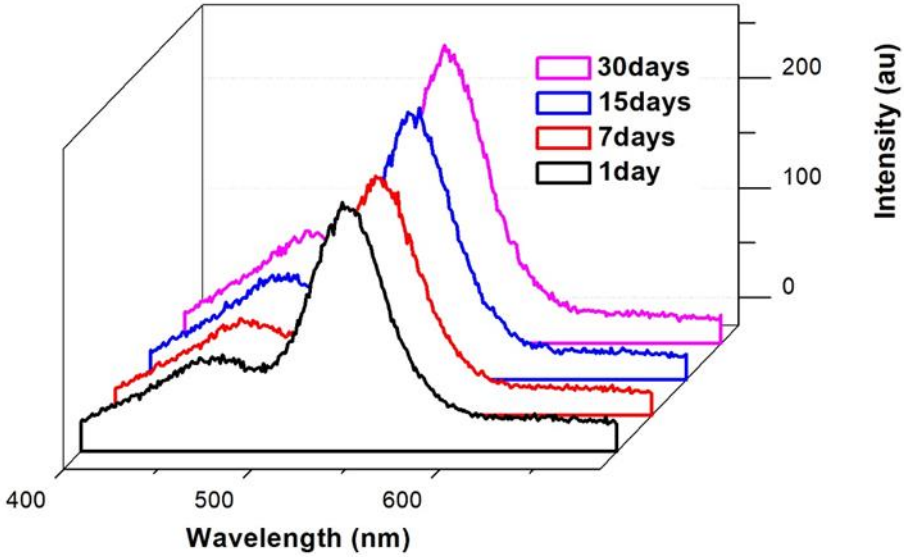

Figure B1 Emission spectra of the coated green QDs in molar ratio between Oct-PEI and QDs of 60:1 after 1 day (black line), 7 days (red line), 15 days (blue line), and 30 days (pink line). The excitation wavelength was 350 nm with 700 PMT applied voltage.

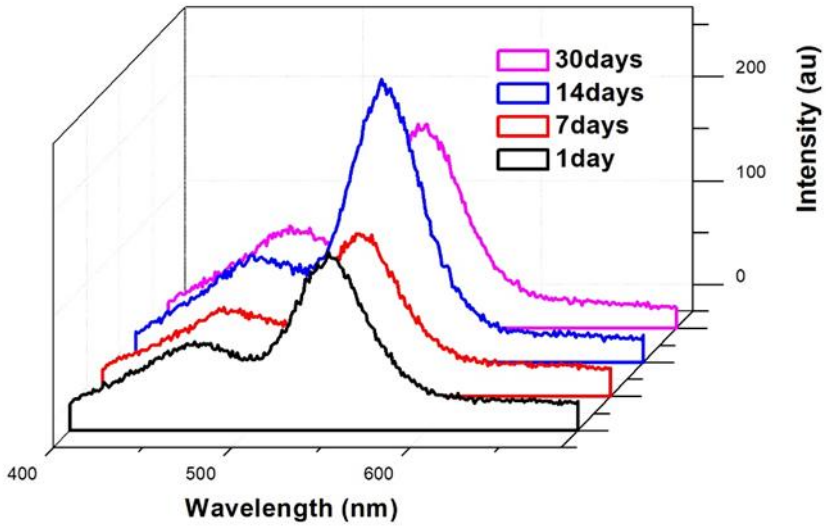

Figure B2 Emission spectra of the coated green QDs in molar ratio between Oct-PEI and QDs of 70:1 after 1 day (black line), 7 days (red line), 15 days (blue line), and 30 days (pink line). The excitation wavelength was 350 nm with 700 PMT applied voltage.

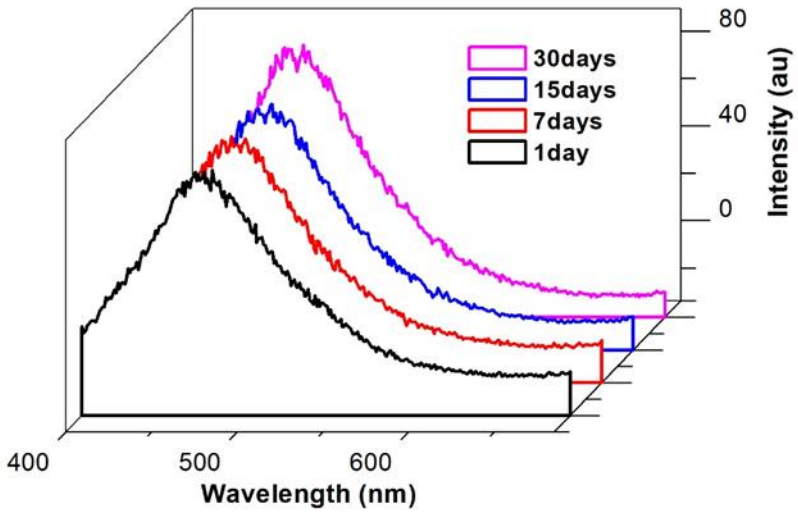

Figure B3 Emission spectra of the coated green QDs in molar ratio between Oct-PEI and QDs of 80:1 after 1 day (black line), 7 days (red line), 15 days (blue line), and 30 days (pink line). The excitation wavelength was 350 nm with 700 PMT applied voltage.

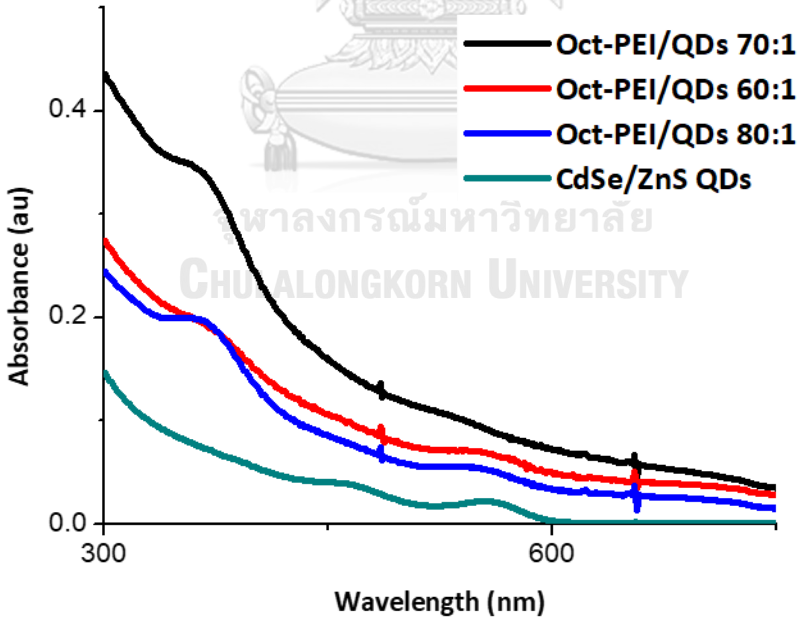

Figure B4 Absorption spectra of CdSe/ZnS core/shell QDs (green line) compared with the Oct-PEI/QDs in different molar ratio of 60:1 (red line), 70:1 (black line), and 80:1 (blue line).

Appendix C

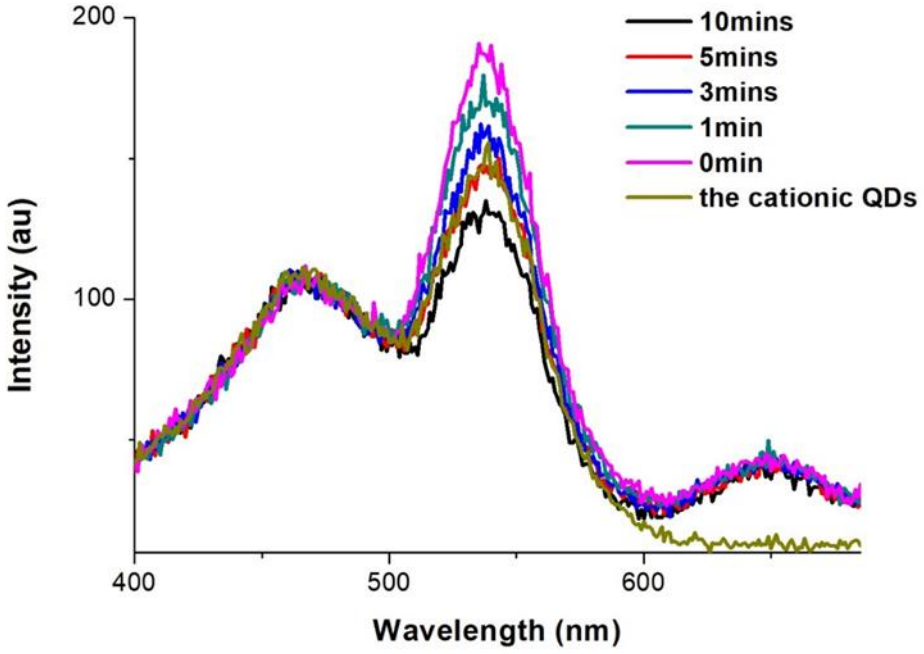

Figure C1 Fluorescent spectra of 0.1 μM of the cationic QDs before interacted with 1 μM of DNA and NR-PNA (dark yellow line), after interacted for 0 minute (pink line), 1 minute (green line), 3 minutes (blue line), 5 minutes (red line), and 10 minutes (black line). The excitation wavelength was 350 nm with 700 PMT applied voltage.

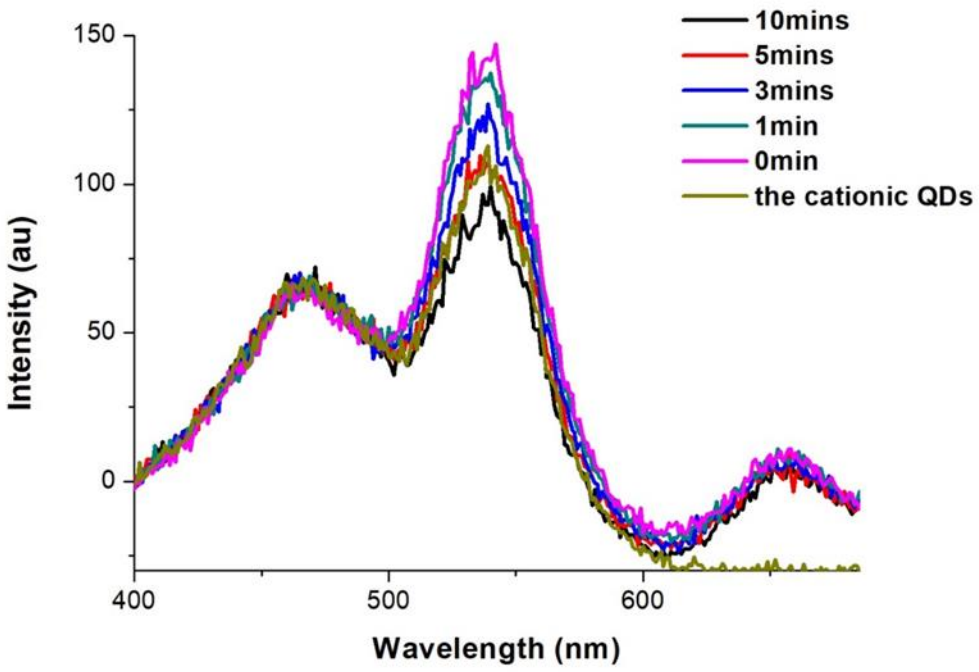

Figure C2 Fluorescent spectra of 0.1 μM of the cationic QDs before interacted with 1 μM of NR-PNA (dark yellow line), after interacted for 0 minute (pink line), 1 minute (green line), 3 minutes (blue line), 5 minutes (red line), and 10 minutes (black line). The excitation wavelength was 350 nm with 700 PMT applied voltage.

VITA

Miss Jamornpan Yangcharoenyuenyong was born on June 24, 1991 in Bangkok, Province, Thailand. She graduated in Bachelor Degree of Science in Chemistry from Chulalongkorn University in 2014. She became a member of Materials Chemistry and Catalysis Research Unit under the supervision of Dr. Numpon Insin since 2013. She continued her Master's Degree of Science in Program in Chemistry, Faculty of Science, Chulalongkorn University. On 7-9 February 2018, she attended Pure and Applied Chemistry International Conference (PACCON) 2018 in the title of "SYNTHESIS OF HYDROPHOBICALLY-MODIFIED POLY(ETHYLENEIMINE) AS SURFACTANT FOR CATIONIC CdSe/ZnS QUANTUM DOTS WITH HIGH COLLOIDAL STABILITY" by oral presentation. Her present address is 369/612 Moo 3, Sukhumvit Road., Bangpumai, Muang, Samutprakarn, Thailand, 10280. Email address: Jamornpan.y@gmail.com